



**Dynamische Reorganization des endoplasmatischen Retikulums und der
Ribosomen in Axonterminalen von Wildtyp- und Spinaler Muskelatrophie
Motoneuronen**

**Dynamic remodeling of endoplasmic reticulum and ribosomes in axon
terminals of wildtype and Spinal Muscular Atrophy motoneurons**

**Doctoral thesis for a doctoral degree
at the Graduate School of Life Sciences,
Julius-Maximilians-Universität Würzburg,
Section Neuroscience**

submitted by

Deng, Chunchu

from

Hunan, China

Würzburg, 2021



Submitted on:

Office stamp

Members of the Thesis Committee

Chairperson: ... Prof. Dr. Christian Wegener

Primary Supervisor: ... Prof. Dr. med. Michael Sendtner

Supervisor (Second): ... Prof. Dr. Markus Sauer

Supervisor (Third): ... Prof. Dr. med. Lars Dölken

Date of Public Defence:

Date of Receipt of Certificates:

Table of contents

1. Summary	3
2. Zusammenfassung.....	4
3. Introduction.....	6
3.1 Axonal endoplasmic reticulum: organization, dynamics and functions.....	6
3.1.1 Organization of axonal ER and its dynamic regulation.....	7
3.1.2 Functions of axonal ER	11
3.1.3 ER in neurodegenerative diseases.....	16
3.2 Local translation in neurons	21
3.2.1 Roles of local translation in neurons.....	22
3.2.2 Regulation of local translation	25
3.3 Spinal Muscular Atrophy	28
3.4 Aim of the present study.....	30
4. Materials and Methods	31
4.1 Materials.....	31
4.1.1 Animals	31
4.1.2 HEK ^{293T} and NSC34 cell Lines.....	32
4.1.3 Chemicals, reagents, solutions, materials and kits	32
4.1.4 List of plasmids	43
4.1.5 Antibodies.....	44
4.1.6 Primers for genotyping and cloning	47
4.1.7 Softwares.....	48
4.2 Methods	49
4.2.1 Isolation and culture of embryonic mouse motoneurons	49
4.2.2 Pharmacological treatments	50
4.2.3 Immunocytochemistry of cultured motoneurons.....	51
4.2.4 Western blotting	52
4.2.5 Live cell imaging	53
4.2.6 Analysis of ER dynamics	54
4.2.7 Confocal microscopy, super-resolution microscopy and data analysis.....	56
4.2.8 Cloning of the constructs.....	57
4.2.9 HEK ^{293T} and NSC34 cell line culture.....	66
4.2.10 Validation of constructs containing fluorescent proteins	67
4.2.11 Virus production, titration, and transduction	68
4.2.12 DNA extraction for genotyping.....	69

4.2.13	Genotyping of transgenic mice.....	70
5.	Results	73
5.1	ER enters growth cone filopodia and moves along actin filaments in filopodia.....	73
5.2	ER movements in growth cones of cultured motoneurons are regulated by actin and microtubule cytoskeleton	78
5.3	Myosin VI and drebrin A are particularly involved in ER dynamics in axon terminals.....	82
5.4	BDNF-induced TrkB activation triggers redistribution of ribosomes in growth cones on a time scale of seconds	89
5.5	Extracellular BDNF stimulation induces ribosome assembly and local translation in axonal growth cones of motoneurons.....	96
5.6	Extracellular BDNF stimulation rapidly induces protein translation in growth cones of motoneurons.....	101
5.7	Activated ribosomes induced by BDNF attach to ER, contributing to protein synthesis in the distal axonal compartment	106
5.8	Dynamics of ER in axonal growth cones are defective in Smn-deficient motoneurons	109
5.9	Deficiency in SMN protein abolishes the effects of BDNF on ribosome activation and local translation in axon terminals	114
5.10	BDNF-induced active ribosomes and their association with ER are disturbed in axonal growth cones of cultured SMA motoneurons.....	116
5.11	Basic TrkB levels are comparable in growth cones of Smn-deficient and control motoneurons.....	119
5.12	BDNF induced TrkB activation is altered in axon terminals of Smn-deficient motoneurons	121
6.	Discussion.....	124
6.1	ER dynamics depend on drebrin A-mediated actin/microtubule crosstalk in axonal growth cones in motoneurons.....	124
6.2	ER associates with active ribosomes and contributes to protein synthesis including transmembrane proteins in axonal growth cones of cultured motoneurons	126
6.3	ER dynamics are impaired in growth cones of SMA motoneurons.....	128
6.4	BDNF/TrkB induced dynamics of translational machinery is defected in SMA.....	130
7.	References.....	130
8.	Appendix.....	146
8.1	List of figures	146
8.2	List of tables.....	147
8.3	List of abbreviations	148
9.	Affidavit	156
10.	Acknowledgments.....	157
11.	Curriculum Vitae.....	159

1. Summary

In highly polarized neurons, endoplasmic reticulum (ER) forms a dynamic and continuous network in axons that plays important roles in lipid synthesis, Ca^{2+} homeostasis and the maintenance of synapses. However, the mechanisms underlying the regulation of axonal ER dynamics and its function in regulation of local translation still remain elusive. In the course of my thesis, I investigated the fast dynamic movements of ER and ribosomes in the growth cone of wildtype motoneurons as well as motoneurons from a mouse model of Spinal Muscular Atrophy (SMA), in response to Brain-derived neurotrophic factor (BDNF) stimulation. Live cell imaging data show that ER extends into axonal growth cone filopodia along actin filaments and disruption of actin cytoskeleton by cytochalasin D treatment impairs the dynamic movement of ER in the axonal filopodia. In contrast to filopodia, ER movements in the growth cone core seem to depend on coordinated actions of the actin and microtubule cytoskeleton. Myosin VI is especially required for ER movements into filopodia and drebrin A mediates actin/microtubule coordinated ER dynamics. Furthermore, we found that BDNF/TrkB signaling induces assembly of 80S ribosomes in growth cones on a time scale of seconds. Activated ribosomes relocate to the presynaptic ER and undergo local translation. These findings describe the dynamic interaction between ER and ribosomes during local translation and identify a novel potential function for the presynaptic ER in intra-axonal synthesis of transmembrane proteins such as the α -1 β subunit of N-type Ca^{2+} channels in motoneurons. In addition, we demonstrate that in *Smn*-deficient motoneurons, ER dynamic movements are impaired in axonal growth cones that seems to be due to impaired actin cytoskeleton. Interestingly, ribosomes fail to undergo rapid structural changes in *Smn*-deficient growth cones and do not associate to ER in response to BDNF. Thus, aberrant ER dynamics and ribosome response to extracellular stimuli could affect axonal growth and presynaptic function and maintenance, thereby contributing to the pathology of SMA.

2. Zusammenfassung

Das Endoplasmatische Retikulum (ER) bildet ein dynamisches und kontinuierliches Netzwerk in Axonen von stark polarisierten Neuronen und spielt dabei eine wichtige Rolle in der Lipidsynthese, dem Ca^{2+} Homöostase und der Aufrechterhaltung von Synapsen. Allerdings sind die Mechanismen, die der Regulierung der axonalen ER-Dynamik und seiner Funktion bei der dynamischen Regulierung der lokalen Translation zugrunde liegen, nicht vollständig aufgeklärt. Im Rahmen meiner Dissertation habe ich die schnellen dynamischen Bewegungen des ERs und Ribosomen in Wachstumskegeln von Wildtyp- und Smn-defizienten Motoneuronen als Reaktion auf einen kurzen Puls von Brain-derived neurotrophic factor (BDNF) untersucht. Daten der Bildgebung lebender Zellen zeigen, dass sich das ER in axonalen Filopodien des Wachstumskegels entlang von Aktin-Filamenten ausbreitet. Die Beeinträchtigung des Aktin-Zytoskeletts mittels Cytochalasin D Behandlung führt zu einer Einschränkung der dynamischen Bewegung des ERs in den axonalen Filopodien. Im Gegensatz zu den Filopodien scheinen die Bewegungen des ERs in Wachstumskegeln von einem koordinierten Zusammenspiel des Aktin- und Mikrotubuli- Zytoskeletts zu beruhen. Myosin VI ist insbesondere für die ER-Bewegungen in Filopodien erforderlich, während Drebrin A die Aktin/Mikrotubuli koordinierte ER-Dynamik vermittelt. Darüber hinaus zeigte sich, dass das BDNF/TrkB Signal die Bildung von 80S-Ribosomen in Wachstumskegeln in Sekundenschnelle auslöst. Aktivierte Ribosomen verlagern sich in das präsynaptische ER und vollziehen eine lokale Translation. Diese Ergebnisse beschreiben die dynamische Interaktion zwischen ER und Ribosomen während der lokalen Translation und zeigen eine neuartige potentielle Funktion des präsynaptischen ER bei der intra-axonalen Synthese von Transmembranproteinen wie die α -1 β Untereinheit der N-Typ Ca^{2+} Kanäle in Motoneuronen auf. Darüber hinaus zeigen wir, dass in Smn-defizienten Motoneuronen die dynamischen ER-Bewegungen in axonalen Wachstumskegeln beeinträchtigt sind, was mit einer gestörten

Polymerisation von Aktinfilamenten zusammenzuhängen scheint. Interessanterweise erfahren Ribosomen in Smn-defizienten Wachstumskegeln keine schnellen strukturellen Veränderungen und assoziieren nicht mit dem ER als Reaktion auf BDNF. Somit könnten eine abweichende ER-Dynamik und die Reaktion der Ribosomen auf extrazelluläre Reize das axonale Wachstum und die präsynaptische Funktion und Aufrechterhaltung beeinträchtigen und damit zur Pathologie von SMA beitragen.

3. Introduction

3.1 Axonal endoplasmic reticulum: organization, dynamics and functions

Endoplasmic reticulum (ER) is a large and dynamic membranous organelle, providing a physically continuous network throughout all eukaryotic cells, including neurons (Terasaki, Slater et al. 1994, Wu, Whiteus et al. 2017, Yalçın, Zhao et al. 2017). According to the density of ribosomes on the surface, ER is divided into rough and smooth ER domains. Rough ER (RER) is studded with substantial ribosomes and predominantly distributes around the nucleus as sheets and cisternae. A crucial function of RER is to serve as the major site for protein synthesis of mainly secretory and integral membrane proteins and some cytosolic proteins (Jan, Williams et al. 2014, Reid and Nicchitta 2015, Rogers 2019). Some proteins that are synthesized in the RER are transported to the Golgi apparatus via packaged vesicles. ER resident proteins remain in the ER and play their specific roles there. Smooth ER (SER) lacks ribosomes and forms predominantly as tubules and occasionally as irregular sheets or cisternae. SER localizes mainly in the cellular peripheral compartments and contributes to Ca^{2+} regulation (Clapham 2007, Stutzmann and Mattson 2011), lipid synthesis (Fagone and Jackowski 2009, Jacquemyn, Cascalho et al. 2017), glucose metabolism (Müller, Fouyssac et al. 2018) and provides contact sites with other organelles (Rowland, Chitwood et al. 2014, Lee, Cathey et al. 2020, Xu, Wang et al. 2020). Elaborate modulation of Ca^{2+} concentration in subcellular compartments initiates and terminates many pivotal cellular responses to different types of signals. For homeostasis of Ca^{2+} concentration, ER functions as a calcium reservoir that takes up and releases Ca^{2+} from/to other subcellular compartments and regulates Ca^{2+} flux of the plasma membrane (PM) (Raffaello, Mammucari et al. 2016). In addition, SER also provides a platform for lipid production including sterols, sphingolipids, phospholipids and neutral lipids which can be transported from ER to other cellular organelles such as mitochondrial and PM after synthesis to sustain lipid compositions of their membranes

(Fagone and Jackowski 2009). In tissues such as liver, glucose-6-phosphate (G6P) consumed to produce adenosine triphosphate (ATP) can be dephosphorylated by glucose-6-phosphatase- α (G6Pase- α) in the ER and then stored there. When necessary, the stored glucose is released, such that detrimental high blood glucose concentration could be prevented (Burchell, Allan et al. 1994). Many recent studies have been investigating the interaction of ER with other organelles via membrane contact sites (MCSs) and their roles in maintenance of cellular homeostasis and function. MCSs provide a conduit between two organelles that offers an alternative channel for rapid exchange of lipids and calcium (Wu, Carvalho et al. 2018). Taken as an example, non-vesicular dependent transport of lipid between organelles is mediated by ER MCSs, as an additional way to the membrane budding and fusion dependent vesicular transport (Muallem, Chung et al. 2017). So far, many proteins such as vesicle-associated membrane protein-associated proteins (VAPs) and the retromer that help tethering ER and other membranes were identified as key components of MCSs (Dong, Saheki et al. 2016).

3.1.1 Organization of axonal ER and its dynamic regulation

Similar as other eukaryotic cells, neurons have RER and SER. While RER is mostly constricted in cell body, axonal ER is primarily composed of tubular ER network. Tubular ER is generated and maintained by a group of ER membrane proteins. Reticulons (RTNs) that localize mainly in the tubular ER in yeast and mammalian cells constitute a large group of membrane associated proteins with diverse functions ER (Voeltz, Prinz et al. 2006, Yang and Strittmatter 2007). For example, a member of RTNs, Rtn4a, also known as Nogo-A, is needed for the formation of tubular ER in vitro (Voeltz, Prinz et al. 2006). Another family member Rtn1p is also proposed to play a role in tubular ER formation via its interaction with deleted in polyposis 1 (DP1) in mammalian cells or with its homolog Yop1p in yeast cells. This interaction is necessarily for the formation of Rtn1p oligomers that results in less mobility of

oligomers in the membrane and facilitating their localization exclusively to the tubular ER (Shibata, Voss et al. 2008). Mutations in Rtn1p impair the ability of oligomerization and affect its localization to the tubular ER, thereby reducing the tubule shaping (Shibata, Voss et al. 2008). The protein Yop1p contains a reticulon homology domain (RHD) with long hydrophobic helices across the membrane and an amphipathic helix (APH) necessary for membrane tubule formation (Brady, Claridge et al. 2015). Among six human DP1 proteins also termed receptor expression-enhancing proteins (REEPs), receptor expression-enhancing protein 1 (REEP1) binds to both microtubules (MTs) and ER to promote ER co-alignment along MTs. A SPG31 mutant in REEP1 that disrupts the interaction between ER and MTs or application of anti REEP1-4 antibodies both disturb formation of ER network (Park, Zhu et al. 2010). In addition, other proteins such as ADP-ribosylation factor-like 6 interacting protein 1 (ARL6IP1), inositol polyphosphate 5-phosphatase K (INPP5K) and protrudin also help to shape tubular ER. Depletion of ARL6IP1, INPP5K or protrudin alters ER morphology, with increased ER sheets and decreased tubules (Chang, Lee et al. 2013, Yamamoto, Yoshida et al. 2014, Dong, Zhu et al. 2018). Homotypic membrane fusion involved in establishment and maintenance of axonal ER requires guanosine triphosphate (GTP) hydrolysis. In *Drosophila* neurons, ultrastructural analysis of ER has shown that depletion of a guanosine triphosphatase (GTPase) atlastin makes ER fragmented and discontinuous, compared to long tubular ER in the control group, while overexpression of atlastin promotes membrane fusion (Orso, Pegini et al. 2009). Atln-1, as an atlastin-1 ortholog in *C. elegans*, is required for tubular ER extension into dendrites. Mutant atln-1 with disturbed GTPase activity impairs tubular ER network, characterized by retraction from dendritic branches (Liu, Guo et al. 2019). In human corticospinal neurons, mutations in atlastin-1 or REEP1 result in distal axonopathy of upper motoneuron (Beetz, Schüle et al. 2008, Salinas, Proukakis et al. 2008). Moreover, it has been suggested that the highly elongated axons may be more sensitive to defective ER

morphogenesis, as the disruptions of orthologues of RTNs, atlastin and DP1/Yop1p in the same haloid yeast strain do not affect growth (Chen, Novick et al. 2012).

Within cells, continuous and interconnected ER sheets and tubules are arranged into a polygonal network, which is balanced by sliding of an ER junction along the side of a polygon until the polygon is lost (Lee and Chen 1988). In addition to proteins contributing to ER tubule formation and fusion, those proteins required for maintenance of ER at a steady state have been also investigated in detail (Chen, Novick et al. 2012). DP1 and RTNs that consist of APHs have the ability to maintain the high membrane curvature essential for the edges of ER sheets and SER tubules (Brady, Claridge et al. 2015). Lnp1p, as a member of Lunapark family, is located at the three-way junctions of ER. Instead of involvement in tubule development, Lnp1p regulates ring closure and loss of polygons of ER junctions via its interaction with RTNs, Sey1p and Yop1p, thereby stabilizing these three-way junctions (Chen, Novick et al. 2012). There are also proteins including small GTPase Rab10, Rab18, Rab3 GTPase-activating protein (Rab3GAP) complex and mitofusin-2 (MFN2) that influence the morphology of ER by influencing the balance between ER sheets and tubules to maintain ER luminal continuity (de Brito and Scorrano 2008, English and Voeltz 2013, Gerondopoulos, Bastos et al. 2014).

Changes in tubular ER distribution play important roles in diverse cellular functions, such as cellular responses to changes in Ca^{2+} concentration or ER stress (Ribeiro, McKay et al. 2000, Schuck, Prinz et al. 2009), and cellular processes including cellular division and cell motility (Bobinnec, Marcaillou et al. 2003, Hernández, Sala et al. 2006). It has been shown that myo4p mediates transport of cytoplasmic ER tubules along actin filaments into newly formed buds in budding yeast (Estrada, Kim et al. 2003, Du, Ferro-Novick et al. 2004). In animal cells, ER moves mainly along MTs, complemented by actin filaments (Waterman-Storer and Salmon 1998). Likewise, in neurons, ER movements in dendrites and axons rely on backbones provided by MTs (Farias, Freal et al. 2019). However, other studies uncovered that an actin-

based motor protein, myosin Va, is required for ER transport along actin filaments into Purkinje dendritic spines. This finding suggests the involvement of actin in ER movements in subcellular compartments (Wagner, Brenowitz et al. 2011).

In axonal growth cones, extension of ER network into the periphery is driven by dynamic ER tubules and this tubular ER can remain still highly dynamic in differentiated cells and neurons (Dailey and Bridgman 1989, Farías, Fréal et al. 2019). While ER cisternae are predominantly restricted in the somatodendritic compartment, axonal compartment harbors exclusively tubular ER. Axonal ER tubules interact with MTs, and this interaction promotes stabilization of both ER tubules and MTs in axons (Farías, Fréal et al. 2019). There are two mechanisms of ER movements along MTs, one of which is mediated by the tip attachment complex (TAC). In TAC, the protein stromal interacting molecule 1 (STIM1) and the MT-associated plus-end binding protein 1 (EB1) form a complex and connect the tip of an ER tubule to the tip of MT plus end, thus ER extends and retracts when MTs extend and retract (Grigoriev, Gouveia et al. 2008, Pavez, Thompson et al. 2019). Faster and more frequently than TAC, ER also can slide along already existing and stable acetylated MTs driven by MT motor proteins: kinesin-1 and dynein (Woźniak, Bola et al. 2009). ER sliding is independent of TAC, since ER sliding still can be detected even after nocodazole treatment that depolarizes non-acetylated MTs, or after destroying functions of STIM1 or EB1 (Terasaki, Chen et al. 1986, Waterman-Storer and Salmon 1998, Grigoriev, Gouveia et al. 2008). STIM1 serves as an ER-calcium sensor and it is required for steering growth cones towards calcium-dependent guidance cues such as BDNF and away from calcium-independent guidance cues such as semaphorin-3a (Mitchell, Gasperini et al. 2012). The steering of growth cones is mediated by the interaction of STIM1 and EB1/EB3, coupled with recruitment and organization of MT, along with which ER is remodeled to the motile side of steering growth cones (Grigoriev, Gouveia et al. 2008, Pavez, Thompson et al. 2019). Loss of both EB1 and EB3 does not impair axonal ER distribution, while knockdown of kinesin-1 or dynein disturbs ER tubules

movements along axons (Farías, Fréal et al. 2019). These findings indicate that ER sliding is more important than TAC in neuronal axons. Different ER adaptors for MTs have been identified. For example, P180 protein is a ribosome-binding protein and localizes on the ER (Savitz and Meyer 1990). This integral ER membrane protein interacts with MTs via a microtubule-binding domain (MTB1) (Ogawa-Goto, Tanaka et al. 2007). In axons, p180 is expressed in ER tubules and binds to kinesin-1, thus regulating MT remodeling (Farías, Fréal et al. 2019). A subunit of the Sec61 translocon complex, Sec61 β , which has direct interaction with MTs, localizes also to axons (Zhu, Zhang et al. 2018). Climp63 also contributes to stabilization of ER network via mediating interactions with MTs (Vedrenne, Klopfenstein et al. 2005). Additionally, ER-shaping proteins are also involved in ER tubule dynamics. For instance, REEP1, spastin and atlastin-1 coordinate interactions between MTs and tubular ER (Park, Zhu et al. 2010). Overexpression of RTN causes an increase in frequency of tubular ER fission and a reduction in retraction speed (Espadas, Pendin et al. 2019). Rab10 can be found at the leading of approximately 50% of dynamic ER tubules tracking along MTs and the tubular extension frequency and fusion efficiency are decreased by depletion of Rab10 (English and Voeltz 2013). ER-associated organelles via MCSs are also supposed to play a role in movement of ER tubules as MCSs still exist while functioning dynamically to regulate organelles' fission and fusion events, lipid metabolism and Ca²⁺ concentration (Wu, Carvalho et al. 2018).

3.1.2 Functions of axonal ER

In neurons, a physically continuous ER provides a potential platform for intra-cellular communication, including in the long axon far away from the cell body (Maday, Twelvetrees et al. 2014). Like other mammalian cells, axonal ER has conserved functions as tubular ER such as Ca²⁺ regulation, lipid metabolism and contacts with other organelles. At presynaptic terminals, ER Ca²⁺ sensor STIM1 helps to modulate presynaptic Ca²⁺ influx and exocytosis

via promoting PM Ca^{2+} uptake (de Juan-Sanz, Holt et al. 2017). In addition, ER can take up Ca^{2+} from cytosolic compartments to buffer Ca^{2+} excess via Sarcoplasmic/endoplasmic reticulum Ca^{2+} ATPase (SERCA) during repetitive firing at the presynapse (Sanyal, Consoulas et al. 2005) and it can release Ca^{2+} back to the cytosol via inositol tris-phosphate receptors (IP3Rs) and ryanodine receptors (RyRs) (Ross 2012). These Elaborate changes in presynaptic Ca^{2+} concentration play a key role in regulation of signaling events and synaptic functions. For another example, the protein multiple C2 domain and transmembrane region proteins (MCTPs) that is located in the ER membrane function to stabilize the synaptic transmission via regulating presynaptic Ca^{2+} flux (Genç, Dickman et al. 2017). The interaction between VAPs and secernin-1 (SCRN1) also can modulate Ca^{2+} homeostasis at the presynapse. Depletion of VAPs or SCRN1 is accompanied by a reduction in Ca^{2+} response evoked by action potential and impaired synaptic vesicle cycling (Lindhout, Cao et al. 2019). Beside Ca^{2+} modulation, homeostasis of lipid composition of membranes is also crucial for cellular functions. So far, there are two mechanisms that have been proved for intracellular lipid trafficking: vesicular and non-vesicular trafficking. Vesicular trafficking is required for lipid transfer to the targets that localize not close enough to the Golgi complex. Non-vesicular lipid trafficking takes place at membrane contacts between ER and other membrane-bound organelles. This non-vesicular mechanism is likely to be especially important in axons of neurons because axons are long and thin. Growing evidence shows that MCSs can serves as a non-vesicular lipid trafficking between ER and other organelles such as mitochondria, lipid droplets and plastids (Helle, Kanfer et al. 2013, Prinz 2014), as ER localizes directly in opposition to the membranes of other organelles and contacts with them via tethering proteins, instead of contacts in a fused manner (Lahiri, Toulmay et al. 2015, Dong, Saheki et al. 2016).

Even though most studies on MCSs and other subcellular organelles were performed in yeast and mammalian non-neuronal cells, ion beam-scanning electron microscopy approaches have

shown that in different neuronal compartments, ER membrane localizes in close opposition to membranes of other organelles, namely ≤ 30 nm (Wu, Whiteus et al. 2017). Furthermore, these studies show that ER-PM contacts are smaller in axons, axon terminals and dendrites than in soma and ER network engulfs mitochondria to form ER-mitochondria contact sites. Additionally, tubulovesicular structures which seem to be endosomes and lysosomes were also found to have small contact sites with the ER. In axons that have narrow dimensions, MCSs seem to play crucial roles in interorganelle communication and different cellular functions including lipid homeostasis, regulation of Ca^{2+} dynamics, control of organelle biogenesis and dynamics (Gould, Pant et al. 1983, Lim, Cho et al. 2015, de Juan-Sanz, Holt et al. 2017, Wu, Whiteus et al. 2017).

There are specialized domains found on the axonal ER membrane which are sites associated with membranes of other organelles such as mitochondria, so called mitochondria-associated membranes (MAMs) (Villegas, Martinez et al. 2014, Bernard-Marissal, Chrast et al. 2018), which were rarely studied because these axonal MAMs were difficult to be visualized technically. MAMs were first observed in 1956 using electron micrographs of the rat liver (Bernhard and Rouiller 1956) and later characterized using biochemical assays (Wieckowski, Giorgi et al. 2009), fluorescent microscopy (Tsukita and Ishikawa 1976, Merianda and Twiss 2013) and in situ proximity ligation assays (Bernard-Marissal, Médard et al. 2015). The intermembrane distance of MAMs is defined as 10 to 30 nm (Herrera-Cruz and Simmen 2017), with around 15 to 20% of mitochondria connected to the ER (Rizzuto, Pinton et al. 1998). Specific proteins are required for the architecture and maintenance of MAMs. The tethering complex of the ER membrane protein vesicle-associated membrane protein-associated protein B (VAPB) and mitochondrial protein tyrosine phosphatase-interacting protein 51 (PTPIP51) mediate MAM connections at presynaptic compartments and these connections are reported important for synaptic functions, since loss of VAPB or PTPIP51 leads to a reduction in synaptic activity (Gómez-Suaga, Pérez-Nievas et al. 2019). PDZD8 is

an ER protein that is also present at MAMs in neurons, and PDZD is required for cytosolic Ca^{2+} regulation after synaptically induced Ca^{2+} release from ER via involvement in Ca^{2+} uptake by mitochondria (Hirabayashi, Kwon et al. 2017). In injured sciatic nerve explants, modulation of Ca^{2+} exchange between ER and mitochondria protects against axonal degeneration (Villegas, Martinez et al. 2014). The importance of MAMs in axons can be additionally addressed by the axonal degeneration caused by mutations in the MAM-associated proteins Sigma 1 receptor (SIGMAR1) (Bernard-Marissal, Médard et al. 2015) and MFN2 (Misko, Sasaki et al. 2012). After inactivation of SIGMAR1, cultured primary motoneurons suffer from axonal degeneration prior to cell death (Bernard-Marissal, Médard et al. 2015). Mutant MFN2 disrupts mainly mitochondrial positioning in axons and causes a reduction in the number of MAMs, resulting in segmental axonal degeneration, but without death of cell bodies (Misko, Sasaki et al. 2012). MAMs also regulate mitochondrial dynamics via mediating mitochondrial fusion and fission events (Hoppins, Lackner et al. 2007). In more detail, ER tubules first contact mitochondria and define constriction sites, followed by the recruitment of dynamin related protein 1 (Drp1) that forms helices around mitochondria to perform division (Friedman, Lackner et al. 2011). The balance of fission and fusion of mitochondria mediated by MAMs also requires regulation of lipid composition. Enzymes essential for mitochondrial lipids are enriched at MAMs, suggesting that MAMs serve as sites for lipid exchange between mitochondria and ER to support fission and fusion events of mitochondria (Steenbergen, Nanowski et al. 2005, Tasseva, Bai et al. 2013, Vance 2014).

Other relatively well studied MCSs in axons are ER-PM MCSs. In axons, approximately 0.5 to 1 % of the PM surface have contacts with ER (Wu, Whiteus et al. 2017). These MCSs provide channels for exchange of lipid and Ca^{2+} between ER and PM via different specific proteins (Saheki and Camilli 2017). In hippocampal neurons, Kv2 ion channels are localized at ER-PM junctions, juxtaposed to clusters of ER receptors RyRs, which induce the formation of these specialized MCSs (Fox, Haberkorn et al. 2015, Kirmiz, Palacio et al. 2018). In

medium spiny neurons of the striatum, the juxtaposed Kv2.1: RyR clusters are associated with regulation of local Ca²⁺ concentration (Mandikian, Bocksteins et al. 2014). Another study has shown that, Cav1, RyRs and KCa3.1 channels form a complex and this complex colocalizes with junctophilin 3 and 4 (JPH3 and JPH4) proteins. These Cav1-RyR2-KCa3.1 complexes tether ER-PM contact sites and contribute to a slow afterhyperpolarization (sAHP) that controls the excitability of CA1 hippocampal pyramidal cells (Sahu, Wazen et al. 2019). Disconnection of the Cav1-RyR2-KCa3.1 complex caused by short hairpin RNA (shRNA) reduces the amplitude of the sAHP current (IsAHP), indicating that this complex as well as JPH 3 and JPH4 proteins are required for calcium modulation between different sources to regulate neuronal activity (Sahu, Wazen et al. 2019). Similar to MAMs, ER-PM MCSs also contribute to lipid transfer between ER and PM, that is facilitated by lipid metabolic enzymes (Lauwers, Goodchild et al. 2016). ER-endosome MCSs are mediated by VAP and lipid binding proteins that allow exchange of lipids such as cholesterol or phospholipids (Eden 2016). Vacuolar protein sorting-associated protein 13A (VPS13A) and 13C (VPS13C) tether ER to late endosomes/lysosomes and lipid droplets (Kumar, Leonzino et al. 2018). These proteins serve as a lipid transporter between ER and other organelles. However, it has not been shown whether lipid transfer between ER and endosomes occurs (Kumar, Leonzino et al. 2018).

In neurons, RER is the major site for protein synthesis, folding, processing and secretion and it appears mainly restricted in the somatodendritic compartment (Horton and Ehlers 2003, Shibata, Shemesh et al. 2010, West, Zurek et al. 2011, Puhka, Joensuu et al. 2012, Lee, Cathey et al. 2020). Function of axonal ER in local translation still remains elusive because pioneering electron microscopy (EM) studies of the axonal ER did not reveal RER (Lasek, Dabrowski et al. 1973, Tsukita and Ishikawa 1976, Krijnse-Locker, Parton et al. 1995), even though there are lines of evidence from other methodologies supporting this possibility, including abundant axonal transcripts for transmembrane proteins (Willis, van Niekerk et al.

2007, Taylor, Berchtold et al. 2009, Zivraj, Tung et al. 2010, Younts, Monday et al. 2016), presence of ribosomes and translational machinery components (Steward and Ribak 1986, Kun, Otero et al. 2007, Kalinski, Sachdeva et al. 2015) and the secretory machinery (González, Cánovas et al. 2016).

3.1.3 ER in neurodegenerative diseases

As ER has crucial roles in lipid metabolism, calcium regulation and organelle homeostasis, its dysfunction could change physical properties of the cells and disturb essential cellular processes, leading to disease pathology of cells. In neurons, the long projection of axons from cell bodies poses great challenge for ER to keep its continuity and dynamics throughout the axon, making axonal compartment more vulnerable to ER dysfunction and more susceptible to degeneration and axonopathy in different disease associated contexts.

The first well known ER-associated disease is Hereditary Spastic Paraplegias (HSPs). HSPs are a group of genetically heterogeneous neurodegenerative diseases and characterized by progressive degeneration of upper motoneurons. The major symptoms are weakness and spasticity of lower limbs, which is accompanied by additional symptoms such as peripheral neuropathy, cerebellar ataxia and optic atrophy in complicated cases, (Bellofatto, De Michele et al. 2019). Among 79 known spastic gait genes that are responsible for HSPs (Parodi, Coarelli et al. 2018), the ER-shaping proteins spastin, REEP1 and atlastin were found in around 50 % of the patients. The main impairment of lower limbs is due to selective degeneration of distal axons of the corticospinal tracts, indicating the importance of ER shaping in axonal maintenance (Boutry, Morais et al. 2019). Autosomal dominant mutations in the spastin-encoding gene termed as SPAST/SPG4 are the most common cause of HSPs, found in up to 40% of autosomal dominant HSP families (Blackstone, O'Kane et al. 2011). Spastin, a MT-severing protein, together with atlastin, regulates ER and MT rearrangement near growing axon tips after nerve injury, thereby contributing to axon regeneration. Decrease

in spastin levels causes a deficit in axon regeneration (Rao, Stone et al. 2016). At ER-endosome membrane contacts, spastin interacts with the ESCRT protein IST1 and they help to drive fission of endosomal tubules (Allison, Edgar et al. 2017). Fission of endosomal tubules and sorting receptors such as the transferrin receptor (TfnR), low-density-lipoprotein receptor (LDLR) and cation-independent mannose 6-phosphate receptor (CI-MPR) determine the fate of transmembrane proteins and growth factor receptors that are carried by endosomes (Maxfield and McGraw 2004, Huotari and Helenius 2011, Gautreau, Oguievetskaia et al. 2014). Primary cortical neurons obtained from a spastin-HSP mouse model bear defective sorting of mannose 6-phosphate (M6PR) and impaired lysosomal morphology, suggesting that the function of spastin in endosomal fission affects lysosome functions (Allison, Edgar et al. 2017). The same results have been observed in induced pluripotent stem cells (iPSCs)-derived neurons from patients diagnosed with spastin-HSP, as well as in SPG4 (spastin)-HSP patients-derived fibroblast lines (Denton, Lei et al. 2014, Allison, Edgar et al. 2017). In corticospinal neurons, REEP1 is also involved in modulating ER shaping and MT dynamics (Park, Zhu et al. 2010). Knockout of REEP1 leads to defects in neurite outgrowth and degeneration (Lim, Cho et al. 2015). The presence of REEP1 at MAMs also indicates that mitochondrial impairment caused by defective Ca^{2+} metabolism via MCSs could play an important role in axonopathy in patients diagnosed with HSPs (Lim, Cho et al. 2015). HSP-associated proteins also contain proteins that localize on the ER or have an influence on the ER morphogenesis such as ARL6IP1, Rab3GAP2 (Novarino, Fenstermaker et al. 2014), REEP2 (Esteves, Durr et al. 2014) and seipin (Windpassinger, Auer-Grumbach et al. 2004). Therefore, mutations in HSPs affect not only ER remodeling itself but also its contacts with other organelles, causing defective function of neurons, especially in long axons.

Alzheimer's disease (AD) is one of the most common neurodegenerative diseases. The pathological hallmarks of AD consist of extracellular deposits of β -amyloid plaques, intracellular tau protein tangles, dystrophic neurites (DNs) and mitochondrial dysfunction

(Serrano-Pozo, Frosch et al. 2011, DuBoff, Feany et al. 2013). Neurite plaques contain amyloid deposits surrounded by DNs and reactive gliosis (Prior, Shi et al. 2010). Reticulon 3 (RTN3) occurs in neurite plaques and regulates the formation of amyloid deposits and DNs via negative modulation of beta-secretase 1 (BACE1) and via the formation of RTN3, respectively. Overexpression of RTN3 in transgenic mice (Tg-RTN3 mice) promotes DNs in the brain (Prior, Shi et al. 2010, Sharoar, Shi et al. 2016). Ultrastructural analysis of fixed hippocampal samples obtained from Tg-RTN3 mice revealed clusters of curvier and shorter tubular ER in the axonal region at the age of 3 months and further the remarkable accumulation of tubular ER and altered ER morphology in terminals of axons surrounding amyloid plaques at the age of 11 months, compared to non-transgenic mice that did not show clustered tubular ER formation (Sharoar, Shi et al. 2016). Using ultrastructural approaches abnormal tubular ER aggregates were also detected in brains of patients diagnosed with AD (Sharoar, Shi et al. 2016). Furthermore, it was found that mitochondria were remarkably smaller near clustering of tubular ER in the brain of the Tg-RTN3 mice at the age of 3 months and became even barely visible at the age of 11 when the clusters were more remarkable. The quantification of size and number of mitochondria indicates increased fission of mitochondria induced by clustered tubular ER in the early stages of DN formation and mitochondrial degeneration at later stages. The same group also performed immunostaining against different proteins together with staining against RTN and found that RTN-immunoreactive DNs are colocalized with tubular ER shaping proteins including REEP2 and REEP5, while not co-immunostained with other ER proteins such as disulfide isomerase, DP1, calnexin and not colocalized with ER stress-associated proteins such as activating transcription factor-6 (ATF-6), inositol-requiring enzyme 1 (IRE1) and glucose-related protein 78 (GRP78) that are enriched in ER cisternae. After depletion of RTN3, RTN-immunoreactive DNs disappeared in aging and AD mouse models (Sharoar, Shi et al. 2016). Thus, irregular pathogenic tubular ER

clusters in brains cause disturbed mitochondrial integrity, DNs formation and impaired cognitive function (Sharoar, Shi et al. 2016).

Amyotrophic lateral sclerosis (ALS) is a fatal neurodegenerative disease with death of upper and lower motoneurons, leading to progressive weakness and atrophy of muscles. Even though half of the familial cases are caused by mutations influencing superoxide dismutase 1 (SOD1), TAR DNA-binding protein 43 (TDP43), fused in sarcoma (FUS) and chromosome 9 open reading frame 72 (C9ORF72) genes, a mutation in vesicle-associated membrane protein-associated membrane protein B (VAPB) was also found in patients diagnosed with typical severe ALS, ALS8 and late-onset SMA (Nishimura, Mitne-Neto et al. 2004). VAPs interact with target lipid binding proteins that carry a two phenylalanine-containing short motif in an acidic tract (FFAT motif) to the cytosolic surface of ER. The mutant P56S in VAPB is related to motoneuron degeneration in ALS diagnosed patients. It has been shown that VAPB is enriched in motoneurons and the substitution of P56S generates mutant VAPB aggregates in immobile clustered tubular ER, therefore interrupting FFAT motif binding and immobilizing endogenous VAP in mutant aggregates. Reduction in expression of VAPA and VAPB was found in human ALS patients and this reduction could contribute to the pathogenesis since in a mouse model with reduced levels of VAPs, lipid binding proteins were found less anchored in ER, and VAPs-deficient motoneurons suffered from degeneration (Teuling, Ahmed et al. 2007). There are other ER-associated proteins contributing to ALS such as BCL2 interacting protein 1 (BNIP1), Sigma-1 receptor (SigR1) and Ataxin-2. BNIP1 mediates ER membrane fusion and organizes the ER network (Nakajima, Hirose et al. 2004). SigR1, a ligand-operated receptor chaperon that is calcium sensitive, forms a complex at MAMs with another chaperon, binding immunoglobulin protein (BiP), to regulate Ca^{2+} exchange between ER and mitochondria via IP3Rs (Hayashi and Su 2007). Ataxin-2 is a RNA-binding protein that is essential for morphogenesis and dynamics of tubular ER (del Castillo, Gnazzo et al. 2019). Analysis of 6 ALS patients and 3 neurologically normal control groups have found

mislocalization of ataxin-2 in spinal cord neurons of the patients. Moreover, genomic DNA analysis of 915 ALS patients and control groups have revealed that an intermediate-length CAG expansion that encodes a polyglutamin (polyQ) stretch in ataxin-2 gene is significantly related to ALS (Elden, Kim et al. 2010). Furthermore, VAPA and VAPB proteins are expressed less in ALS patients and SOD1-ALS mice. VAPA and VAPB are shown to be involved in maintenance of proper ER morphology and synaptic vesicle (SV) cycling regulation (Lindhout, Cao et al. 2019).

Parkinson's disease (PD), characterized by tremor, rigid muscles, bradykinesia and postural abnormalities, is caused by genetic and environmental factors, leading to loss of dopaminergic neurons in the substantia nigra with accumulation of α -synuclein in Lewy bodies as hallmark pathologies (Spillantini, Schmidt et al. 1997). Disease-associated mutant genes contain SNCA encoding α -synuclein and Pten-induced putative kinase 1 (Pink1). It has been shown that Pink1 mutations disturb mitochondrial activity (Marongiu, Spencer et al. 2009). Infected with viral-derived Pink1, neuronal cell models of PD present enhanced intracellular calcium concentration and exacerbated alterations in mitochondrial activity promoted by mutant α -synuclein (A53T) (Marongiu, Spencer et al. 2009). Co-expression of mutant Pink1 and mutant α -synuclein changes mitochondrial morphology and neurite outgrowth, severer than that of expressing either mutant Pink1 or mutant α -synuclein (Marongiu, Spencer et al. 2009). This alteration could be completely restored by application of Ruthenium, a calcium influx blocker for mitochondria, while other calcium blockers only partially or rarely rescued mitochondrial morphology (Marongiu, Spencer et al. 2009). In familial PD patient iPSC-derived neurons which harbor a mutation in the α -synuclein gene, VAPB-PTPIP51 complex that interacts with α -synuclein and forms a scaffold to tether ER and mitochondria in control groups was, however, disturbed and impaired ER-mitochondria contacts (Paillusson, Gomez-Suaga et al. 2017). The disruption in ER-mitochondria contacts could cause defects in exchange of Ca^{2+} between these two organelles and lead to neuronal damage in PD. Another gene, MFN2,

could also be linked to ER functions via mediating ER-mitochondria physical contact, since loss of MFN2 in dopaminergic neurons causes disrupted localization of Parkin that mediates mitophagy occurring at ER-mitochondria contacts and axonal loss (Tanaka, Cleland et al. 2010, Böckler and Westermann 2014, Puri, Cheng et al. 2019). Moreover, sleep disorder is one of the PD symptoms and this disorder has been found in patients, parkin and pink1 PD models as well as in patient iPSCs differentiated hypothalamic neurons. In these PD models, there were excessive ER-mitochondria contacts that cause abnormal lipid trafficking, resulting in depletion of phosphatidylserine from ER. This sleep disorder can be rescued by feeding mutant animals with phosphatidylserine, suggesting the sleep problem in PD can be explained by excessive ER-mitochondria contacts (Valadas, Esposito et al. 2018).

3.2 Local translation in neurons

Neurons are spatially highly compartmentalized with multiple dendrites, a long axon and specialized synapses. In these specialized synapses, signals from other cells are received, processed and stored, and corresponding information is sent out to other cells. These functions provide a network for information transmission. While most proteins in subcellular compartments are transported from the cell body, some specific subtypes of proteins are locally translated in response to extracellular signals. First, factors required for protein synthesis such as different transcripts supplied as translation template and ribosomes serving as the translational machinery were both detected in axons and synapses in different studies (Cajigas, Tushev et al. 2012, Saal, Briese et al. 2014, Shigeoka, Jung et al. 2016, Hafner, Donlin-Asp et al. 2019). Second, neuronal processes physically isolated from cell bodies were detected capable of protein synthesis induced by different triggers, which provides more evidence to support the presence of protein synthesis in neuronal processes (Martin, Casadio et al. 1997, Kim and Martin 2015).

Additional posttranslational machineries that consist of ER, the Golgi apparatus, the trans-Golgi network and ER-Golgi intermediate compartment (ERGIC) are needed for folding, assembly and glycosylation of secreted and membrane proteins before these proteins are delivered to their destinations. While ER has been detected in axons and dendrites (Gardiol, Racca et al. 1999, Merianda, Lin et al. 2009), the conventional Golgi apparatus is considered to be not available in neuronal processes even though some Golgi components are detected in dorsal root ganglion (DRG) axons such as trans-Golgi network protein 38 (TGN38) and Golgi matrix protein 130 (GM130) and sparse small Golgi outposts have also been observed at postsynaptic compartments of hippocampal neurons (Hanus and Ehlers 2008, Merianda, Lin et al. 2009). However, an unconventional highly core-glycosylation of surface membrane proteins was uncovered in neuronal processes, which is related to immature intracellular proteins. This glycosylation pattern is different from N-glycosylation in other cells. This unclassical glycosylation can be due to a bypass or hypo-function of the Golgi apparatus (Hanus, Geptin et al. 2016).

3.2.1 Roles of local translation in neurons

The detection of transcripts and translation machineries in neuronal processes and successful visualization of local protein synthesis in dendrites and distal axons (Dahm, Zeitelhofer et al. 2008) raise up the question about the function of local translation in neuronal development, survival and plasticity. During development, neurons extend their axons that navigate over long distances to reach their postsynaptic targets. The specialized tips of growing axons are named growth cones and they contain specific groups of cellular messenger ribonucleic acids (mRNAs), ribosomes and other translational machinery-like structures (Bunge 1973, Bassell, Zhang et al. 1998, Kun, Otero et al. 2007, Zivraj, Tung et al. 2010). In response to axonal guidance cues, specific mRNAs are rapidly translated in sub-regions of the growth cone; consequently, the growth cone undergoes morphological changes that enable it to turn

towards the attractive signals but away from the repulsive cues to ensure that the axon moves along the correct path (Jung, Yoon et al. 2012). For example, netrin 1 and BDNF induce redistribution of β -actin mRNAs to the region of growth cones near the cues and induce asymmetrical translation of β -actin, leading to steering towards them (Leung, van Horck et al. 2006, Yao, Sasaki et al. 2006). Conversely, factors such as Semaphorin 3A (Sema3A) and Slit2 trigger protein production of Ras homolog family member A (RHOA) and cofilin that depolymerize actin filaments, resulting in collapse of growth cones and repulsion (Wu, Hengst et al. 2005, Piper, Anderson et al. 2006). Without cell bodies, growth cones can still respond to guidance signaling in vitro (Ming, Wong et al. 2002). Factors such as netrin-1 and nerve growth factor (NGF) increase the rate of axonal elongation by stimulating local translation of a cytoskeleton regulator Par complex and thus promoting axon outgrowth (Goldstein and Macara 2007, Hengst, Deglincerti et al. 2009). Once axons reach their targets, they start to form branches and growth cones transform into presynaptic terminals. Synapse formation alters mRNA localization and regulates translation at synapses. mRNA that encodes the neuropeptide sensorin localizes at synapses in isolated *Aplysia* sensory neurons only when they are cultured together with their targeting motoneurons and form synapses. Reduction of sensorin mRNA using dsRNA inhibits synapse formation, indicating that mRNAs also influence synapse formation (Lyles, Zhao et al. 2006). This suggests that specific protein synthesis at synaptic sites could contribute to synapse formation. Furthermore, Fragile X mental retardation protein (FMRP) regulates metabotropic glutamate receptors (mGluRs)-stimulated protein synthesis and in turn regulates protein synthesis-dependent synaptic plasticity. In Fragile X syndrome (FXS) mental retardation patients, loss of function of FMRP impairs dendritic spine structure and mGluRs-induced synaptic plasticity (Ronesi and Huber 2008). In brain slices from mosaic mouse models of FXS it was found that lack of synaptic functional regulator (*Fmr1*) expression lessened the formation of synaptic connections at presynaptic terminals (Hanson and Madison 2007). Up to 200 μ m, a

single axon can form around up to 50,000 synapses. At the axonal bouton, scaffolding and regulatory molecules, synaptic vesicles containing neurotransmitter and other organelles coordinate to regulate and promote neurotransmitter release. Metabolism of neurotransmitters at synapses is regulated by different enzymes such as tyrosine hydroxylase that regulates catecholamine biogenesis and acetylcholinesterase (AChE) that degrades acetylcholine. mRNA encoding tyrosine hydroxylase was detected in catecholamine terminal regions (Melia, Trembleau et al. 1994). Additionally, oxytocin and vasopressin mRNAs were also detected in the neurohypophysis using different methods, suggesting that in nerve terminals neuropeptide and hormones might also be produced locally (Jirikowski, Sanna et al. 1990, Mohr, Fehr et al. 1991, Trembleau, Melia et al. 1995, Trembleau, Morales et al. 1996, Jung, Yoon et al. 2012). At neuromuscular synapses of *Xenopus*, potentiation of synaptic transmission that is induced by neurotrophin-3 (NT3) requires protein synthesis at presynapses (Lohof, Ip et al. 1993, Yang, He et al. 2001, Je, Ji et al. 2011).

Axonal protein synthesis is crucial for cellular survival and axon maintenance via regulating different signaling pathways as well as promoting mitochondrial function. For example, in sensory axons, mRNA encoding the cAMP-responsive element (CRE)-binding protein (CREB) is locally translated upon NGF application and the produced proteins are retrogradely transported into the cell body. These proteins are required for survival since a deficiency in axonal CREB mRNA translation destroys NGF promoted survival of sensory neurons (Cox, Hengst et al. 2008). In addition, transcripts encoding different mitochondrial proteins or mitochondrial function associated proteins were also detected in axons (Gioio, Eyman et al. 2001, Hillefors, Gioio et al. 2007, Saal, Briese et al. 2014). For instance, en1, a target-derived cue, can induce local translation of lamin B2 and nuclear-encoded mitochondrial protein, thus sustaining mitochondrial function and neuronal survival (Alvarez-Fischer, Fuchs et al. 2011, Yoon, Jung et al. 2012). A neuropathic disorder Charcot-Marie-Tooth disease type 2, characterized by chronic axonal degeneration, is caused by mutations in lamins or

mitochondrial proteins (Capell and Collins 2006, Pareyson and Marchesi 2009). Interestingly, axonal synthesis is decreased in mature neurons; but after injury, the protein synthesis is increased again during the regeneration process (Tobias and Koenig 1975, Gummy, Tan et al. 2010). One important pathway for regeneration is mammalian target of rapamycin (mTOR) pathway. It has been shown that mTOR mRNAs localize into axons and their translation is induced at the injured site of the axon. In the meantime, the locally translated mTOR upregulates its own translation, thereby promoting the regeneration. When mTOR 3'UTR is depleted in mice to reduce the axonal mRNA levels, the local translation of mTOR is decreased after nerve injury. Furthermore, mTOR 3'UTR depletion or pharmacological inhibition of mTOR in axons causes a reduction in proprioceptive neuronal survival after nerve injury (Terenzio, Koley et al. 2018).

3.2.2 Regulation of local translation

Proteins used as sensors and effectors in neuronal processes have a limited half-life and constantly undergo degradation and synthesis in a precisely coordinated manner. The precise regulation of the local translation is critical for cellular functions. Some cellular cues such as NGF, BDNF and netrin1 increase protein production locally. For example, upon BDNF binding to its receptor tropomyosin receptor kinase B (TrkB), signaling pathways including the phosphatidylinositol 3-kinase (PI3K) pathway, Ras/ERK (extracellular signal-regulated protein kinase) pathway and the phospholipase C γ (PLC γ) pathway are activated in parallel (Manadas, Santos et al. 2009). Parts of these signaling pathways modulate sub-compartmental proteome via modulating initiation and elongation steps, the rate-limiting steps for translation (Takei, Inamura et al. 2004, Esvald, Tuvikene et al. 2020). In cultured cortical neurons, mTOR, ERK and PI3K downstream cascades have been shown to be involved in this regulation (Takei, Kawamura et al. 2001). For translational initiation, three subunits of eukaryotic initiation factors (eIFs): eIF4G, eIF4E and eIF4A first form the eIF4F complex and

this complex connects ribosomes to the mRNA. Components of eIF4F perform different functions: eIF4G connects the mRNA to the 43S pre-initiation complex, eIF4E binds to 5' capped mRNAs and eIF4A changes the secondary structures of mRNA. eIF4E-binding proteins (4EBPs) regulate assembly of eIF4F by changes between non-phosphorylated and phosphorylated forms. Non-phosphorylated 4EBPs bind to eIF4E and suppress translation, while phosphorylation of 4EBPs releases eIF4E, promotes formation of eIF4F complexes and activates the translation. After initiation, elongation factors including the eukaryotic elongation factor 2 (eEF2) are recruited for the elongation step. eEF2 is required for translocation of the nascent protein chain from the A-site to the P-site of the ribosomes and this step is GTP-dependent. BDNF promotes the phosphorylation of 4EBP1 that binds to eIF4E in a non-phosphorylated form. This BDNF-induced phosphorylation of 4EBP1 is blocked by chemical inhibitors of the PI3K and ERK signaling pathways, respectively. The phosphorylation of 4EBP1 is also shown to be mediated by the activation of the mTOR pathway (Takei, Inamura et al. 2004). In addition, BDNF also increases the rate of protein synthesis via regulating the elongation step by upregulation of the active and non-phosphorylated eukaryotic elongation factor 2 (eEF2) in cerebral cortex of BDNF transgenic mice, which is however controversial in BDNF knockout mice (Takei, Kawamura et al. 2009). This BDNF-induced decreased eEF2 phosphorylation is abolished with rapamycin that blocks mTOR pathway (Inamura, Nawa et al. 2005). Another mechanism of BDNF-regulated protein synthesis at synapses is related to the selective targeting of mRNAs to dendrites such as transcripts for translational machinery components (Poon, Choi et al. 2006, Manadas, Santos et al. 2009).

Additionally, there is also evidence to suggest that guidance cues may directly regulate ribosomes. It has been shown that a netrin 1 receptor, deleted in colorectal carcinoma (DCC), binds directly to the 60S ribosomal subunit component ribosomal protein L5 (RPL5) (Koenig, Martin et al. 2000, Tcherkezian, Brittis et al. 2010). Cytoskeleton is as well supposed to be

involved in the spatial organization and regulation of translation (Kim and Coulombe 2010). Axonal transcriptome analyses from diverse neurons have identified thousands of different mRNAs in their axons (Taylor, Berchtold et al. 2009, Andreassi, Zimmermann et al. 2010). Axonal transcriptomes change dynamically during development, which suggests that axons may recruit specific and biologically relevant mRNAs using active transport. Some mRNAs were specifically enriched in some cell types (Gumy, Yeo et al. 2011).

The cis-acting and trans-acting elements also participate in local translation regulation. The cis-acting elements that mostly localize in 3'UTR are responsible for mRNA transport into distinct subcellular compartments which determines local translation of specific subsets of transcripts. These cis-acting elements can be regulated by extracellular factors such as BDNF, NT3 and NGF via distinct downstream signals (Willis, van Niekerk et al. 2007). For instance, BDNF, netrin1 and en1 all induce global protein synthesis, but only BDNF and netrin1 can induce translation of β -actin mRNA in axons of *Xenopus laevis* retina (Leung, van Horck et al. 2006, Yao, Sasaki et al. 2006, Yoon, Jung et al. 2012). In contrast to protein synthesis promoting factors, there are also factors that can suppress translation of specific mRNAs (Yoon, Jung et al. 2012). Trans-acting elements help specific mRNAs to form RNA granules reversibly, thus regulating mRNA stability, transport and translation (Kiebler and Bassell 2006). RNA-binding proteins (RBPs) and microRNAs, as components of RNA granules are present in axons and growth cones and their localization can be modulated by different cues. Zipcode binding protein 1 (ZBP1) binds to the 3'UTR of β -actin mRNA to suppress its translation. When the ZBP1-RNA complex arrives at its destination, it can be activated by factors such as BDNF. Upon activation, the protein kinase Src phosphorylates ZBP1 and consequently induce β -actin synthesis (Hüttelmaier, Zenklusen et al. 2005, Chao, Patskovsky et al. 2010, Sasaki, Welshhans et al. 2010). FMRP, as another RBP that is detected in axons and growth cones, recognizes and represses the translation of its target mRNAs via binding to them. This repression is relieved upon neuronal activity that leads to dephosphorylation of

FMRP by protein phosphatase 2A (Narayanan, Nalavadi et al. 2008, Melko and Bardoni 2010). As another group of trans-acting factors, microRNAs repress the protein synthesis of target mRNAs in RNA granules in a sequence-specific manner (Wu, Hengst et al. 2005, Schratt, Tuebing et al. 2006). For example, miR-338 is approved to inhibit axonal translation of mRNAs encoding components of mitochondrial complexes cytochrome c oxidase subunit 4 isoform 1 (COX4I1) and ATP synthase lipid-binding protein (ATP5G1) (Hillefors, Gioio et al. 2007, Aschrafi, Schwechter et al. 2008).

3.3 Spinal Muscular Atrophy

Spinal muscular atrophy (SMA) is caused by loss or mutation of the survival motor neuron 1 (SMN1) gene which results in low expression levels of its protein product survival motor neuron (SMN) (Burghes and Beattie 2009). SMA is characterized by degeneration of spinal motoneurons and atrophy of muscles (Crawford and Pardo 1996, Jablonka and Sendtner 2003, Burghes and Beattie 2009). SMN is a part of SMN complex that plays a role in the assembly of small nuclear ribonucleoproteins (snRNPs) that are crucial for pre-mRNA splicing via recognizing and removing introns from pre-mRNA in the nucleus (Pellizzoni, Yong et al. 2002). Each snRNP consists of a small nuclear RNA (snRNA), several Sm proteins and a variety of specific proteins. SMN complex is required for mediating the ATP-dependent assembly of the core of seven Sm proteins on uridine-rich, small nuclear ribonucleic acids (U snRNAs) (Pellizzoni, Yong et al. 2002). Experiments performed *in vitro* demonstrate that the SMN complex functions as an essential factor for correct assembly of Sm proteins on U snRNA and specific binding of Sm cores assembly on RNA targets to prevent unspecific binding with other RNAs (Pellizzoni, Yong et al. 2002). Another important function of SMN protein is proposed to regulate axonal RNA metabolism as SMN localizes in transport

granules in axons and interacts with a number of mRNA-binding proteins that do not participate in splicing regulation (Fallini, Bassell et al. 2012).

So far, there are two main hypotheses about how low expression of SMN protein causes SMA. One hypothesis proposes that loss of SMN affects the ability of snRNP in splicing via altered snRNP assembly, while another one states that the transport of mRNA that is regulated by SMN into subcellular compartments such as axons is disrupted (Liu, Fischer et al. 1997, Pellizzoni, Charroux et al. 1999, Paushkin, Gubitza et al. 2002, Rossoll, Jablonka et al. 2003, Wan, Battle et al. 2005, Eggert, Chari et al. 2006, Saal, Briese et al. 2014). In addition to these two mechanisms, intra-axonal protein synthesis and altered actin dynamics also contribute to SMA (Kye, Niederst et al. 2014, Moradi, Sivadasan et al. 2017). A direct interaction between SMN and F-actin has not been confirmed yet, but there is growing evidence that supports the connection between SMN and actin filaments. Profilin is a regulator of actin dynamics via promoting actin assembly, thus regulating neuronal motility and transport processes and modulating synaptic function (Hensel and Claus 2017). G/F-actin ratio is increased in motoneurons obtained from SMA mice but not in primary fibroblast cell lines from SMA patients. This altered G/F-actin ratio is caused by hyper-phosphorylation of profilin2 that affects the link between SMN and the Rho-associated protein kinase (ROCK) pathway (Nölle, Zeug et al. 2011). Profilin2, a neuronal specific isoform of profilin, is predominantly expressed in nerve tissues and interacts directly with SMN *in vivo* (Nölle, Zeug et al. 2011). In SMA patients with S230L mutations, it has been shown that interaction between SMN and profilin2 is reduced. This reduced interaction results in increased targeting of profilin2 to ROCK regulation and thus hyperphosphorylation of profilin2 (Nölle, Zeug et al. 2011). ROCK coordinates the activity of an actin regulatory network containing profilins and phosphorylates actin-based molecules cofilin and myosin II. Cofilin regulates the balance between F-actin and G-actin and increases the dynamics of filament assembly via severing actin filaments (Pavlov, Muhrad et al. 2007). F-actin severing increases polymerization of

readily usable ATP-G-actin and increases barbed (+) ends. However, without an enhancement in actin recycling, increase in cofilin activity results in filament breakdown with less F-actin (Pavlov, Muhrad et al. 2007, Gomez and Letourneau 2014, Hosseinibarkooie, Peters et al. 2016). In presynaptic terminals of a SMA mouse model, immunostaining showed that fluorescence signals of F-actin was much less than that of heterozygote control group and overexpression of Plastin3 (PLS3) rescued the F-actin levels (Ackermann, Kröber et al. 2013). In Zebrafish, SMN depletion leads to a significant decrease in PLS3 levels (Hosseinibarkooie, Peters et al. 2016), however in severe SMA mouse models the expression levels of PLS3 are not altered (Ackermann, Kröber et al. 2013). *In vivo* it has been shown that PLS3 associates with SMN in the mouse spinal cord, but an *in vitro* pull-down assay did not detect direct interaction between these two proteins (Oprea, Kröber et al. 2008). Moreover, triple labeling of primary murine motoneurons with antibodies have found colocalization of endogenous PLS3 with SMN in axons and they also accumulate at F-actin enriched growth cones (Oprea, Kröber et al. 2008). Upregulation of PLS3 expression rescued the defects in axon length and outgrowth defects caused by loss of SMN in motoneurons from SMA mouse models (Oprea, Kröber et al. 2008).

3.4 Aim of the present study

Mechanisms underlying ER dynamic remodeling and the importance of maintaining its remodeling are intensively studied in mammalian cells. ER-shaping proteins, MTs and MCSs have been shown to play critical roles in shaping ER structure, regulating ER dynamics and maintaining interactions between ER and other organelles. In neurons, axonal ER is composed of tubular ER that is mainly involved in calcium storage, lipid metabolism and contacts with other organelles. The interaction of axonal ER and actin filaments and its role in local translation in distal axon terminals of motoneurons are poorly understood. Rapid and

precise regulation of protein synthesis in axonal growth cones is essential for diverse cellular functions, especially cellular responses to different cues. The fast and slow axonal transport for replenishing proteins in subcellular compartments have been extensively studied, but local translation especially in axonal growth cones, the dynamics of BDNF-induced ribosome assembly and the interaction between ribosomes and ER still need to be investigated. Furthermore, an important question one would need to answer refers to the alterations in ER dynamics and its interaction with ribosomes in the context of SMA motoneurons, and how these changes contribute to axonopathy in SMA.

The aim of this study was to investigate the mechanisms of ER dynamic regulation in distal axons of motoneurons and its function in local translation, as well as dynamics of translational machinery (ribosomes) and its interaction with ER induced by extracellular BDNF stimulation in distal axons of cultured wildtype (WT) and *Smn*-deficient motoneurons.

4. Materials and Methods

4.1 Materials

4.1.1 Animals

The used SMA mouse model is a transgenic mouse expressing two copies of the human *SMN2* gene, mated onto a mouse null *SMN*^{-/-} background, resembling a severe type I SMA in humans (Monani, Sendtner et al. 2000). TrkB knockout (KO) mice (Rohrer, Korenbrot et al. 1999) were obtained from the University of California, Davis (MMRRC: 000188, B6; 129S4-Ntrk2 < tm1Rohr >) and maintained on a C57B1/6 background. CD1 mice (Charles River) were used for motoneuron cell cultures from WT mice. All mice were housed in the animal facility of the Institute of Clinical Neurobiology, University Hospital of Wuerzburg. All mouse procedures were performed according to the regulations on animal protection of the

German federal law and of the Association for Assessment and Accreditation of Laboratory Animal care, approved by the local authorities

4.1.2 HEK^{293T} and NSC34 cell Lines

Human embryonic kidney HEK^{293T} cells (System Biosciences, 293TN producer cell line) were used to produce lentiviral particles, validate the expression of constructed plasmids. Mouse motor neuron-like hybrid cell line NSC34 (tebu-bio, CLU140-A) was used for virus titration as previously described (Subramanian, Wetzel et al. 2012).

4.1.3 Chemicals, reagents, solutions, materials and kits

(-)-blebbistatin	Sigma-Aldrich, B0560
1.5 ml microcentrifuge tube	Sarstedt, 1083121
10 x NEBuffer TM 3.1	New England Biolabs
10 cm Nunc TM petri dish	Thermo Scientific TM , 150350
10 x Key buffer (15 mM MgCl ₂)	VWR
12-well dish	Sarstedt, 83.3921
15 ml falcon	Lager, 10114572
18 mm Ø coverslips	Carl Roth, LH23.1
2,4,6-triiodophenol	Sigma-Aldrich, 137723
24-well dish	Sarstedt, 83.3922
2-mercaptoethanol	Sigma-Aldrich, M-6250
30% Acrylamide/Bis solution	Bio-Rad, 1610154
4-(2-hydroxyethyl)-1-piperazineethanesulfonic acid (HEPES)	Sigma-Aldrich, H3375
4-well dish	Greiner Bio-One, 627170
Agarose	Biozym, 840004

Ammonium persulfate (APS)	Merck, A3678
Ampicillin sodium salt	Merck, A9518
Anisomycin	EMD Millipore, 176880
Aqua Poly/Mount	Polysciences, 18606-20
B-27™ supplement (50x), serum free	Thermo Fisher, 17504044
Betaine monohydrate	Sigma-Aldrich, 61962
Boric acid	Roth, 5935
Bovine serum albumin (BSA)	Sigma, A7030
Brain-derived neurotrophic factor (BDNF)	Institute of clinical neurobiology
Bromophenol blue	Sigma-Aldrich, B8026
Calcium chloride dihydrate (CaCl ₂ x2H ₂ O)	Sigma-Aldrich, C-7902
Chelex	Bio-Rad, 1432832
Chloroform	Merck, 32211
Ciliary neurotrophic factor (CNTF)	Institute of clinical neurobiology
Coverslips, round 10 mm	Laborversand, DKRO
Cytochalasin D (CytoD)	Sigma-Aldrich, C2618
Deoxyribonucleotides (dNTPs)	GeneOn, 110-012
Dimethyl sulfoxide (DMSO)	AppliChem, A3672,0100
Donkey serum	Bio-Rad, C06SB
Dulbecco's modified eagle medium (DMEM)	Gibco™, 61965059
EcoRI restriction enzyme	Thermo Fisher, ER0275
Ethanol	Sigma, 32205
Ethylenediaminetetraacetic acid (EDTA)	Roth, CN06.3
Fetal calf serum (FCS)	Linarisblue, SBF3119KYA
Filter, 0.2 µm	Lager, 10107293

GeneRuler 100 bp DNA Ladder	Thermo Scientific, SM0242
GeneRuler 1kb plus DNA Ladder	Thermo Scientific, SM1331
Glacial acetic acid	Sigma-Aldrich, 33209
Glucose	Sigma-Aldrich, G7021
GlutaMAX	Gibco™, 35050-038
Glycerol	AppliChem, 151339.1211
Glycine	Carl Roth, 3790.5
Hanks balanced salt solution (HBSS)	Gibco™, 1417-138
Horse Serum (HS)	Linaris
Isopropanol	Sigma-Aldrich, 33539
KAPA HiFi HorStart ReadyMix	KAPA Biosystems
Lipofectamine 2000	Invitrogen, 11668-030
Lysogeny broth (LB)	Sigma-Aldrich, L3022
Magnesium chloride	Merck, 7786303
Merosin (Human)	Millipore, CC085
Methanol	Merck, 32213
Milk powder	Carl Roth, T145.3
MyoVin-1	Calbiochem, 475984
Neurobasal medium	Gibco™, 21103049
NheI restriction enzyme	Thermo Fisher, ER0972
N-Lauroylsarcosine sodium salt (Sarcosyl)	Sigma-Aldrich, 137-16-6
Nocodazole	Sigma-Aldrich, M1404
NotI restriction enzyme	Thermo Fisher, ER0595
Nonidet P-40 (NP-40)	Roche
Opti-MEM medium	Invitrogen, 51985-026

PageRuler plus prestained protein ladder, 10-250 kDa	Thermo Fisher, 26619
Paraformaldehyde (PFA)	Millipore Sigma, 1040051000
Penicillin-Streptomycin	Thermo Fisher, 15070063
PfuUltra II fusion HotStart DNA polymerase	Agilent Technologies, 600670
Phosphate buffered saline (PBS)	Sigma, D8537
Pierce™ 16% formaldehyde, methanol free	Thermo Fisher, 28908
Poly D-L-Ornithine (PORN)	Merck
Potassium chloride	Carl Roth, 7447-40-7
Potassium dihydrogen phosphate (KH ₂ PO ₄)	Merck, 7778-77-0
Prestained protein ladder (10-180 kDa)	Abcam, 1b116027
Protease Inhibitor Cocktails	Thermo Fisher, 87785
Proteinase K	GeneOn, 405-010
Puromycin	Merck, P8833
PVDF membranes	Bio-Rad, 1620177
SaII restriction enzyme	New England Biolabs, R0138T
Select Agar, powder	Thermo Fisher, 30-391-023
Sodium chloride (NaCl)	Carl Roth, 9265.2
Sodium dihydrogen phosphate (NaH ₂ PO ₄)	Merck, 7558-80-7
Sodium dihydrogen orthophosphate (Na ₂ HPO ₄)	Carl Roth, 7558-79-4
Sodium dodecyl sulfate (SDS)	AppliChem, A7249,10000
Sodium hydroxide (NaOH)	Carl Roth, 6771.1
Sucrose	Fluka/Honeywell, 84100H
T4 DNA ligase	Thermo Fisher, EL0011
T4 DNA ligase buffer	Thermo Fisher
Taq DNA polymerase	VWR, 733-1303

Tetramethylethylenediamine (TEMED)	Carl Roth, 2367.1
Tris Base	Carl Roth, 4855.3
Tris-hydrochloride (Tris-HCl)	Carl Roth, 9090.3
Triton-X 100	Sigma-Aldrich, X100
Trypsin, TRL3	Worthington, LS003707
Trypsin inhibitor	Sigma-Aldrich, T6522
Trypsin/EDTA	Thermo Scientific, 25300062
Tween 20	Sigma-Aldrich, P1379
X-ray film	Fuji super RX
XbaI restriction enzyme	Thermo Fisher, ER0681
Xylene cyanol FF	Sigma-Aldrich, X-4126
μ -Dish, 35 mm, high	Ibidi, 81158

Solutions and media for motoneuron culture

Dissection medium	HBSS
1% trypsin	100 mg trypsin 9.75 ml HBSS 250 μ l 1 M pH=7.3 HEPES Filter using sterile filters with pore size of 0.2 μ m
1% trypsin inhibitor	100 mg trypsin inhibitor 250 μ l 1 M pH=7.3 HEPES 9.75 ml HBSS Filter using sterile filters with pore size of 0.2 μ m
1 M HEPES buffer	238.3 g HEPES Dissolve in 1 L ddH ₂ O

	Check the pH and adjust to 7.3
	Autoclave to be sterilized
Borate buffer	0.15 M boric acid
	Double-distilled water (ddH ₂ O)
	Check the pH and adjust to 8.35
	Autoclave to be sterilized
P ⁷⁵ panning	anti-p ⁷⁵ antibody (1:10000; MLR2) diluted in 10 mM pH 9.5 Tris-buffer
Depolarization solution	0.8% NaCl
	2 mM CaCl ₂
	30 mM KCl
	Dissolve in ddH ₂ O
	Autoclave to be sterilized
100 × PORN stock solution	500 mg PORN
	Dissolve in 10 ml borate buffer
	Final concentration: 0.5 mg/ml
Merosin	Merosin
	HBSS
	Final concentration: 2.5 µg/ml
Full motoneuron medium	NeuroBasal Medium
	500 µM GlutaMAX
	2% horse serum
	2% B-27 TM supplement

Media for Cell lines

Culture medium for	DMEM
--------------------	------

HEK^{293T} and NSC34
500 μ M GlutaMAX
10% FCS
1 \times P/S

Solutions for live cell imaging

Tyrode buffer (pH 7.4)
125 mM NaCl
2 mM KCl
2 mM CaCl₂ \times 2H₂O
2 mM MgCl₂
30 mM glucose
25 mM HEPES
Check the PH and adjust to 7.4

Solutions for immunocytochemistry

4% PFA
1 ml PierceTM 16% Formaldehyde
3 ml 1xPBS

Home-made 16% PFA
32 g paraformaldehyde
Dissolve in 100 ml ddH₂O
A few drops of NaOH
Dissolve at 60°C (Celsius grad)
82 ml of 0.2 M Na₂HPO₄
18 ml of 0.2 M NaH₂PO₄
Check the pH and adjust to 7.4

10 × PBS	80 g NaCl
	2.0 g KCl
	14.4 g Na ₂ HPO ₄
	2.4 g KH ₂ PO ₄
	Add ddH ₂ O to 1 L and adjust pH to 7.4
	Autoclave to be sterilized
Block solution	10 % donkey serum
	2% BSA
	In 1 x PBS

Buffers and stock solutions for western blotting

2 × Laemmli buffer	4% SDS
	20% glycerol
	125 mM pH 6.8 Tris-HCl
	0.004% bromophenol blue
	10% 2-mercaptoethanol (freshly added)
1.5 M Tris pH 8.8	15.8 g Tris-HCl
	24.2 g Tris-base
	180 ml Millipore water
	Adjust the pH to 8.8
	Fill up to 200 ml with Millipore water
1 M Tris pH 6.8	24.2 g Tris-base
	180 ml Millipore water
	adjust the pH to 6.8
	Fill up to 200 ml with Millipore water

10% APS	1 g Ammonium persulfate
	10 ml Millipore water
10 × Running buffer	30.3 g Tris-base (250 mM)
	143.6 g glycine (1.9M)
	10 g SDS (1%)
	1 L Millipore water
1 x Transfer buffer	10 ml 10 × Running buffer
	40 ml methanol
	150 ml Millipore water
Blocking solution	5 g milk powder
	100 ml 1× TBST
10 × TBS	88 g NaCl
	24 g Tris-HCl
	5.6 g Tris-base
	900 ml Millipore water
	adjust the pH to 7.6
	Fill up to 1 L with Millipore water
1 x TBST	100 ml 10 x TBS (pH 7.6)
	900 ml Millipore water
	1 ml Tween 20

Stacking gel 4%

Reagents	Volume
30% Acrylamide/Bis solution	850 μ l
1 M Tris-HCl pH 6.8	625 μ l

10% SDS	50 μ l
10% APS	50 μ l
TEMED	5 μ l
Millipore water	3.4 ml

Separating gel

Reagents	Gel %				
	4%	6%	8%	10%	12%
30% Acrylamide/Bis solution	260 μ l	400 μ l	520 μ l	680 μ l	800 μ l
1.5 M Tris-HCl pH 8.8	520 μ l	520 μ l	520 μ l	520 μ l	520 μ l
10% SDS	20 μ l	20 μ l	20 μ l	20 μ l	20 μ l
10% APS	20 μ l	20 μ l	20 μ l	20 μ l	20 μ l
TEMED	2 μ l	2 μ l	2 μ l	2 μ l	2 μ l
Millipore water	1180 μ l	1000 μ l	920 μ l	760 μ l	640 μ l

Solutions for DNA extraction and genotyping

Lysis buffer	5 g Chelex
for quick and dirty DNA extraction	2 ml 5 M NaCl
	5 ml 10% sarkosyl solution
	Add ddH ₂ O up to 100 ml
Lysis buffer	150 mM NaCl
for chloroform DNA extraction	10 mM Tris-HCl pH 7.5
	0.5% SDS
	100 mM EDTA pH 8.0

5 M betaine	33.8 g betaine monohydrate, 50 ml ddH ₂ O
6 × loading buffer	250 mg bromophenol blue 250 mg xylene cyanol FF 33 ml glycerol Add Millipore water up to 100 ml
50 × TAE buffer	57.1 ml glacial acetic acid 242 g Tris-base 100 ml of 0.5 M EDTA pH 8 Add ddH ₂ O up to 1 L

Solutions for Cloning

LB-Agar	20 g LB 15 g select agar 1 ml 50 mg/ml ampicillin stock 1 L ddH ₂ O Autoclave to be sterilized
LB medium	20 g LB 1 L ddH ₂ O Autoclave to be sterilized

Commercial Kits

Kits	Company
Plasmid DNA purification kit	Macherey-Nagel, 740727.250
NucleoBond® Xtra Midi/Maxi plasmid purification kit	Macherey-Nagel, 740420.50

QIAEX II gel extraction kit

Qiagen, 20021

NEBuilder HiFi DNA Assembly cloning kit

New England Biolabs, E5520S

ECL Western Blotting-Substrat

Thermo Fisher, 32106

4.1.4 List of plasmids

Vector	Insert	Vector Source or references
pRSV-REV	Helper plasmids for lentivirus packaging	(Dull, Zufferey et al. 1998, Zufferey, Dull et al. 1998)
pCMV R8.91		
pMDLg/pRRE		
pMD.G VSVG		
pSIH-H1		SBI, SI500A-1
pCMV-CES2-CMV	Myc-KDEL	Institute of Clinical Neurobiology, provided by Robert Blum (Samtleben, Wachter et al. 2015)
FuValentine-ubiquitin promoter	mCherry-Rab7a	Institute of Clinical Neurobiology, provided by Patrick Lüningschrör
pSIH-CMV	GFP-actin	Institute of Clinical Neurobiology (Sivadasan, Hornburg et al. 2016)
PH-PLCD1	mScarlet-I_IRES_sYFPs_PH_N1	Addgene, 110623
pSIH-CMV	GFP	Institute of Clinical Neurobiology

Table 4.1.4.1 List of plasmids used for cloning and lentivirus production

4.1.5 Antibodies

Primary antibodies used for immunofluorescence

Antibody	Host	Working dilution	Company
monoclonal anti- α -Tubulin	mouse	1:1000	Sigma-Aldrich, T6168
monoclonal anti-beta actin	mouse	1:1000	GeneTex, GTX26276
polyclonal anti-TrkB	goat	1:500	Bio-Techne Sales Corp, AF1494
Monoclonal anti-rRNA(Y10b)	mouse	1:500	Thermo Fisher Scientific, MA116628
polyclonal anti-ribosomal protein L8	goat	1:500	Sigma-Aldrich, SAB2500882
Polyclonal anti-Tau	rabbit	1:1000	Sigma-Aldrich, T6402
polyclonal anti-eEF2	rabbit	1:50	Cell signaling Technology, 23325
monoclonal anti-S6 ribosomal protein	mouse	1:100	Thermo Fisher Scientific, MA515123
polyclonal anti-RPL24	rabbit	1:500	Thermo Fisher Scientific, PA530157
polyclonal antiserum RFP	Guinea pig	1:500	Synaptic Systems, 390004
monoclonal anti-mCherry	rat	1:1500	Thermo Fisher Scientific, M11217
monoclonal anti-puromycin	mouse	1:1000	Merck Millipore, MABE343
Polyclonal anti-Ca ²⁺ channel N-type alpha-1B channel	guinea pig	1:250	Synaptic System, 152305

Alexa Fluor® 647 conjugated Phalloidin	-	1:100	Invitrogen, A22287
polyclonal anti-calreticulin	chicken	1:500	Thermo Fisher Scientific, PA1-902A
polyclonal anti- synaptophysin 1	guinea pig	1:1000	Synaptic Systems, 101004

Table 4.1.5.1 List of primary antibodies used for immunofluorescence

Secondary antibodies used for immunofluorescence

Antibody	Host	Working dilution	Company
Alexa Fluor® 488 anti-mouse IgG (H+L)	donkey	1:500	Life Technologies, A21202
Alexa Fluor® 488 anti-rabbit IgG (H+L)	donkey	1:500	Jackson ImmunoResearch (JIR), 711-545-152
Alexa Fluor® 488 anti-chicken IgY (H+L)	donkey	1:500	JIR, 703-545-155
Cy3 anti-guinea pig IgG (H+L)	donkey	1:500	JIR, 706-165-148
Cy3 anti-rat IgG (H+L)	donkey	1:500	JIR, 712-165-150
Cy3 anti-rabbit IgG (H+L)	donkey	1:500	JIR, 711-165-152
Cy3 anti-goat IgG (H+L)	donkey	1:500	JIR, 705-165-147
Cy3 anti-mouse IgG (H+L)	donkey	1:500	JIR, 715-165-151
Cy3 anti-mouse IgG (H+L)	goat	1:500	JIR, 115-165-146
Alexa Fluor® 647 anti-goat IgG (H+L)	donkey	1:500	JIR, 705-605-003

Alexa Fluor® 647 anti-mouse IgG (H+L)	donkey	1:500	Invitrogen, A31571
Cy5 anti-rabbit IgG (H+L)	donkey	1:500	JIR, 711-175-152
Cy5 anti-guinea pig IgG (H+L)	donkey	1:500	JIR, 706-175-148

Table 4.1.5.2 List of secondary antibodies used for immunofluorescence

Primary antibodies used for western blot analysis

Antibody	Host	Working dilution	Company
polyclonal anti-TrkB	goat	1:500	Bio Techne Sales Corp, AF 1494
monoclonal anti- α -Tubulin	mouse	1:5000	Sigma-Aldrich, T5168
monoclonal anti-phospho-TrkA(Tyr674/675)/TrkB(Tyr706/707)	rabbit	1:1000	Cell Signaling Technology, C50F3
monoclonal anti-phospho-TrkA(Tyr490)/TrkB(Tyr516)	rabbit	1:1000	Cell Signaling Technology, 4619
monoclonal anti- β -III-tubulin	mouse	1:4000	Sigma Aldrich, T8578
monoclonal anti-drebrin	mouse	1:500	Santa Cruz, sc-374269
Monoclonal anti-GAPDH	mouse	1:1000	Sigma-Aldrich, CB1001

Table 4.1.5.3 List of primary antibodies used for western blot

Secondary antibodies used for western blot analysis

Antibody	Host	Working dilution	Company
Peroxidase AffiniPure anti-rabbit IgG (H+L)	donkey	1:10000	JIR, 711-035-152

Peroxidase AffiniPure anti-goat IgG (H+L)	donkey	1:10000	JIR, 115-035-146
Peroxidase AffiniPure anti-rabbit IgG (H+L)	goat	1:10,000	JIR
Peroxidase AffiniPure anti-mouse IgG (H+L)	goat	1:10000	JIR, 115-035-146

Table 4.1.5.4 List of secondary antibodies used for western blot

4.1.6 Primers for genotyping and cloning

Primers for genotyping

Name	Sequence
SMN 201f	5'-CTG GAA TTC AAT ATG CTA GAC TGG CCT G-3'
SMN 1049r	5'-AAT CAA TCT ATC ACC TGT TTC AAG GGA GTT G-3'
SMN ko	5'-GAT GTG CTG CAA GGC GAT TAA GTT G-3'
Tw3	5'-TCA TAC CTT AAA GGA AGC CAC -3'
Tw7	5'-AGG TTC TGA GGT CAG AAC AGC -3'
TrkB-n2	5'-ATG TCG CCC TGG CTG AAG TG -3'
TrkB-c8	5'-ACT GAC ATC CGT AAG CCA GT -3'
Pgk3-1	5'-GGT TCT AAG TAC TGT GGT TTC C -3'

Table 4.1.6.1 List of used primers for genotyping

Primers for cloning

Name	Sequence
mCherry-for	5'- ACT CGT CGA CGT GAG CAA GGG CGA GGA GGA T-3'
mCherry-rev	5'- GAA TGC GGC CGC CTT GTA CAG CTC GTC CAT GCC -3'
mCherry-KDEL-for	5'-TTT GAC CTC CAT AGA AGA TTC CAC CAT GGG ATG

	GAG CTG-3
mCherry-KDEL-rev	5'-TGT AAT CCA GAG GTT GAT TGC TAC AGC TCG TCC TTC TCG-3'
GFP-actin-for	5'-ACT CTC TAG AGC CCA CCA TGG TGA GCA AG-3'
GFP-actin-rev	5'-GAA TGC TAG CCT AGA AGC ACT TGC GGT G -3'
shDrebrin A	5'-GTCCGTA CTGCCCCTTTCATAA-3'
shDrebrin A+E	5'-GGCTGTGCTAACCTTCTTAAT-3'
drebrin A for	5'-CCTGATAACCCACGGGAGTT-3'
drebrin A rev	5'-GGAAGAGAGGTTTGGGGTGC-3'
drebrin E for	5'-CCCACGGGAGTTCTTCAGACA-3'
drebrin E rev	5'-TCCAGGTGGCTGCATGGGAGGGAG-3'

Table 4.1.6.2 List of used primers for cloning

4.1.7 Softwares

- Adobe Acrobat DC
- Adobe Illustrator 2020
- Adobe Photoshop CS6
- ApE plasmid editor
- GraphPad Prism 9.0
- Fiji, ImageJ
- Microsoft Office 2019, Excel, Word, Power Point
- Nikon Element image software
- Olympus FV10-ASW imaging software
- ZEN 2.1 SP-1 software

4.2 Methods

4.2.1 Isolation and culture of embryonic mouse motoneurons

For preparation of motoneuron culture on coverslips, coverslips were placed in 4-well dishes (Greiner Bio-One, 627170) or 12-well dishes (Sarstedt, 83.3921) and coverslips together with dishes were sterilized with UV for 30 min, followed by adding Poly D-L-Ornithine (PORN) (Merck) onto coverslips and incubation overnight at 4°C. The next day, PORN was removed, and coverslips were washed 3 times with HBSS. Then, coverslips were coated with merosin (Merck-Millipore, CC085) at room temperature (RT) for at least 1 h before usage. Merosin contains Laminin211 ($\alpha2\beta1\gamma1$) and Laminin221 ($\alpha2\beta2\gamma1$) which is highly expressed in extra-synaptic basal lamina and at the cleft of neuromuscular junctions (NMJs), respectively. Merosin is involved in formation, maturation, and maintenance of NMJs (Fox, Sanes et al. 2007, Rogers and Nishimune 2017). Therefore, motoneurons cultured on merosin form relatively matured presynaptic structures on their axon terminals (Jablonka, Beck et al. 2007). For SIM analysis, cells were cultured on coverslips with precise thickness 0.17 ± 0.005 mm (18 mm \varnothing , Carl Roth, LH23.1). For conventional confocal microscopy analysis, cells were cultured on 10 mm \varnothing coverslips (Laborversand, DKRO). For live cell imaging, μ -Dishes with glass bottom (Ibidi, 81158) were coated with PORN/merosin. Lumbar spinal cords were isolated from E13.5 embryos from CD1 or SMA mice, removed of meninges and DRGs and digested with 1% trypsin (Worthington, LS003707) in a water bath for 15 min at 37°C, followed by enrichment of motoneurons with anti-p75 antibody (MLR2, Abcam), as previously described (Wiese, Herrmann et al. 2009). After incubation with anti-p75 antibody in a 10 cm NuncTM petri-dish (Thermo ScientificTM, 150350) with neurobasal medium (NB) (GibcoTM, 21103049), the plate was washed twice with NB medium. Motoneurons attached to anti-p75 antibody coated plate were depolarized with depolarization buffer for 10-20 s and full motoneuron medium was added inside. The supernatant was collected into 15 ml falcons

(Lager, 10114572) and centrifuged at the speed of 400 g for 5 min. Following the aspiration of the supernatant, the left cell pellet at the bottom of the falcon was re-suspended with full motoneuron medium. After counting the number of cells using a hemacytometer (Neubauer chamber), merosin on the coverslips or μ -Dishes were removed and motoneurons were immediately seeded onto PORN/merosin-coated coverslips or onto μ -Dish and maintained in full motoneuron medium containing NB medium, 2% heat-inactivated horse serum (Linaris), 500 μ M GlutaMAX (GibcoTM, 35050-038) and 2% B-27TM supplement (Thermo Fisher, 17504044). For the first 5 days, motoneurons were cultured with full motoneuron medium containing 5 ng/ml BDNF (home-made) at 37°C in a humid incubator with 5% CO₂. Full motoneuron medium was first replaced 24 h after plating and then every second day.

4.2.2 Pharmacological treatments

Drugs for pharmacological treatments were all commercially available: nocodazole (Sigma-Aldrich; M1404), cytochalasin D (Sigma-Aldrich; C2618), anisomycin (EMD Millipore; 176880-10MG), (-)-blebbistatin (Sigma-Aldrich; B0560), MyoVin-1 (Calbiochem; 475984) and 2,4,6-triiodophenol (Sigma-Aldrich; 137723). All the chemicals were dissolved or diluted in DMSO (AppliChem, A3672,0100). For depolymerization of microtubules, motoneurons were treated with 10 μ M nocodazole for 2 h. For inhibition of translation, cells were incubated with 100 ng/ml anisomycin for 1 h. 1 μ g/ml cytochalasin D for 30 min treatment was performed to disturb polymerization of actin filaments. For inhibition of myosin proteins, toxicity of the chemicals was first examined by survival assay of cultured motoneurons after treatment with three myosin inhibitors at concentrations ranging from 1-100 μ M and incubation time from 30 min up to 12 h. As a control the same volume of DMSO was added. Percentage of survived neurons was determined for each condition and different incubation times. After toxicity testing, 5 μ M (-)-blebbistatin, 30 μ M MyoVin-1 and 1 μ M 2,4,6-triiodophenol were incubated with cells for 15 min to inhibit myosin II, myosin V and myosin

VI, respectively. All the pharmacological treatments were performed in a humid cell culture incubator at 37°C with 5% CO₂.

4.2.3 Immunocytochemistry of cultured motoneurons

At days in vitro (DIV) 6, cells were fixed with 4% PFA (Thermo Fisher, 28908) in phosphate buffered saline (PBS) for 10 min at RT. After fixation, cells were washed 3 times with PBS, each time for 5 min. Then 0.1% or 0.3% Triton X-100 (Sigma-Aldrich, X100) in PBS were incubated for 10 min at RT for permeabilization. Following permeabilization, cells were washed 3 times with PBS and incubated with block solution containing 10% donkey serum (Bio-Rad, C06SB) and 2% BSA (Sigma-Aldrich, A7030) for 1 h at RT. After washing with PBS, cells were incubated with primary antibodies diluted in block solution overnight at 4°C. The next day, primary antibodies were washed with PBS for 3 times, each time 10 min, followed by incubation with secondary antibodies in PBS at RT for 1 h. Secondary antibodies were washed 3 times with PBS and the cells were embedded using Aqua Poly/Mount (Polysciences, 18606-20). For phalloidin staining, motoneurons were fixed with 4% PFA for 15 min and permeabilized with 0.3% Triton X-100 for 20 min. Alexa Fluor647-conjugated Phalloidin (Invitrogen, A22287) was used to label F-actin. For β -actin staining, permeabilization was performed with ice-cold methanol (Merck, 32213) at -20°C for 5 min. For Cav2.2 staining, fixation was performed with 4% PFA for 5 min and 0.1% Triton X-100 was incubated for 5 min at RT for permeabilization. For BDNF stimulation, motoneurons were cultured with full motoneuron medium supplemented with 5 ng/ml BDNF for 5 days. At DIV5, BDNF containing full motoneuron medium was removed and the cells were washed with full motoneurons medium to completely remove BDNF from the cells and the culture dish. After this, the cells were cultured in full motoneuron medium without BDNF overnight. The following day, motoneurons were stimulated with 40 ng/ml BDNF diluted in the full motoneuron medium for 10 s, 1 min or 10 min and fixed immediately after stimulation. No

BDNF control group was incubated with the same volume of full motoneuron medium without BDNF. For chemical treatment, cells were incubated with 10 μ M nocodazole for 2 h, 100 ng/ml anisomycin for 1 h or 1 μ g/ml cytochalasin D for 30 min prior to BDNF stimulation as well as during BDNF stimulation. For puromycin incorporation assay, 10 μ g/ml puromycin (Merck, P8833) was added to motoneurons and incubated for 10 min in a cell culture incubator. BDNF stimulation was performed during 10 min incubation time of puromycin. Following treatment, neurons were immediately fixed and immunostained using an anti-puromycin antibody.

Surface TrkB staining was performed by a colleague Luisa Hennlein. Cultured motoneurons were placed on ice and antibody against TrkB that was diluted in cold full motoneuron medium was added onto cells and incubated for 45 min on ice, followed by a washing step with cold PBS (Sigma, D8537). Then cells were incubated with secondary antibody diluted in cold full motoneuron medium. After incubation, cells were washed three times with cold PBS, and then fixed with 4% PFA for 5 min on ice. After fixation, a conventional immunostaining was performed to cells.

4.2.4 Western blotting

For western blot (WB) analysis, approximately 300,000 motoneurons were plated in one well of a 24-well dish (Sarstedt, 83.3922) that was pre-coated with PORN/laminin. Gradient gels were prepared one day before the performance of a western blotting and wrapped into wet tissues and sealed for storage at 4°C overnight. At DIV 6, motoneurons were first washed twice with pre-warmed PBS and then lysed with 2 x Laemmli buffer. Protein lysates were collected into 1.5 ml tubes (Sarstedt, 1083121) and boiled at 99°C for 10 min, followed by a short centrifugation step at 8000 g. Samples were stored at -80°C or directly used for western blotting. For all the samples, the same volumes of protein lysates were loaded into the wells of gradient gels. Gels were first run at 80 mV for 20 min and then at 120 mV for 1.5 to 2 h.

PVDF membranes (Bio-Rad, 1620177) were first immersed in 100% methanol for 1 min till it became translucent. Then the membranes were transferred into transfer buffer and incubated for 5 min for equilibration. Together with PVDF membranes, filter papers and gels were also immersed in the transfer buffer. After this step, the gels were blotted on PVDF membranes in a semi dry chamber at 1000 mA for 1 h or in a wet chamber at 120 V for 1.5 h. When transfer was finished, membranes were taken out and washed with TBST (0.1% Tween 20 in Tris-buffered saline) shortly. After blocking with 5% milk (Carl Roth, T145.3) in PBST for 1 h on a shaker at RT, the membranes were washed with TBST shortly and incubated with primary antibodies in TBST overnight at 4°C on a shaker. On the next day, membranes were washed with TBST three times each time for 15 min and incubated with secondary antibodies at RT for 1 h. After this, 3 x 15 min wash with TBST was performed and the membranes were developed with Enhanced chemiluminescence (ECL) Western Blotting-Substrat (Thermo Fisher, 32106) and X-ray films (Fuji super RX). For BDNF stimulation, DIV5 cells were first deprived of BDNF and cultured in full motoneurons medium without BDNF. At DIV6, 40 ng/ml BDNF was added to cells for 10 s, 30 s, 1 min and 10 min, followed by directly adding 2 x Laemlli buffer for lysis.

4.2.5 Live cell imaging

For live cell imaging, motoneurons were transduced with lentiviruses expressing mCherry-KDEL or co-expressing mCherry-KDEL and GFP-actin, or co-transduced with a lentivirus that expresses mCherry-KDEL and another lentivirus expressing GFP and incubated with corresponding lentiviruses for 10–15 min at RT. Then 30,000 – 50,000 cells were seeded into μ -Dishes that were pre-coated with PORN/merosin. At DIV6, live cell imaging was performed. First, pharmacological treatments were performed by directly adding the drugs into full culture medium and incubated in a cell culture incubator. Following drugs were used: 10 μ M nocodazole for 2 h, 1 μ g/ml cytochalasin D for 30 min, 5 μ M (-)-blebbistatin for 15

min, 30 μ M MyoVin-1 for 15 min and 1 μ M 2,4,6-triiodophenol for 15 min. After incubation, cells were washed twice with pre-warmed Tyrode's buffer to remove the drugs and imaged in Tyrode's buffer. For nocodazole and cytochalasin D experiments, nocodazole and cytochalasin D were again added into the Tyrode's buffer before imaging and imaged in presence of these drugs. For (-)-blebbistatin, MyoVin-1 and 2,4,6-triiodophenol experiments, drugs were not added into Tyrode's buffer before and during imaging. For all the live cell imaging, an inverted widefield epifluorescence microscope (Nikon Eclipse TE2000-E) was applied. This epifluorescence microscope was equipped with a Plan Apo 60x 1.4 NA objective, a perfect focus system (PFS), an Orca Flash 4.0 V2 camera (Hamamatsu Photonics), a heated stage chamber (TOKAI HIT CO, LTD), CO₂ supply, LED light source CoolLED pE-4000 and Nikon Element image software. Prior to imaging, the stage chamber was heated to 37°C and a continuous 5% CO₂ was supplied. During the whole process of imaging, the temperature and CO₂ supply were controlled and perfect focus system was on. For single channel imaging of motoneurons transduced with lentiviruses expressing mCherry-KDEL, light at excitation wavelength of 580 nm and a broadband DsRed Filter (HQ-Set, F41-035) were used. Images were captured with 100 ms exposure time, 2x2 Binning, fast scan mode over 15 min at intervals of 2 sec per frame. For imaging of motoneurons transduced with lentiviruses that express mCherry-KDEL and co-express GFP-actin or GFP, light with excitation wavelength of 470 nm and 580 nm, together with a multi-band filter ET-Sedat Quad (Chroma Technology, 8900) were applied. Exposure time 100 ms, 2x2 Binning and fast scan mode were set for image acquisition. At the end, 12-bit images of 1.024 x 1.024 pixels were acquired.

4.2.6 Analysis of ER dynamics

Image Correlation Spectroscopy (ICS) implemented in python was applied for analysis of ER dynamics (Wiseman 2015). In the implementation, N and M indicate two dimensions in

space, and T indicates the time dimension. i, j, t designate the corresponding running indices. Flow or diffusion in an image time series $\{I\}_{i,j,t}^{N,M,T}$ determines molecular movements of ER or other organelles. As a start of the workflow, a space-time window, namely a subspace of $K = L = 10 \text{ px}$ over $\Delta t = 10$ consecutive frames, was first defined. Rasterization of this subspace over the image at a sampling rate of $\Delta i = \Delta j = 4$ was performed, followed by a computed correlation window $\{C\}_{x,y}^{K,L}$ for each of these samples. In this way, overlap of signal for a given shift x, y per time frame was given. The point of maximum correlation was indicated by the maximum of this spectrum, and the shift of signal from one image to the next was also indicated by $(\Delta i, \Delta j) = (x_{max} - K/2, y_{max} - L/2)$. For a better sub-pixel accuracy, a 2D Gaussian function was applied to the correlation spectrum using the Levenberg-Marquardt-Algorithm. Parameters includes amplitude $A = \max(C)$, center coordinates in x , $x_0 = K/2$, center coordinates in y , $y_0 = L/2$, standard deviation in x , $\sigma_x = K/4$, standard deviation in y , $\sigma_y = L/4$ and θ that indicates rotation of the coordinated system was initialized as 0. Directed shift of a signal was indicated by the fit results for x_0 and y_0 . A larger σ_x or σ_y indicates an overall lower correlation, that is the signal losing its shape. Three distinctive subspaces were classified according to the intensities in images: First, subspaces with a mean intensity $< 10\%$ of the maximum intensity were classified as noise. Second, subspaces with a mean intensity $> 40\%$ of the maximum intensity were considered as core. Third, subspaces with a mean intensity in between were classified as filopodia. The values given as average dynamics were the mean dynamics in filopodia or core of each cell. The accuracy test of ICS analysis was evaluated using fixed cells. First, motoneurons transduced with a lentivirus expressing mCherry-KDEL in μ -Dishes were fixed with 4% PFA for 10 min at DIV6. After 3 times PBS washing, cells were covered by Tyrode buffer. Imaging and quantification were performed in the same way with single channel imaging abovementioned. This ICS analysis was performed by a collaborator Sebastian Reinhard.

As an additional analysis method, ER dynamics were measured using multiple kymographs produced using Multi Kymograph plugin of ImageJ, as previously described (Moradi, Sivadasan et al. 2017). To obtain multiple kymographs, maximum projection was performed to time series of a live cell image for visualization of all ER tubules detected by the microscope during the whole imaging time and a line was drawn along a moving ER. After acquisition of multiple kymographs along these drawn lines, distance moved by each ER movements and the corresponding spending time were measured. The velocity was calculated by distance divided by time. Frequency of ER movements was also counted from the multiple kymographs manually. If ER movements were not visible or detectable in a growth cone, this growth cone was classified into cells with failure in filopodia or core ER movements.

4.2.7 Confocal microscopy, super-resolution microscopy and data analysis

For analysis of fluorescence signals, we performed immunofluorescence staining to cultured motoneurons and a standard confocal laser microscope Olympus Fluoview 1000 was used for image acquisition. Images were captured using a 60x NA 1.35 oil objective, Olympus FV10-ASW imaging software (RRID:SCR_014215) and corresponding lasers: 473 nm, 559 nm, and 633 nm lasers. For quantification of immunofluorescence signals, we first performed average intensity of Z-projection to Z-stack images using ImageI-win64. Mean gray values of ROIs in images were measured from unprocessed raw images or Z-projection applied images after subtraction of mean gray values of background. For super-resolution imaging, we used a commercial ELYRA S.1 microscope (Zeiss AG), Structured Illumination Microscopy (SIM). Images were captured using a Plan-Apochromat 63x/ 1.40 NA immersion-oil based objective and three excitation lasers: a 488 nm OPSL (100 mW), a 561 nm OPSL (100 mW) and a 642 nm diode laser (150 mW), controlled by the Zeiss “ZEN 2.1 SP-1” software. Z-stacks with intervals at 0.12 nm were set up for image acquisition. For quantification of SIM data, we performed both automatic and manual analysis using ImageJ. For automatic analysis,

Pearson's correlation coefficient was measured using Coloc2 of ImageJ and colocalizing clusters were calculated by Just Another Colocalization Plugin (JACoP) plugin of ImageJ. For manual co-cluster analysis and Pearson's correlation coefficient analysis, maximum projections were obtained for each channel, followed by automatic linear adjustment of contrast and brightness. Then, channels of different labeling were merged into RGB images, and co-clusters were manually quantified when signals from corresponding channels were overlapping with a diameter of co-clusters larger than 350 nm. For analysis using JACoP, images were adjusted using the threshold of ImageJ and objects-based methods were applied to the corresponding images. Colocalizing particles with size larger than $0.096 \mu\text{m}^2$ (diameter = 350 nm) were calculated as co-clusters using Analyze Particles of ImageJ. 3D reconstruction of SIM images was performed using Imaris software. Linear contrast enhancement was applied to all representative images using Adobe Photoshop for a better visibility. The gamma correction was not performed for the images.

4.2.8 Cloning of the constructs

For cloning of the construct pSIH-mCherry-KDEL, mCherry was first amplified by Polymerase chain reaction (PCR) using a plasmid FuValentine-mCherry-Rab7 (provided by Patrick Lüningschrör) as the template and PfuUltra II fusion HotStart DNA polymerase (Agilent Technologies, 600670). The PCR products were run onto 2% agarose gels and the bands corresponding to the correct size were cut and purified using a DNA purification kit QIAEX II PCR purification kit (Qiagen, 20021). After purification, PCR products were digested by restriction enzymes SalI (New England Biolabs, R0138T) and NotI (Thermo Fisher, ER0595). The vector pCMV-CES2-CMV-myc-KDEL ((Samtleben, Wachter et al. 2015)) containing KDEL sequence was cut by restriction enzymes SalI and NotI. The fragments from the vector and mCherry were ligated with T4 DNA ligase (ThermoFisher, EL0011) according to manufacturer's protocol. First, the ligation reaction was prepared by

adding insert DNA, 10x T4 DNA ligase buffer, T4 DNA ligase and nuclease-free water and incubated for 1 h at RT. For negative control, ligation reaction was prepared and incubated in the absence of insert DNA. 10 min before finishing of the incubation, competent *Escherichia coli* (*E.coli*) TOP10 cells in a 1.5 ml microcentrifuge tube were taken out from -80°C and placed on ice for 10 min before usage. After incubation, 2 µl of the ligation reaction was taken out and mixed with *E.coli* TOP10 cells. The mixture was incubated on ice for 15 min, followed by a heat shock at 42°C for 50 sec. The mixture was then transferred onto ice for another 10 min incubation. Next, 1 ml LB medium that was placed at RT before usage was added into transformed *E.coli* TOP10 cells and incubated for 1 h at 37°C and 850 rpm in a thermomixer. After shaking, cells were spined down by centrifugation at 400 g for 5 min. Then, 900 µl of the supernatant was removed from the tube and cell pellet was resuspended in the left 150 µl LB medium. From the left 150 µl, half was plated onto an Agar plate that contains Ampicillin. The Agar plates were incubated in an incubator at 37°C overnight. For screening of positive colonies, 8 to 10 single colonies were picked from the positive plate and grew in 5 ml LB with ampicillin (1:1000 dilution from stock at 50 mg/ml) in a microbiological incubator for 12 h at 37°C under constant shaking with 180 rpm. Next day, 2 ml out of 5 ml medium was taken out for plasmid purification using a Plasmid DNA purification kit (Macherey-Nagel, 740727.250) following manufacturer's protocols. After DNA purification, the concentration of purified plasmids was measured using a NanoDrop (ND-1000, Spectrophotometer). For screening of positive colonies, extracted plasmids were digested with restriction enzymes SalI and NotI. Colonies which contained CMV-mCherry-KDEL fragment were selected for the next cloning step. As a next step, mCherry-KDEL fragments were amplified by PCR using KAPA HiFi HotStart ReadyMix (KAPA Biosystems) and purified with DNA purification kit. Lentivirus vector pSIH-H1 (SBI, SI500A-1) was digested by restriction enzymes XbaI and SalI. These two types of fragments were ligated at 50°C for 1 h using NEBuilder HiFi DNA Assembly Master Mix (New England Biolabs,

E5520S). After transformation, the colonies were screened by restriction enzyme NotI. Positive colonies were further checked for the expressing of corresponding inserts by transfection into NSC34 cells. Positive colonies were sent for sequencing and the correct ones were chosen and prepared for a maxi preparation using NucleoBond® Xtra Midi/Maxi plasmid purification kit (Macherey-Nagel, 740420.50) to harvest enough plasmids for lentivirus production. To construct plasmids that knockdown drebrin isoforms, shRNAs were designed to target the mouse drebrin A or target both drebrin A and E. The following antisense oligonucleotides were cloned and inserted into a modified version of pSIH-H1 shRNA vector: for shDrebrin A: 5'-GTCCGTA CTGCCCTTTCATAA-3', for shDrebrin A+E: 5'-GGCTGTGCTAACCTTCTTAAT-3'. Empty pSIH-H1 vector that expresses only EGFP was used as Control (shCtrl). The knockdown constructs were produced by a colleague Changhe Ji. To test the efficiency of constructs that knockdown drebrin isoforms, motoneurons were transduced first with shDrebrin A or shDrebrin A+E lentiviral particles before they were plated into 24-well plates. At DIV7, transduced motoneurons were washed with RNAase free PBS twice and lysed in RNA lysis buffer. NucleoSpin RNA extraction kit (Macherey-Nagel) was purchased for RNA extraction and First Strand cDNA Synthesis kit (Thermo Fisher) and random hexamers were used for reverse transcription of extracted RNA. Reversed transcripts were proceeded with qRT-PCR. For qRT-PCR reactions, the following primers were used: drebrin A: forward: 5'-CCTGATAACCCACGGGAGTT-3', reverse: 5'-GGAAGAGAGGTTTGGGGTGC-3'; drebrin E: forward: 5'-CCCACGGGAGTTCTTCAGACA-3', reverse: 5'-TCCAGGTGGCTGCATGGGAGGGAG-3').

PCR reaction for amplification of KDEL fragments (711 bp)

Components	50 µl reaction	Final concentration
Template	2	20-100 ng

dNTPs (10 mM)	1	0.2 mM
forward primer (10 μ M)	1	0.3 mM
reverse primer (10 μ M)	1	0.3 mM
PfuUltra II fusion HS DNA polymerase	1	3 units
buffer	5	1 \times
water	38	

PCR program for amplification of KDEL fragments (711 bp)

Steps	Number of cycles	Temperature ($^{\circ}$ C)	Duration
Initial denaturation	1	95	2 min
Denaturation	30	95	20 sec
Annealing		60	20 sec
Extension		72	15 sec
Final extension	1	72	5 min
Hold		4	∞

Table 4.2.8.1 PCR program for amplification of KDEL fragments

mCherry PCR products digested with SalI and NotI:

Reagents	Volume
mCherry PCR products	All of it (124 ng/ μ l)
SalI	2 μ l
NotI	2 μ l
10 \times NEBuffer TM 3.1	2 μ l
Water to	50 μ l

Vector 593-CES2-CMV-myc-ER digestion

Reagents	Volume
Vector	5 μ l
SalI	2 μ l
NotI	2 μ l
10 \times NEBuffer TM 3.1	2 μ l
Water to	50 μ l

Ligation setup of vector-593-CMV-ER and mCherry

Positive ligation

Reagents	Volume
Vector	25 ng
mCherry	17,625 ng
	$n(\text{insert}) = 5 \times \text{bp}(\text{insert})/\text{bp}(\text{vector}) \times n(\text{vector})$
T4 ligase	2 μ l
10 \times Ligase buffer	2 μ l
Water to	20 μ l

Ligation setup of vector-593-CMV-ER and mCherry

Negative ligation

Reagents	Volume
Vector	25 ng
No insert	0
T4 ligase	2 μ l
10 \times Ligase buffer	2 μ l
Water to	20 μ l

Screening for 593-CMV-mCherry-ER

Reagents	Volume
Purified plasmid	500 ng
SalI	0,5 μ l
NotI	0,5 μ l
10 \times NEBuffer TM 3.1	2 μ l
Water to	20 μ l

PCR reaction for amplification of mCherry-KDEL fragments (942 bp)

Components	25 μ l reaction
Template (30-100 ng)	1.5 μ l
forward primer (10 μ M)	1 μ l
reverse primer (10 μ M)	1 μ l
KAPA 2x	12.5 μ l
Water to 25 μ l	9 μ l

PCR program for amplification of mCherry-KDEL fragments (942 bp)

Steps	Number of cycles	Temperature ($^{\circ}$ C)	Duration
Initial denaturation	1	95	3 min
Denaturation	30	98	20 sec
Annealing		60	15 sec
Extension		72	15 sec
Final extension	1	72	5 min
Hold		4	∞

Table 4.2.8.2 PCR program for amplification of mCherry-KDEL fragments

Vector pSIH-tomato digestion

Reagents	Volume
pSIH-tomato	5 μ g
XbaI	1 μ l
SalI	1 μ l
10 \times NEBuffer TM 3.1	5 μ l
Water to	50 μ l

Ligation setup of vector pSIH-tomato and mCherry-KDEL

Reagents		Volume
Vector	0.1 pmol	2 μ l
Insert (mCherry-KDEL)	0.2 pmol	1 μ l
NEBuilder HiFi DNA Assembly		10 μ l
Master Mix		
Water to		20 μ l

Screening for pSIH-mCherry-ER

Reagents	Volume
Purified plasmid	500 ng
NotI	1 μ l
10 \times NEBuffer TM 3.1	2 μ l
Water to	20 μ l

To achieve the construct of pSIH-GFP-actin-IRES-mCherry-KDEL, GFP-actin fragments were amplified by PCR from the previous existing plasmid pSIH-GFP-actin (Sivadasan,

Hornburg et al. 2016). From already existing plasmid pSIH-CMV-TrkB-EGFP-IRES-mCherry-KDEL (the IRES fragment was originally from the construct PH-PLCD1-mScarlet-I_IRES_sYFPs_PH_N1, addgene, 110623), TrkB-EGFP fragment was cut out by restriction enzymes XbaI (Thermo Fisher, ER0681) and NheI (Thermo Fisher, ER0972). GFP-actin was amplified by PCR using a template pSIH-CMV-GFP-actin available in our lab. Finally, fragments were ligated using T4 ligase. After transformation, 30 colonies were picked and screened by digestion with restriction enzyme EcoRI (Thermo Fisher, ER0275).

PCR reaction for amplification of GFP-actin (1900 bp)

Components	50 μ l reaction	Final concentration
Template	2	20-100 ng
dNTPs (10 mM)	1	0.2 mM
forward primer (10 μ M)	1	0.3 mM
reverse primer (10 μ M)	1	0.3 mM
PfuUltra II fusion High-fidelity DNA polymerase	1	3 units
buffer	5	1 \times
water	38	

PCR program for amplification of GFP-actin (1900 bp)

Steps	Number of cycles	Temperature ($^{\circ}$ C)	Duration
Initial denaturation	1	95	2 min
Denaturation	30	95	20 sec
Annealing		60	20 sec
Extension		72	15 sec
Final extension	1	72	3 min

Hold		4	∞
------	--	---	---

Table 4.2.8.3 PCR program for amplification of GFP-actin fragments

Vector pSIH-CMV-TrkB-EGFP-IRES-mCherry-KDEL digestion

Reagents	Volume
Vector	5 µg
XbaI	2 µl
NheI	2 µl
10 × NEBuffer™3.1	2 µl
Water to	50 µl

Ligation setup of vector and GFP-actin

Positive ligation

Reagents	Volume
vector	25 ng
Insert (GFP-actin)	29.75 ng
T4 ligase (Fermentas)	2 µl
10 × T4 ligase buffer (Fermentas)	2 µl
Water to	20 µl

Negative ligation

Reagents	Volume
vector	25 ng
No insert	0
T4 ligase (Fermentas)	2 µl

10 × T4 ligase buffer (Fermentas)	2 µl
Water to	20 µl

Screening pSIH-GFP-actin-IRES-mCherry-KDEL with restriction enzyme EcoRI

Reagents	Volume
Plasmid	500 ng
EcoRI	2 µl
10 x EcoRI buffer	2 µl
Water to	20 µl

4.2.9 HEK^{293T} and NSC34 cell line culture

HEK^{293T} and NSC34 cells were maintained in a humid incubator, supplied with 5% CO₂, and controlled at 37°C. Complete growth medium contains 2 mM GlutaMAX, 10% fetal calf serum (FCS) (Linarisblue, SBF3119KYA), and 1% penicillin-streptomycin (P/S) (Thermo Fisher, 15070063) in high glucose Dulbecco's Modified Eagle Medium (DMEM) (Gibco™, 61965059). To maintain the cell lines, cells were passaged approximately three times per week. Once the confluency reached 80-90%, cells were passaged to a new T-75 cm² flask (ThermoFisher), with fresh complete growth medium to maintain an optimal density. For passaging cells, spent culture medium was removed with vacuum pump and discarded. Then, cells were washed twice with pre-warmed PBS to remove cell debris. At this step, PBS was carefully added to the side of the flask. After washing, 2 ml trypsin/EDTA (Thermo Scientific, 25300062) was added directly to the center of cells and the flask was gently fluctuated to let trypsin/EDTA cover all the cells, followed by an incubation for 2 min at 37°C. Then cells were observed under microscope and when the detachment of cells reaches 90%, prewarmed complete culture medium was added into the flask. After pipetting the complete culture medium to blow the cell layer surface, the medium containing cells was

collected and transferred to a 15 ml falcon and centrifuged at the speed of 400 g for 5 min. The pellet at the bottom of the falcon was resuspended using 5 ml pre-warmed complete culture medium after removal of the suspension. For cell counting, 10 μ l of the cell suspension was diluted and cells were counted using Neubauer chamber (Marienfeld). At the end, around 5×10^4 cells/cm² were seeded into a new T-75 cm² flask and 25 ml complete growth medium was added for the maintenance. During the cell culture, complete medium was changed each 2-3 days.

4.2.10 Validation of constructs containing fluorescent proteins

HEK^{293T} and NSC34 cells were used to test whether the constructed plasmids could express fluorescence proteins successfully. For this purpose, approximately 50,000 cells were plated into one well of a 24-well dish and cultured in complete culture medium containing DMEM, 10% FCS, 2 mM GlutaMAX and 1% P/S. When the cells were 70-90% confluent, LipofectamineTM 2000 transfection reagent (Invitrogen, 11668-030) was used for transfection of plasmids. According to the protocol, 2 μ l of Lipofectamine 2000 reagent was diluted in 50 μ l Opti-MEM Medium (Invitrogen, 51985-026) in a 1.5 ml reaction tube and 1 μ g DNA diluted in 50 μ l Opti-MEM Medium in another reaction tube. After mixing the reagents in each tube, diluted DNA was added into diluted Lipofectamine 2000 reagent, and the mixture was incubated at RT for 5 min. Next, 50 μ l of the DNA-lipid complex was added into one well. The cells were cultured with complete culture medium in a humid incubator at 37°C with 5% CO₂. On the next day, the culture medium was completely sucked up to remove the transfection reagent and cells were fed with pre-warmed complete culture medium. 1-3 days after transfection, the expression of corresponding fluorescent proteins was examined using a fluorescent cell culture microscope.

4.2.11 Virus production, titration, and transduction

As previously described, HEK^{293T} cells and helper plasmids including pCMVΔR8.91 and pCMV-VSVG were used for lentiviral production (Rehberg, Lepier et al. 2008, Subramanian, Wetzel et al. 2012). Our technical colleague Christian-Albrecht Mehling was responsible for providing HEK^{293T} cells and another colleague Hildegard Troll performed the virus production. First, HEK^{293T} cells were transfected with plasmid constructs using calcium-phosphate reagents and then cultured in a humid 5% CO₂ containing incubator at 37°C with full culture medium. After 47 h, the cultured medium containing viral particles was transferred into a tube and lentivirus particles were collected by ultracentrifugation. Viral titration was performed using HEK^{293T} cells. 80,000 HEK^{293T} cells were transduced with a serial dilution of lentiviruses and seeded into a 24-well dish and then cultured in full culture medium (DMEM + 10% FCS +1% P/S) in a 5% CO₂ humid incubator at 37°C. For a serial dilution of lentiviral particles, 12 × 1.5 ml tubes were first prepared. 50 µl full culture medium was added into the first tube and 25 µl to the rest 11 tubes. 2 µl of the virus pellet was added into the first tube and mixed by pipetting up and down. Then, 25 µl of the suspension from the first tube was transferred into the second tube, mixed again by pipetting up and down and again 25 µl of the suspension in the second tube was transferred into the third tube. This step was repeated for all the tubes such that a serial dilution of 10-fold was achieved. Finally, each serial dilution was added into one well that was seeded previously with HEK^{293T} cells and incubated overnight. On the second day, the full culture medium was replaced and 48 h after the transduction, colonies expressing corresponding fluorescent proteins were counted under a cell culture fluorescent microscope. The last dilution in which fluorescent signal was still detected determines the number of infectious particles. After the virus titration, the desired volume of lentiviral particles was added into the supernatant of motoneurons and incubated for 10-15 min at RT before plating cells onto coverslips or dishes.

4.2.12 DNA extraction for genotyping

For genotyping of DNA, a quick and dirty method or a chloroform method was applied for DNA extraction. One fourth of the head or tails were obtained from mouse embryos. For fast method with quick and dirty lysis buffer, 20 µl proteinase K (from 10 mg/ml stock) was added into each 200 µl quick and dirty lysis buffer in a 2 ml tube. The thermomixer (Eppendorf) was set to the temperature of 60°C. During dissection of the embryos, ¼ of head or tail was transferred into corresponding labelled tube containing lysis buffer and proteinase K (GeneOn, 405-010). The tubes were then placed in the thermomixer at 60°C and shaken at the speed of 850 rpm for 30 min-1 h till the samples were completely lysed. Then, lysed samples were incubated at 99°C for 20 min to inactivate proteinase K, followed by centrifugation at 20,000 g for 5 min. 100 µl supernatant was added into a new 1.5 ml collection tube and diluted with 100 µl 10 mM Tris-HCl (pH 8). 1 µl DNA was used as template for the PCR reaction. For chloroform method, biopsies from heads or tails were placed in a 2 ml tube containing 20 µl proteinase K and 500 µl lysis buffer and incubated in a thermomixer at 60°C for shaking overnight at the speed of 750 rpm. On the next day, 430 µl 5 % SDS and 170 µL 3 M NaCl were added into each 2 ml tube, followed by a vortex for 30 sec. Then, 750 µl chloroform was added to each tube. These tubes were whirled using a reagents mixer (Hartenstein) around 30 sec till the suspension became white. Suspensions were centrifuged at the speed of 400 g for 5 min at 4 °C. After centrifugation, 700 µl of the upper phase was taken out and transferred into a new 1.5 ml collection tube. 700 µl isopropanol (Sigma-Aldrich, 33539) was added to the collection tubes, followed by centrifugation at the speed of 20,000 g for 5 min at 4°C to get the DNA pellet. Then the supernatant was discarded, and the pellets were washed with 70% ethanol. Ethanol was removed after 2 min centrifugation at 20,000 g at 4°C. The pellets were then placed at RT for 10 min till they were dry. Dissolve and Reconstruction were performed by adding 100 µl 10 mM Tris-HCl (pH 8) and incubation at 65 °C for 15 min.

4.2.13 Genotyping of transgenic mice

Genotyping PCR and DNA electrophoresis

DNA was extracted from heads or tails using quick and dirty method or chloroform method. The obtained samples were used for PCR reactions using Taq DNA polymerase (VWR, 733-1303) to determine the genotypes of Smn KO or TrkB KO mice. According to the protocol of VWR, corresponding DNA sample, corresponding primers, dNTPs, Betaine, Key buffer and Taq DNA polymerase were mixed in one microtube for one reaction. PCR reaction was performed using a Mastercycler machine (Eppendorf). For DNA electrophoresis, 2% agarose gels were prepared using 2 g agarose (Biozym, 840004) in 100 ml 1 x TAE buffer. After PCR reaction, 5 μ l 6 x DNA loading dye was added into each tube containing 25 μ l PCR reaction. 15 μ l of PCR reaction was loaded onto the 2% agarose gel and run at 150 mV for 20-30 min.

Genotyping PCR for Smn KO and WT (products: Smn KO ~600 bp; Smn WT 879 bp)

Components	25 μ l reaction	Final concentration
DNA	1 μ l	150-300 ng
primer SMN 201f (10 μ M)	0.5 μ l	0.2 μ M
Primer SMN1049r (10 μ M)	0.5 μ l	0.2 μ M
Primer SMN ko (10 μ M)	0.5 μ l	0.2 μ M
dNTPs (10 mM)	0.5 μ l	200 μ M
Betaine (5 M)	5 μ l	1 M
10 \times Key buffer (15 mM MgCl ₂)	2.5 μ l	1 \times
Taq DNA polymerase (VWR)	0.2 μ l	1 unit
water	14.3	

Genotyping PCR program for Smn KO and WT (products: Smn KO ~600 bp; Smn WT 879 bp)

Step	Number of cycles	Temperature (°C)	Duration
Initial denaturation	1	94	3 min
Denaturation	30	94	30 sec
Annealing		57	30 sec
Extension		72	1 min 30 sec
Final extension	1	72	5 min
Hold		4	∞

Table 4.2.13.1 Table of PCR program for Smn KO and WT genotyping

Genotyping PCR for *SMN2tgtg* (products: 424 bp)

Components	25 µl reaction	Final concentration
DNA	1 µl	150-300 ng
primer Tw3 (10 µM)	0.5 µl	0.2 µM
Primer Tw7 (10 µM)	0.5 µl	0.2 µM
dNTPs (10 mM)	0.5 µl	200 µM
Betain (5 M)	5 µl	1 M
10 × Key buffer (15 mM MgCl ₂)	2.5 µl	1 ×
Taq DNA polymerase (VWR)	0.2 µl	1 unit
water	14.8	

Genotyping PCR program for *SMN2tgtg* (products: 424 bp)

Step	Number of cycles	Temperature (°C)	Duration
Initial denaturation	1	94	3 min
Denaturation	30	94	30 sec
Annealing		56	30 sec
Extension			

		72	30 sec
Final extension	1	72	5 min
Hold		4	∞

Table 4.2.13.2 Table of PCR program for *SMN2tgtg* genotyping

Genotyping PCR for TrkB KO (products: KO 179 bp; WT 369 bp)

Components	25 µl reaction	Final concentration
DNA	1 µl	150-300 ng
Primer TrkB-n2 (10 µM)	0.75µl	0.3 µM
primer TrkB-c8 (10 µM)	0.75 µl	0.3 µM
Primer Pgk3-1 (10 µM)	0.75 µl	0.3 µM
dNTPs (10 mM)	0.5 µl	200 µM
Betain (5 M)	5 µl	1 M
10 × Key buffer (15 mM MgCl ₂)	2.5 µl	1 ×
Taq DNA polymerase (VWR)	0.15 µl	0.75 unit
water	13.6	

Genotyping PCR program for TrkB KO and WT (products: KO 179 bp; WT 369 bp)

Step	Number of cycles	Temperature (°C)	Duration
Initial denaturation	1	94	3 min
Denaturation	30	94	30 sec
Annealing		59	30 sec
Extension		68	30 sec
Final extension	1	68	5 min

Hold		4	∞
------	--	---	----------

Table 4.2.13.3 Table of PCR program for TrkB KO and WT genotyping

5. Results

5.1 ER enters growth cone filopodia and moves along actin filaments in filopodia.

In developing neurons, the stability of MTs regulates axonal ER and the extension of ER tubules into the axon depends on MT plus-end motor kinesin heavy chain isoform 5A (KIF5) (Farías, Fréal et al. 2019). In the growth cone of rat sympathetic neurons, ER structures labeled by a fluorescent lipophilic dye 3,3'-Dihexyloxacarbocyanine iodide (DiOC6(3)) have been shown to co-align with MTs but barely move beyond them (Dailey and Bridgman 1989). In addition to MTs, an actin-based motor myosin Va can drive ER transport into dendritic spines of Purkinje neurons (Wagner, Brenowitz et al. 2011), indicating the important role of actin in ER movements in neuronal processes. However, little is known about the ER distribution and dynamics in growth cone filopodia that are enriched in actin filaments but mostly lack MTs (Geraldo and Gordon-Weeks 2009). To study whether ER could enter in actin-rich filopodia, primary cultured mouse motoneurons were transduced with lentiviral particles expressing the fluorescent protein mCherry fused KDEL, an ER-resident protein, to visualize ER (mCherry-ER) and then immunostained against mCherry-ER with anti-mCherry antibody, F-actin with phalloidin and MTs with anti- α -tubulin antibody. SIM microscope was applied for assessment of the association of ER with microtubules or actin filaments (Fig.5.1.1 A). 3D reconstruction (Fig. 5.1.1 B) and line scan analysis (Fig. 5.1.1 C) of mCherry-ER, F-actin and microtubules indicated that ER distributes in both growth cone filopodia and core. Interestingly, in growth cone filopodia, ER overlaps mainly with F-actin where there is a lack of MTs, while it colocalizes with both MTs and F-actin in the core. To confirm that ER moves into filopodia and whether its movements are associated with actin

filaments, I first performed live cell imaging of growth cones of motoneurons transduced with a lentivirus expressing cell volume marker GFP and co-transduced with lentiviral particles expressing mCherry-ER at the speed of 2 sec/frame over 15 min (Fig. 5.1.2 A). Consistent with observation of immunostaining, live cell imaging and analysis of mCherry-ER and GFP in filopodia demonstrated that ER enters in some but not all the filopodia during the imaging time (Fig. 5.1.2 A and B). As the next step, motoneurons were transduced with lentiviral particles co-expressing GFP-actin to visualize actin filaments and mCherry-ER. Live cell imaging of GFP-actin and mCherry-ER was performed to assess the association of movements of actin filaments and ER at the intervals of 2 sec for 8 min (Fig. 5.1.3 A and B). ICS python implementation (Wiseman 2015) (Fig. 5.1.3 C) was applied for analysis of dynamics of actin filaments and mCherry-ER in filopodia by calculating intensity movements ($\mu\text{m}/\text{sec}$). Notably, ER extends and retracts with F-actin in some filopodia (Fig. 5.1.3 A), while in some other filopodia, ER moves along F-actin but F-actin itself does not move (Fig. 5.1.3 B). Image Correlation Spectroscopy (ICS) analysis shows significantly higher dynamics of actin filaments than those of mCherry-ER in filopodia (Fig. 5.1.3 D). Taken together, ER enters growth cone filopodia of cultured motoneurons along actin filaments and filopodia ER movements are not passively forced by movements of actin filaments.

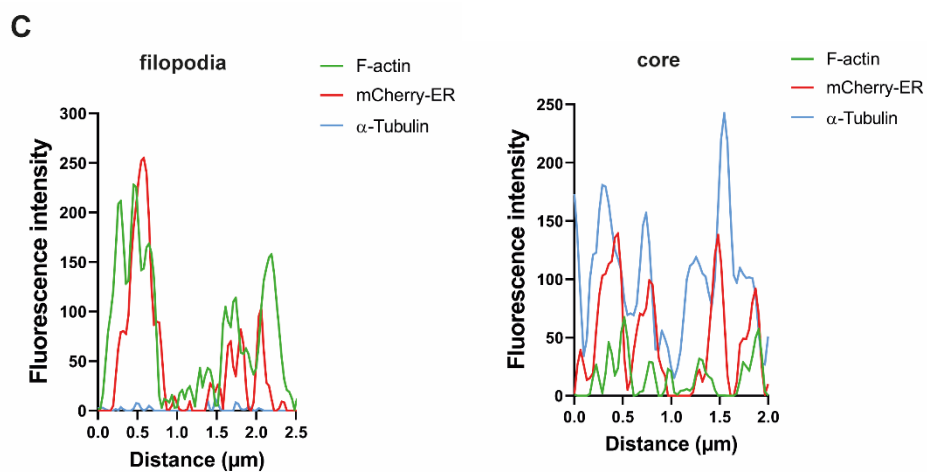
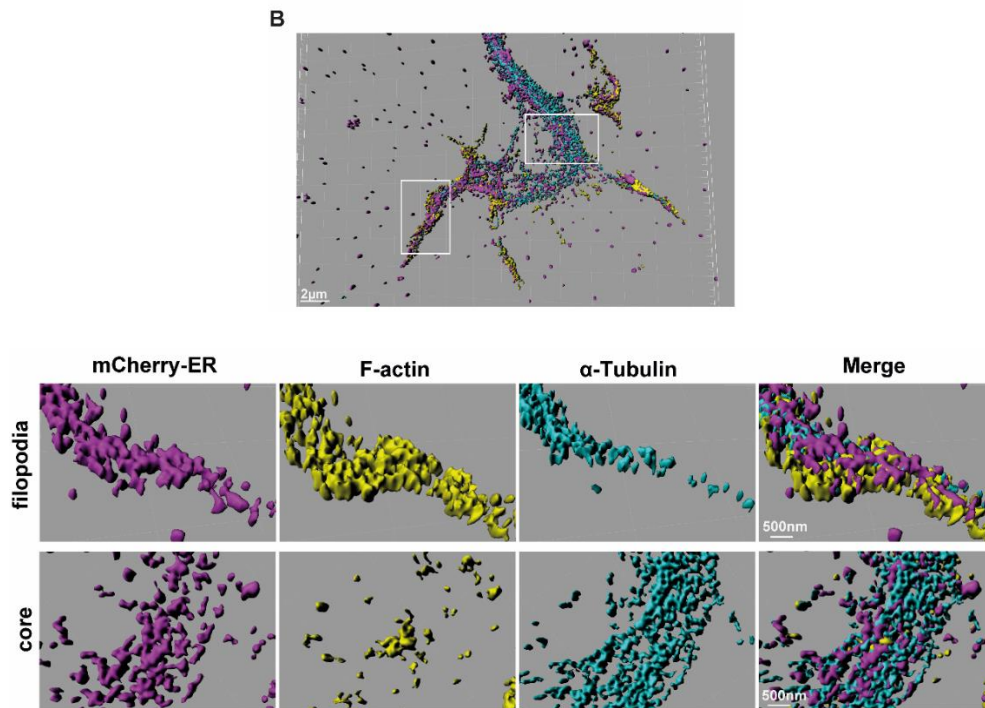
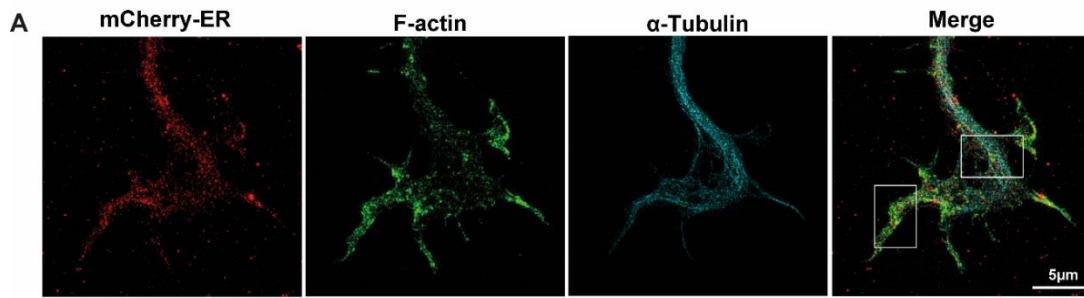


Figure 5.1.1 ER distributes in the growth cone core and filopodia of cultured motoneurons. (A) Cultured motoneurons were transduced with a lentivirus expressing mCherry-KDEL (mCherry-ER) to mark ER structure. Fixed cells were immunostained with antibodies against mCherry-ER, F-actin (Phalloidin) and MTs (α -Tubulin). (B) 3D reconstruction of representative image of the growth cone immunostained against mCherry-ER (purple),

F-actin (green) and α -Tubulin (cyan). Magnified images indicated by white square boxes show that in filopodia, mCherry-ER mainly overlaps with F-actin, while it connects with both α -Tubulin and F-actin in core. (C) Representative line scan analysis of mCherry-ER (red), F-actin (green) and α -Tubulin (cyan) in filopodia and core, showing overlapping of ER with F-actin in filopodia and with both F-actin and α -Tubulin in core.

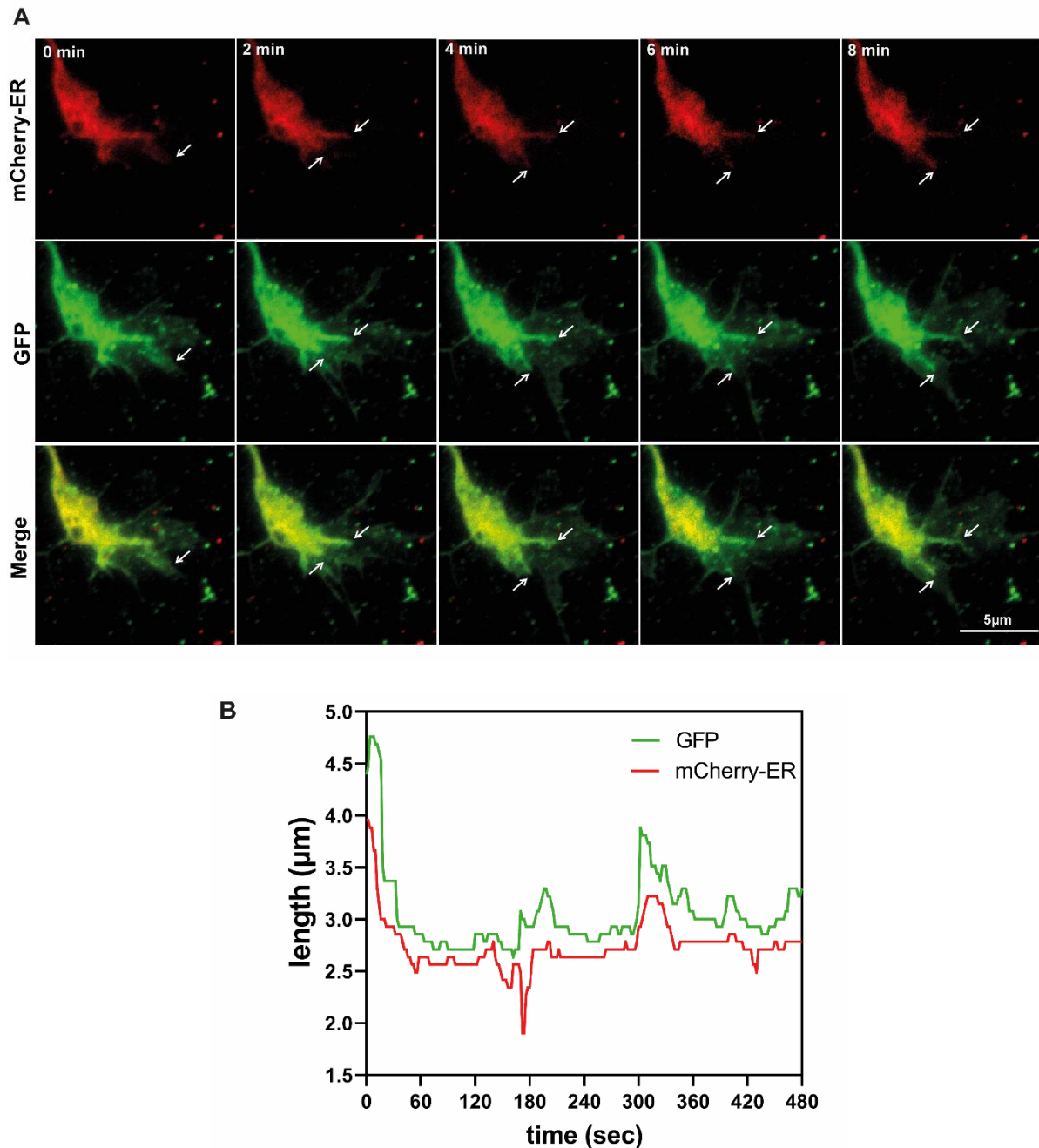


Figure 5.1.2 ER moves into growth cone filopodia and these movements are different from membrane filopodia movements. (A) Motoneurons were co-transduced with a lentivirus expressing GFP and another lentivirus that expresses mCherry-ER to visualize the whole growth cone and ER. Arrows in representative time lapse images indicate movements of ER filopodia into GFP marked filopodia. (B) The graph shows a representative movement event of ER filopodia and GFP labeled membrane filopodia over 8 min.

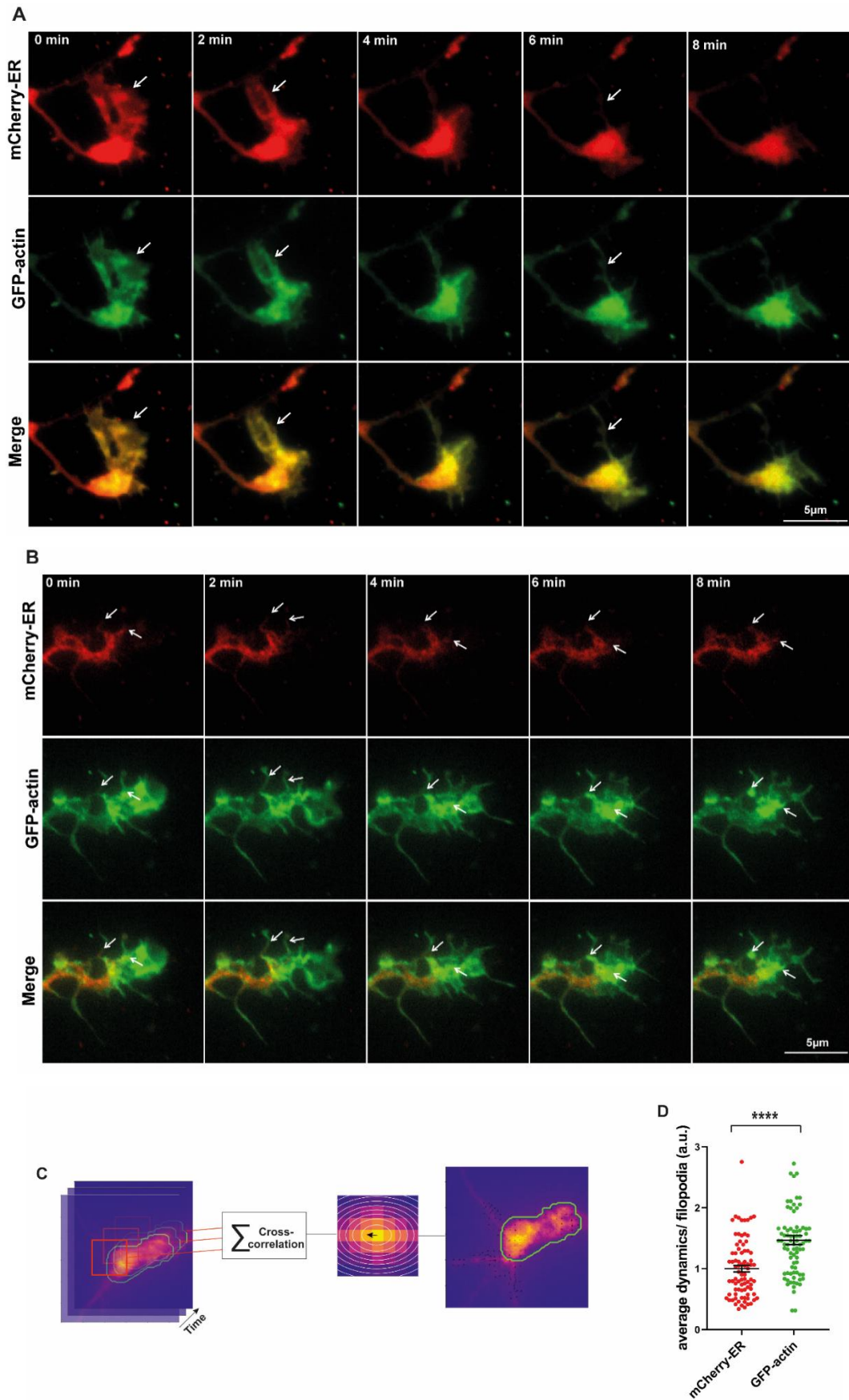


Figure 5.1.3 In cultured motoneurons, ER movements in filopodia are coordinated by actin filaments. (A and B) Motoneurons were transduced with a lentivirus co-expressing mCherry-ER and GFP-actin and live cell imaging was performed to assess association of ER and F-actin movements. Arrows in representative time lapse

images of the growth cone in Fig. A show the co-movements of mCherry-ER and GFP-actin in some filopodia. In Fig. B, arrows indicate that mCherry-ER retracts and extends along F-actin in some filopodia, but F-actin itself does not move together with mCherry-ER. (C) ER dynamics in growth cones were analyzed using ICS python implementation. The graph shows the workflow. (D) ICS analysis of mCherry-ER and GFP-actin in the same filopodia indicates that dynamics of actin filaments are significantly higher than those of filopodia ER (****, $P < 0.0001$; $n = 83$ filopodia, 3 independent experiments). Statistical analysis: two-tailed Mann Whitney test. Data are shown in scatter dot plot, with mean \pm SEM.

5.2 ER movements in growth cones of cultured motoneurons are regulated by actin and microtubule cytoskeleton

Observations from SIM analysis and live cell imaging implicate that ER movements in filopodia might be regulated mainly by actin but not MTs, while in the core it might be associated with both actin and MTs. To check this hypothesis, pharmacological treatments with 1 $\mu\text{g/ml}$ cytochalasin D (CytoD) for 30 min and 10 μM nocodazole for 2 h were applied to motoneurons to disrupt actin filaments and MTs, respectively. Motoneurons were transduced with lentiviral particles expressing mCherry-ER to visualize ER and live cell imaging was performed at the speed of 2 sec/frame over 15 min (Fig. 5.2.1 A, B and C). For analysis of ER dynamics, we performed both ICS analysis and manual analysis using multiple kymographs. To test the error of ICS analysis, we analyzed fixed cells and almost no ER dynamics can be detected (Fig. 5.2.2 A), which indicates the low error of this analysis. Using manual analysis, we analyzed the frequency of ER movements and the distance moved in each movement event. Strikingly, ICS analysis discovered that ER dynamics in growth cone filopodia are notably higher, compared to those in the growth cone core. Moreover, manual analysis revealed that the velocity of ER movements in filopodia is higher, and the distance moved in individual ER movement in filopodia is also greater, in contrast to those in the growth cone core (Fig. 5.2.2 B and C). Differences in filopodia and core ER dynamics further indicate that movements of ER in distinct sub-regions of growth cones might be controlled by different mechanisms. As shown in Fig. 5.2.3 A, CytoD treatment causes 80% of

motoneurons suffering from a failure of ER movements in filopodia, while nocodazole treatment results in 50% of cells failing to show ER movements. Double treatments with CytoD and nocodazole destroy ER dynamics in 90% of motoneurons (Fig. 5.2.3 A). Furthermore, ICS analysis showed a significant decrease in filopodia ER dynamics after CytoD or nocodazole treatment, as well as double treatments (Fig. 5.2.3 B), indicating that movements of ER in growth cone filopodia rely on both actin and MTs. More interestingly, the frequency of ER movements in filopodia was significantly reduced by CytoD treatment but not by nocodazole treatment, even though there was a slight reduction (Fig. 5.2.3 C), providing the evidence that filopodia ER movements depend mainly on actin cytoskeleton. In the growth cone core, CytoD or nocodazole treatment both resulted in approximately 40% of cells that had a failure in ER movements and upon double treatments around 80% of cells did not show ER movements (Fig. 5.2.4 A). Results from ICS analysis revealed a disruption in ER dynamics upon either CytoD or nocodazole treatment, as well as double-treatments (Fig. 5.2.4 B). Different from filopodia, the frequency of ER movements in the core was reduced after treatment with either CytoD or nocodazole (Fig. 5.2.4 C), implying a comparable importance of actin and MTs for regulation of ER dynamics in the growth cone core.

In conclusion, these data revealed high ER dynamics in axon terminals of cultured developing mouse motoneurons. The ER in axon terminals shows higher dynamics in filopodia than in the core. Filopodia ER dynamics are mainly coordinated by actin filaments, while core ER dynamics seem to rely on both actin and MTs cytoskeleton.

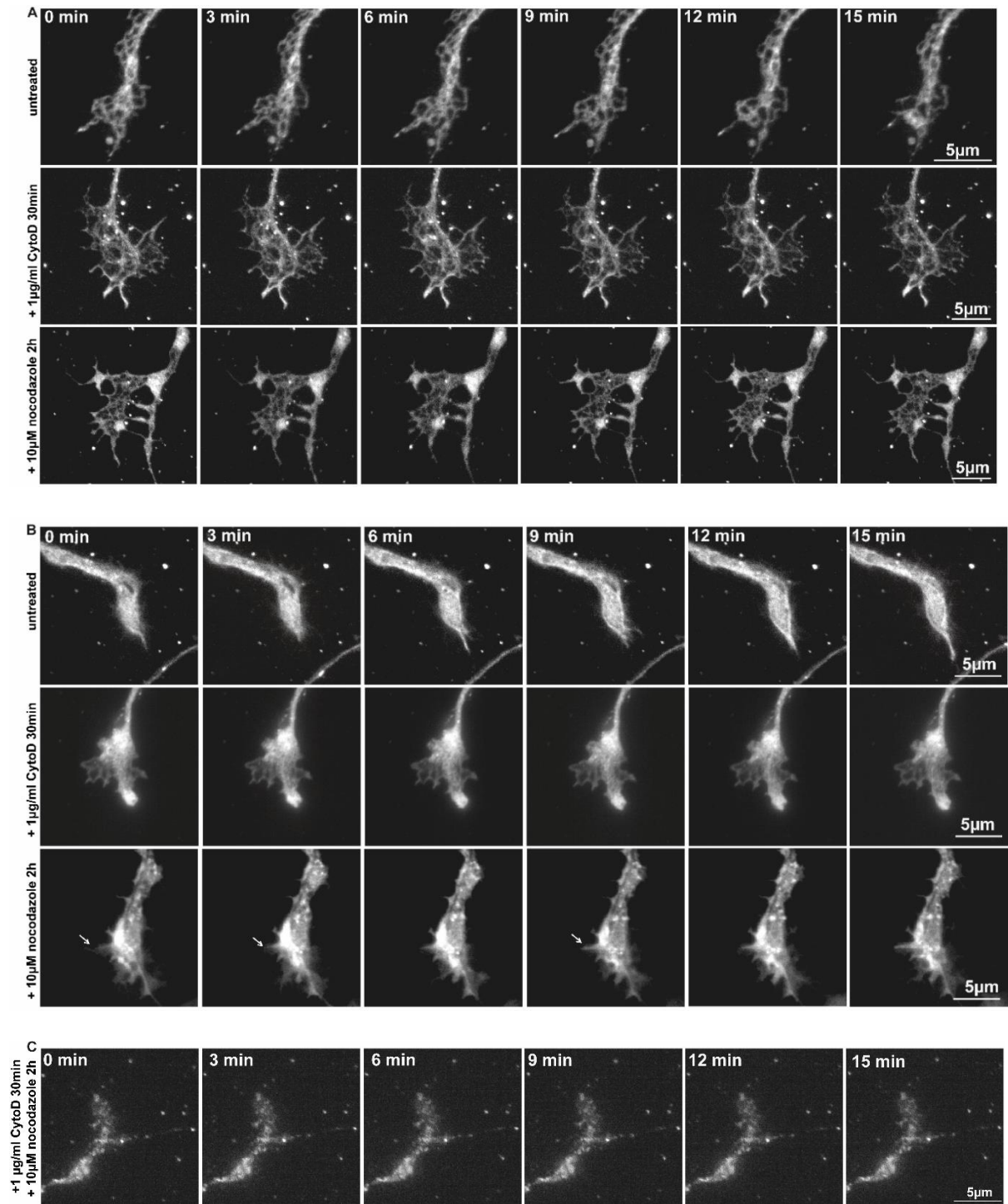


Figure 5.2.1 ER dynamics in growth cone filopodia and core after different treatments. (A) Representative time lapse images of growth cone cores of motoneurons transduced with a lentivirus expressing mCherry-ER after CytoD and nocodazole treatments. (B) Representative time lapse images of growth cone filopodia of motoneurons expressing mCherry-ER in untreated, CytoD or nocodazole-treated neurons. Arrows indicate filopodia ER movements after nocodazole treatment. (C) Representative time lapse images of the growth cone after a double treatment with CytoD and nocodazole.

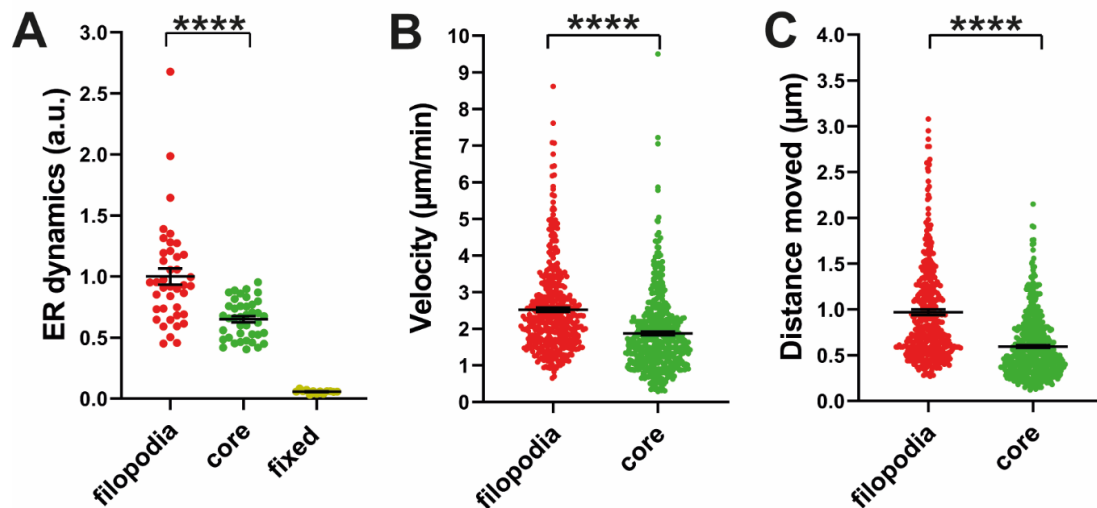


Figure 5.2.2 ER dynamics in growth cone filopodia are higher than those in the growth cone core. (A) Quantification of ER dynamics in growth cone filopodia and core using ICS revealed significantly higher dynamics in filopodia, compared to the core (****, $P < 0.0001$; $n = 40$ cells, 6 independent experiments). In fixed cells, ICS analysis detects almost no movements. (B and C) Analysis of multiple kymographs shows that filopodia ER presents a higher velocity (B) and longer distance (C) moved by individual movements, in comparison to core ER (****, $P < 0.0001$; $n = 25-29$ cells, 3 independent experiments). Statistical analysis: two-tailed Mann Whitney test. Data are shown in scatter dot plot, with mean \pm SEM.

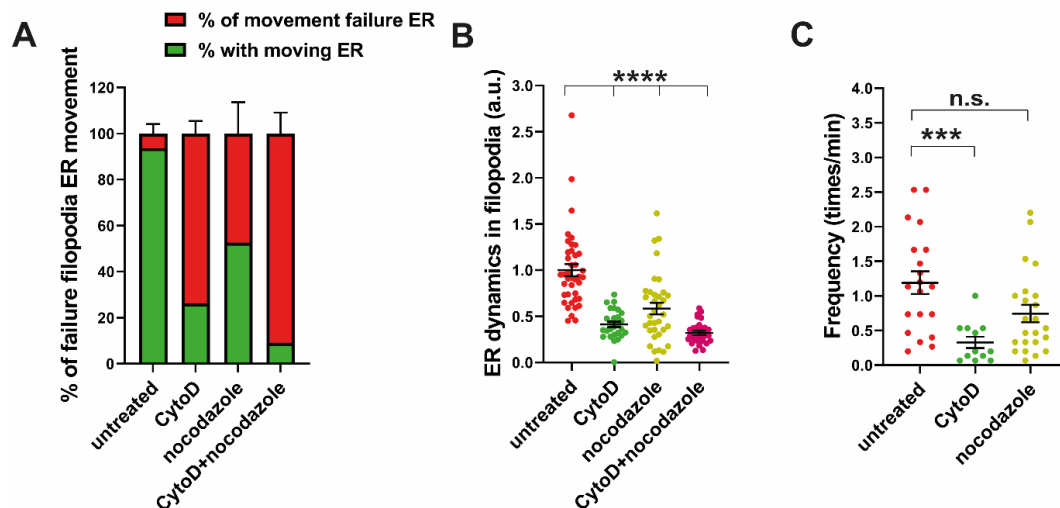


Figure 5.2.3 Filopodia ER are correlated especially with actin filaments. (A) Graph shows average percentage of motoneurons, which failed to show ER movements in filopodia after CytoD or nocodazole treatments. CytoD and nocodazole cause failure of filopodia ER movements in 78% and 65% of motoneurons, respectively. CytoD+nocodazole double-treatments result in an even higher percentage of ER movement failure, approximately 90%. Without treatment, only 10% of cells failed to show filopodia ER movements ($n = 32-55$

cells, 3 independent experiments). (B) ICS analysis of ER dynamics in filopodia shows that treatments with CytoD, nocodazole and double-treatments significantly reduce ER dynamics in filopodia (****, $P < 0.0001$; $n = 27-40$ cells, 3-5 independent experiments). (C) Frequency of ER movements in filopodia is decreased after CytoD treatment (***, $P = 0.0004$; $n = 12-20$ cells, 3 independent experiments), but not nocodazole treatment (n.s., $P = 0.1079$; $n = 20-23$ cells, 4-5 independent experiments). Statistical analysis: one-way ANOVA with Dunn's post-test. Data are shown in scatter dot plot, with mean \pm SEM.

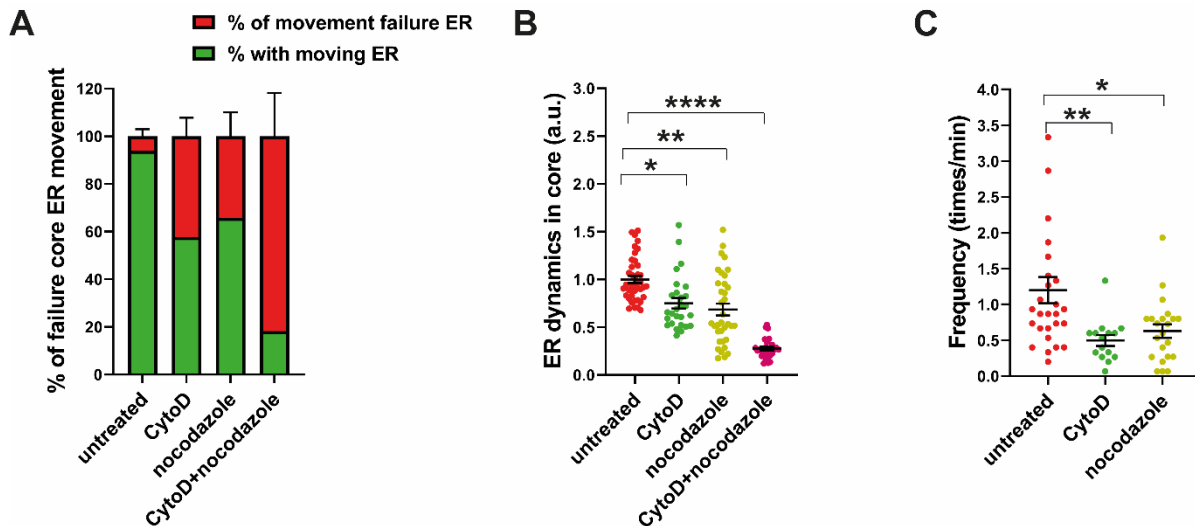


Figure 5.2.4 Core ER dynamics are regulated by actin and microtubules. (A) Quantification of average percentage of cells with failure in core ER movements discloses that with CytoD or nocodazole treatment, around 40% of cells do not show core ER movements, while double-treatments cause 80% failure in ER movements ($n = 32-55$ cells, 3 independent experiments). (B) ICS analysis of ER dynamics indicates that CytoD, nocodazole and double-treatments all reduce ER dynamics in growth cone core (*, $P = 0.0353$; **, $P = 0.0012$; ****, $P < 0.0001$; $n = 27-40$ cell, 3-5 independent experiments). (C) Frequency of core ER dynamics exhibits a significant reduction both after CytoD and nocodazole treatment (**, $P = 0.0016$; *, $P = 0.0271$; $n = 15-27$ cells, 4-6 independent experiments). Statistical analysis: one-way ANOVA with Dunn's post-test. Data are shown in scatter dot plot with mean \pm SEM.

5.3 Myosin VI and drebrin A are particularly involved in ER dynamics in axon terminals

The next question should be whether there are actin-based motor proteins that are involved in regulation of ER movements in growth cone filopodia. Myosin V and VI were found

expressed in cell bodies, neurites and growth cones of cultured chicken dorsal root ganglion neurons (Suter, Espindola et al. 2000). In isolated rat dorsal root ganglion neurons, Myosin II was also detected in growth cones, neurite processes and cell bodies (Miller, Bower et al. 1992). Previous studies have shown that myosin motor proteins are involved in local transport systems in postsynaptic compartments. For example, in Purkinje neurons, myosin Va serves as a transporter of ER into dendritic spines (Wagner, Brenowitz et al. 2011). As another example, myosin VI is highly expressed in the mouse brain and enriched at postsynapses (Osterweil, Wells et al. 2005). In myosin VI-deficient hippocampal neurons, the number of synapses is reduced, dendritic spines become shorter and internalization of α -amino-3-hydroxy-5-methyl-4-isoxazole propionic acid-type glutamate receptors (AMPA) induced by α -amino-3-hydroxy-5-methyl-4-isoxazole propionic acid (AMPA) and insulin stimulation is impaired (Osterweil, Wells et al. 2005). Myosin II regulates actin-bundle length and influences retrograde actin flow and cellular motility in neuronal growth cones (Medeiros, Burnette et al. 2006). However, little is known about functions of myosin proteins in presynaptic compartments of motoneurons. Here, pharmacological treatments were applied to inhibit myosin proteins. First, survival assay of motoneurons was carried out after treatment of specific myosin II inhibitor ((-)-blebbistatin), myosin V inhibitor (MyoVin-1) and myosin VI inhibitor (2,4,6-triiodophenol) at different concentrations and for different incubation time to test the toxicity of these drugs and find the proper dosage (Fig. 5.3.1 A, B and C). Next, 5 μ M (-)-blebbistatin, 30 μ M MyoVin-1 and 1 μ M 2,4,6-triiodophenol for 15 min were decided to be added to cultured motoneurons transduced with lentivirus expressing mCherry-ER and live cell imaging was performed at intervals of 2 sec/frame over 15 min (Fig 5.3.2 A). Astonishingly, myosin V and VI inhibitors impaired ER dynamics in filopodia, especially myosin VI that reduced ER dynamics to the highest extent, while myosin II inhibitor did not alter ER dynamics in filopodia (Fig. 5.3.2 B). Consistently, Myosin VI and myosin V

inhibitors but not myosin II caused a significant reduction in ER dynamics in the growth cone core (Fig. 5.3.2 C).

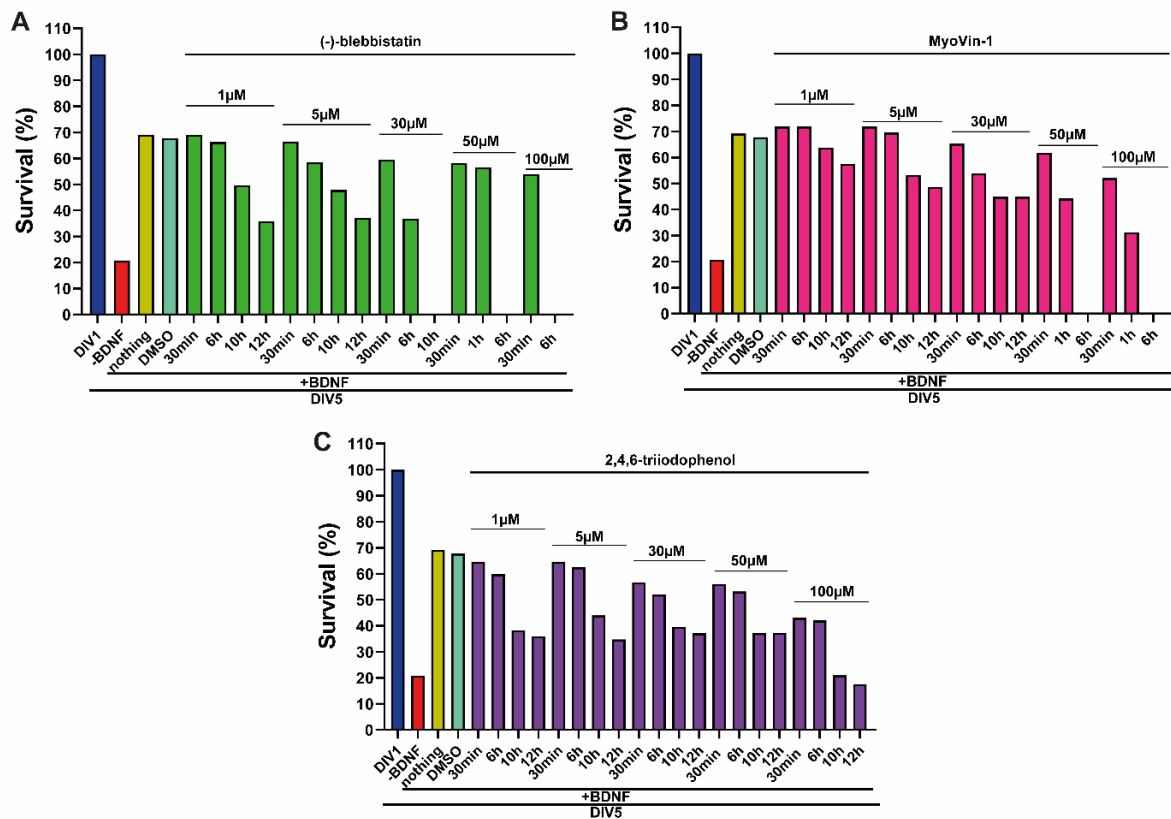


Figure 5.3.1 Survival assay of cultured motoneurons after pharmacological treatments with myosin inhibitors. (A, B and C) Motoneurons were treated with myosin II inhibitor ((-)-blebbistatin), myosin V inhibitor (MyoVin-1) and myosin VI inhibitor (2,4,6-triiodophenol) at different concentrations from 1 μ M to 100 μ M and incubation time ranges from 30 min up to 12 h. Graphs show percentage of survived motoneurons, respectively.

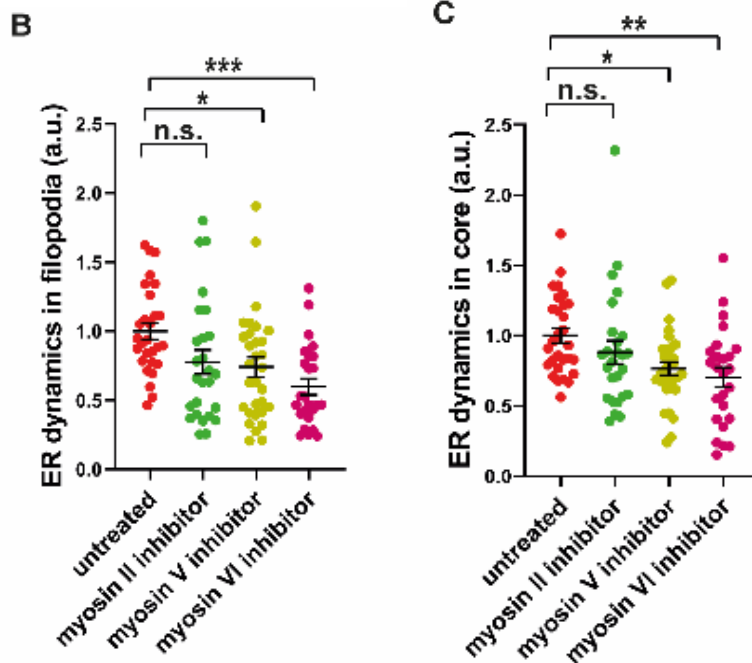
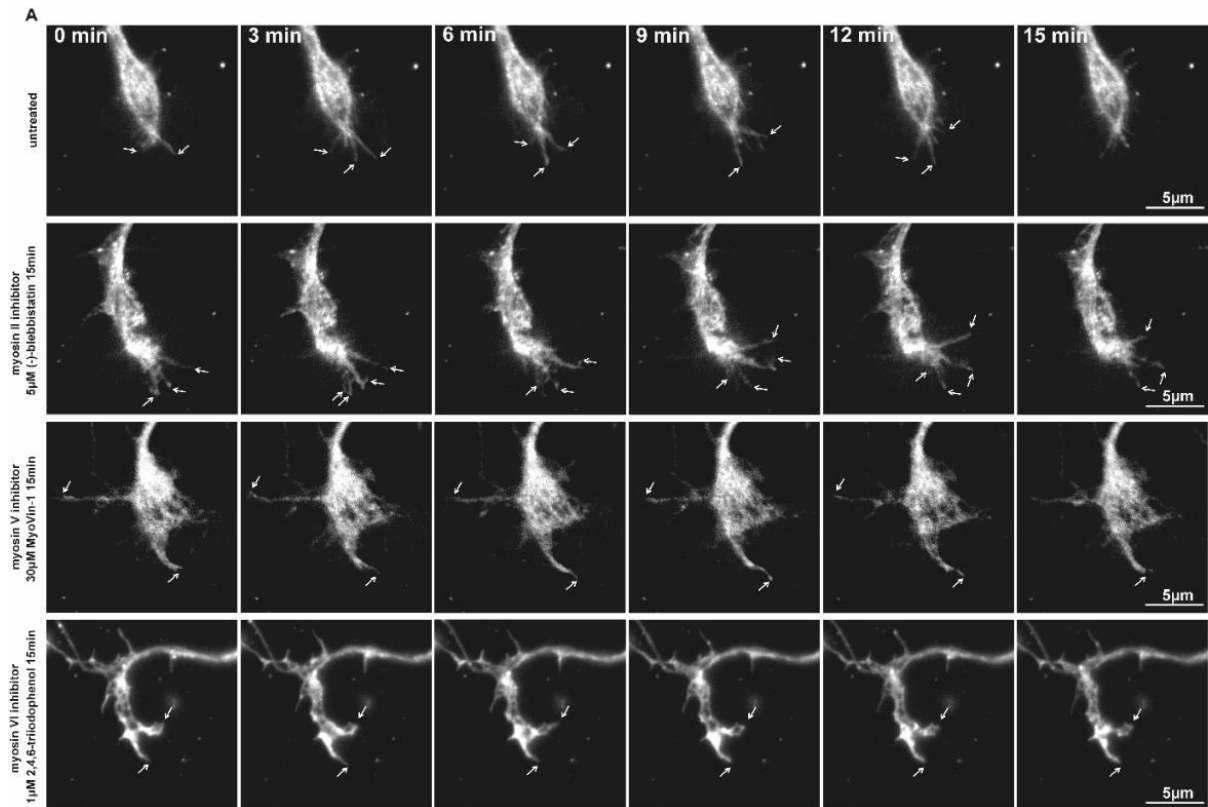
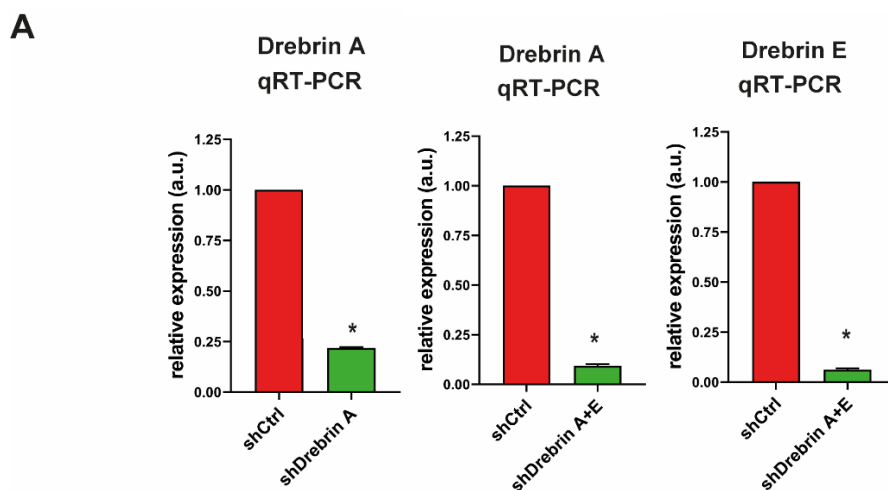


Figure 5.3.2 Myosin VI mediates filopodia ER movements in growth cones of cultured motoneurons. (A) Motoneurons transduced with lentiviral construct expressing mCherry-ER were first incubated with myosin II inhibitor (5 μM (-)-blebbistatin), myosin V inhibitor (30 μM MyoVin-1) and myosin VI inhibitor (1 μM 2,4,6-triiodophenol) for 15 min and then imaged at the intervals of 2 sec over 15 min. White arrows in time lapse images indicate the movements of filopodia ER in growth cones. (B) ICS analysis of ER dynamics in filopodia

uncovers that myosin V (*, $P < 0.0361$; $n = 28-31$ cells, 4 independent experiments) and myosin VI (***, $P < 0.0005$; $n = 25-28$ cells, 4 independent experiments) inhibitors reduce ER dynamics in filopodia, compared to untreated cells, among which myosin VI causes a higher reduction, approximately 40%. (C) Graph depicts a significant reduction of ER dynamics in core after myosin V (*, $P < 0.0339$; $n = 29-31$ cells, 4 independent experiments) and myosin VI inhibition (**, $P < 0.0099$; $n = 25-29$ cells, 4 independent experiments). Statistical analysis: one-way ANOVA with Dunn's post-test. Data are shown in scatter dot plot with mean \pm SEM.

Another question was asked whether disruption of actin/microtubule crosstalk affects core ER movements. Drebrin interacts with microtubule end-binding protein EB3 to link F-actin and MTs and this interaction mediates formation of growth cones and the extension of neurites (Geraldo, Khanzada et al. 2008, Trivedi, Stabley et al. 2017). Drebrin contains two isoforms: drebrin A and drebrin E (Shirao, Hanamura et al. 2017). Drebrin A is a neuron specific F-actin binding protein and specially enriched in synapses receiving excitatory inputs and regulates synaptic transmission (Ivanov, Esclapez et al. 2009). Inhibition of drebrin A delays synapse formation and retards accumulation of postsynaptic proteins such as postsynaptic density protein 95 (PSD-95) (Shirao, Hanamura et al. 2017). Drebrin E is present in axon growth cones and decorates F-actin to link F-actin to microtubules (Shirao, Hanamura et al. 2017). To examine this question, constructs of shDrebrin A was designed to knockdown drebrin A and shDrebrin A+E was also made to knockdown drebrin A and E together. These constructs also express GFP to mark the infected cells. An empty shRNA vector (shCtrl) that was only expressing GFP was used as control. First, lentiviruses of shDrebrin A and shDrebrin A+E were verified by evaluation of mRNA levels of motoneurons transduced with lentiviruses using qRT-PCR (Fig. 5.3.3 A) and assessment of protein levels using western blot (WB) (Fig. 5.3.3 B). Fig. 5.3.3 A showed that shDrebrin A lentivirus reduced approximately 90% of drebrin A mRNA after transduction to motoneurons and shDrebrin A+E causes around 90% and 94% reduction in drebrin A and drebrin E mRNA, respectively. For WB probed against drebrin, drebrin antibody detecting both drebrin A and drebrin E was applied

here. After knockdown of drebrin A by lentiviral transduction, drebrin protein level was remarkably reduced, compared to shCtrl and after shDrebrin A+E transduction, drebrin protein was hardly detectable (Fig. 5.3.3 B). These data confirmed efficient knockdown of drebrin using lentiviral transduction to motoneurons. Next, motoneurons were co-transduced with lentivirus expressing mCherry-ER and lentiviral particles shDrebrin A or shDrebrin A+E or shCtrl. Images of positively transduced live cells, recognized by GFP expression, were acquired at intervals of 2 sec over 15 min to assess ER dynamics in growth cones after drebrin knockdown (Fig. 5.3.4 A). Surprisingly, knockdown of drebrin A caused 40% reduction in ER dynamics in filopodia (Fig. 5.3.4 B) and 30% decrease in ER dynamics in the core (Fig. 5.3.4 C), compared to shCtrl. However, neither ER dynamics in filopodia nor in core were reduced further by additional knockdown of the drebrin E isoform (Fig. 5.3.4 B and C). Taken together, ER movements in filopodia depend especially on actin-based motor myosin VI. Drebrin A that mediates crosslink of actin and MTs is also required for ER dynamics in the growth cone.



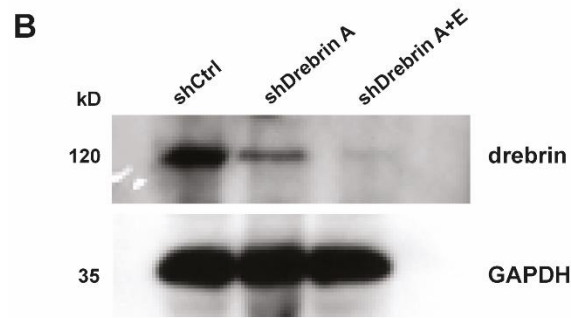
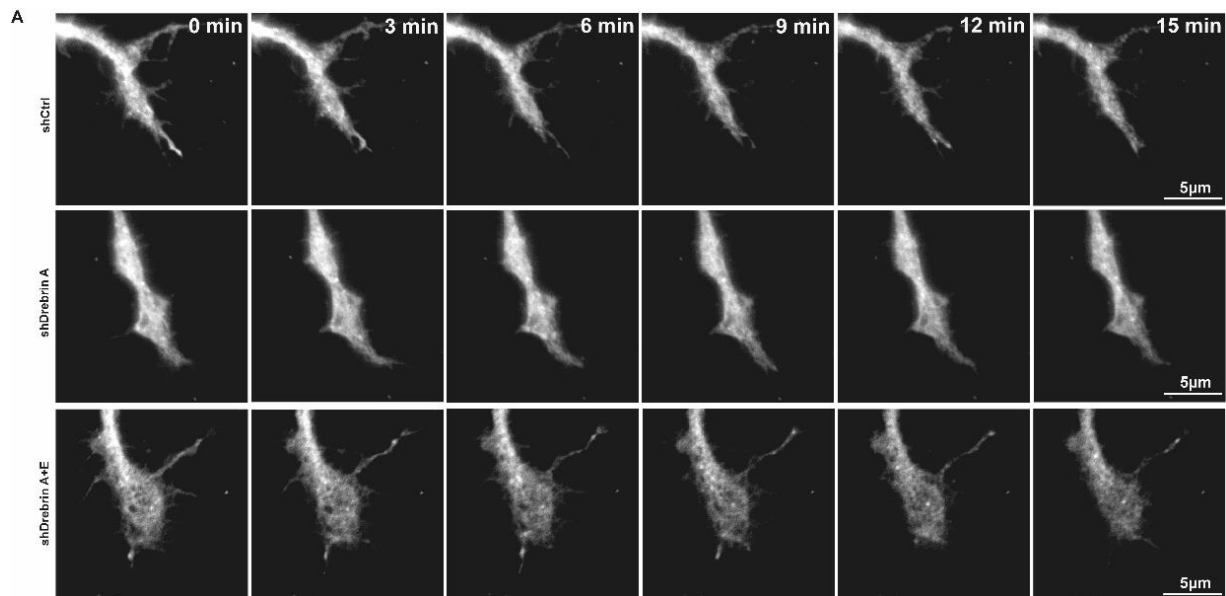


Figure 5.3.3 Knockdown of drebrin isoforms in cultured motoneurons. (A) Constructs of shDrebrin A were transduced to motoneurons to knockdown drebrin A and shDrebrin A+E to knockdown drebrin A and drebrin E. Quantification of mRNA expression of drebrin A and drebrin E of shDrebrin A and shDrebrin A+E transduced motoneurons confirms that shDrebrin A reduces around 80% of drebrin A mRNA (*, $P < 0.05$, 3 independent experiments) and shDrebrin A+E causes a 90% decrease in drebrin A mRNA ((*, $P < 0.05$, 3 independent experiments) and 94% in drebrin E mRNA levels ((*, $P < 0.05$, 3 independent experiments). (B) Western blot of lysates obtained from motoneurons transduced with constructs shDrebrin A and shDrebrin A+E confirms that shDrebrin A transduction results in much lower level of drebrin protein, compared to the control (shCtrl) and after shDrebrin A+E transduction, drebrin protein is not detected. Statistical analysis: one-tailed Mann Whitney test. Data are shown in scatter dot plot, with mean \pm SEM.



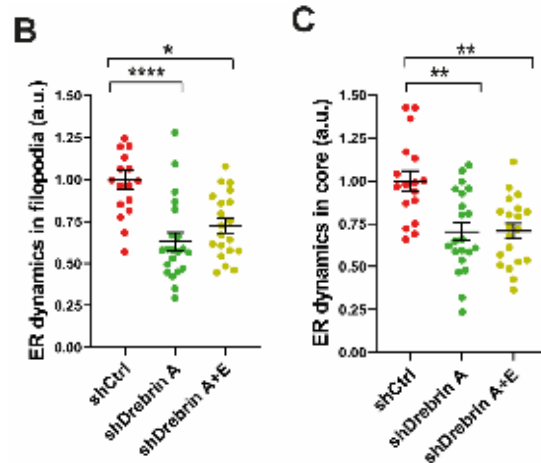


Figure 5.3.4 Drebrin A facilitates actin and microtubule regulated ER dynamics in axon terminals. (A) Representative time lapse images of growth cones of mCherry-ER expressing neurons transduced with shDrebrin A and shDrebrin A+E. (B) ICS analysis shows that knockdown of drebrin A reduces ER dynamics in filopodia (****, $P < 0.0001$; 3 independent experiments). Additional knockdown of drebrin E does not further decrease ER dynamics in filopodia (*, $P = 0.0133$; $n = 17-21$ cells, 3 independent experiments). (C) Graph shows a significant reduction of ER dynamics in core after knockdown of drebrin A (**, $P = 0.0026$), while additional knockdown of drebrin E does not escalate the reduction level (**, $P = 0.0019$; $n = 17-21$ cells, 3 independent experiments). Statistical analysis: one-way ANOVA with Dunn's post-test. Data are shown in scatter dot plot with mean \pm SEM.

5.4 BDNF-induced TrkB activation triggers redistribution of ribosomes in growth cones on a time scale of seconds

Numerous mRNAs (Briese, Saal et al. 2016, Holt, Martin et al. 2019) and translational machineries including ribosomes and ER (Merianda, Lin et al. 2009, Shigeoka, Jung et al. 2016) were observed in axonal compartment of neurons. In distal axons specific transcripts were confirmed to be locally translated (Moradi, Sivadasan et al. 2017, Terenzio, Koley et al. 2018, Biever, Glock et al. 2020) and locally synthesized proteins play critical roles in proteomic homeostasis and replenishment and response of neurons to distinct extracellular signals, contributing to neuron survival, development, and plasticity (Casadio, Martin et al. 1999, Campbell and Holt 2001, Ming, Wong et al. 2002, Jung, Yoon et al. 2012). During

development, guidance cue-induced asymmetrical protein synthesis in growth cones mediates attractive or repulsive turning towards or away from corresponding cues that are required for neurons to find their correct paths (Leung, van Horck et al. 2006, Piper, Anderson et al. 2006). BDNF binds its receptor TrkB, activates parallelly different signaling pathways including mTOR, ERK and PI3K and consequently initiates translation (Takei, Kawamura et al. 2001, Santos, Comprido et al. 2010). BDNF/TrkB signaling is involved in regulation of cytoskeleton dynamics via modulation of local translation of specific mRNAs such as β -actin and actin regulators or via activation of CREB that regulates the transcription of MTs bound factors such as the mitogen-activated protein kinase (MAPK) phosphatase 1 (MKP-1) (Gonzalez, Moya-Alvarado et al. 2016). Here, I am interested in extracellular BDNF induced dynamics of ribosomes in presynaptic compartments of cultured motoneurons. To study precisely how fast TrkB is activated by BDNF stimulation and to study the kinetics of ribosome activation, a series of BDNF stimulation for 10 s, 1 min and 10 min were carried out with cultured motoneurons. The same volumes of medium without BDNF were applied to the control group. After BDNF stimulation, medium was washed out and cells were directly fixed and immunostained against TrkB and phosphorylated TrkB (pTrkB), namely the activated form of TrkB. First, the specificity of antibodies against pTrkB and TrkB was tested by immunostaining of wildtype (WT) and TrkB knockout (KO) motoneurons after 10 min BDNF stimulation (Fig. 5.4.1 A and B). Next, WT motoneurons were stained against pTrkB and TrkB after 10 sec, 1 min and 10 min BDNF pulse (Fig. 5.4.2 A). Surprisingly, upon 10 sec BDNF stimulation a significant increase in pTrkB was detected (Fig. 5.4.2 B). Immunocytochemistry assays showed increased TrkB levels in growth cones upon 1 min BDNF pulse (Fig. 5.4.2 C). However, using WB of the whole lysates of cultured motoneurons, an increase in pTrkB was first detectable after 1 min BDNF stimulation, but no obvious augmentation was detectable in total TrkB levels in whole cell lysates (Fig. 5.4.2 D). Additionally, the levels of TrkB in soma detected by immunostaining did not increase (Fig.

5.4.2 E), combined with the result of WB suggesting that the transcription and translation of TrkB were not induced by a short time BDNF stimulation. But it raised the question from where this increased level of TrkB in growth cones came. An extremely rapid enhancement in immunoreactivity of TrkB within < 1 min in growth cones of motoneurons could be elucidated by the fast conformational changes or the release of TrkB from intracellular storages, thus exposing its antigens to the antibodies. The late increase within 10 min BDNF pulse could be interpreted by locally synthesized TrkB in growth cones and/or by transport of TrkB proteins from proximal axons into growth cones. Furthermore, Fig. 5.4.2 F and G show that anisomycin as a translation inhibitor or nocodazole that destroys MT-dependent axonal transport abolishes the enhancement in TrkB in the growth cone. This indicates that BDNF induces redistribution of TrkB and local translation and subsequently increases its immunoreactivity.

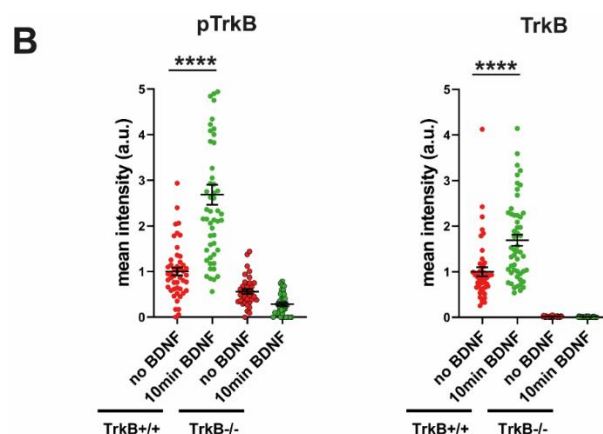
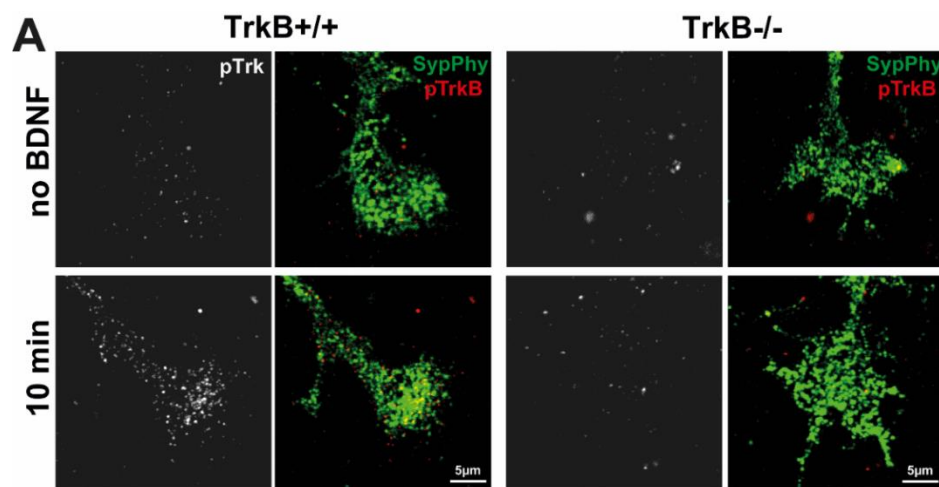
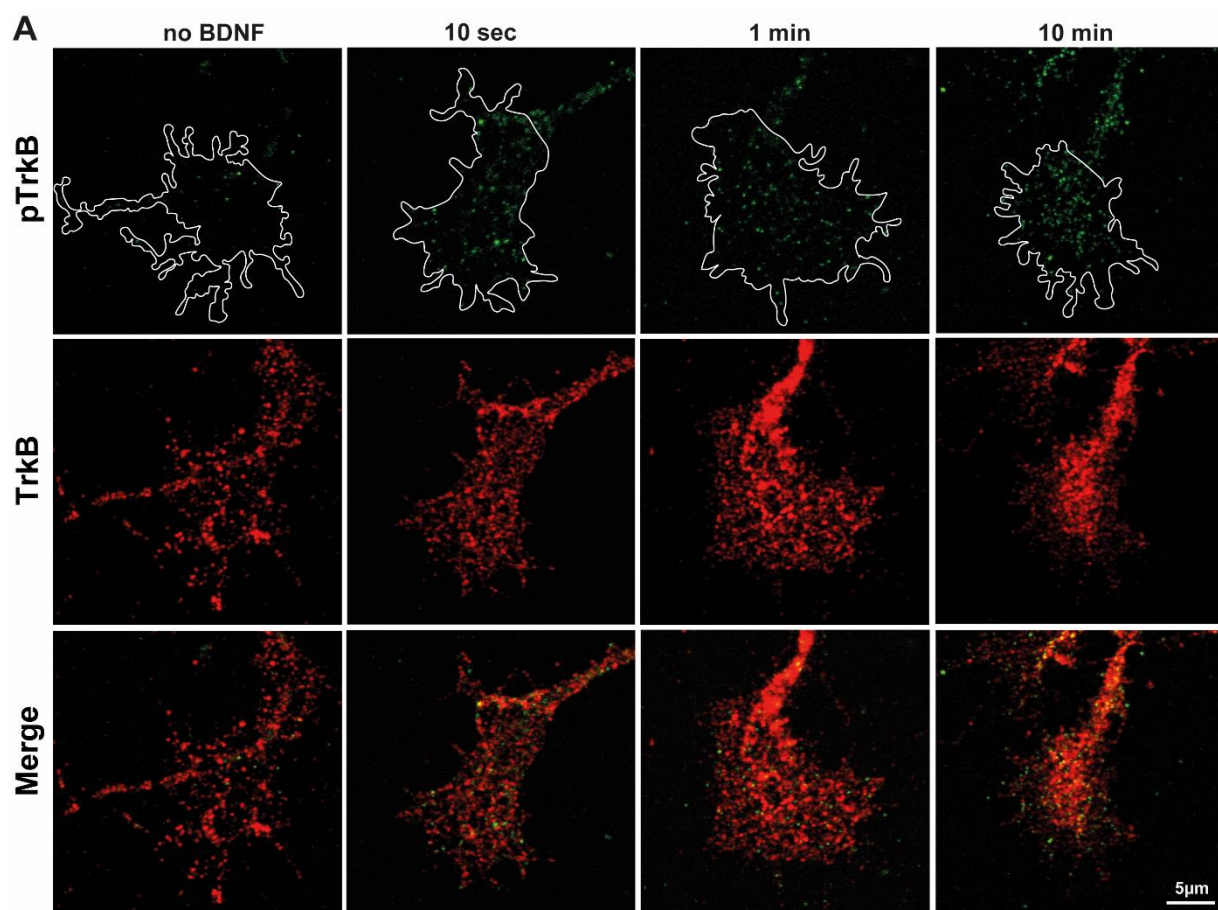


Figure 5.4.1 Specificity of antibodies against pTrkB and TrkB. (A) specificity of used anti-phosphorylated TrkB (pTrkB) and anti-TrkB antibodies was evaluated by immunostaining of WT and TrkB KO motoneurons after 10 min BDNF stimulation. Anti-synaptophysin antibody was applied for visualization of the growth cone. Shown are representative images of growth cones immunostained against pTrkB and synaptophysin or TrkB and synaptophysin. (B) Quantification of mean intensities of pTrkB and TrkB in TrkB KO motoneurons. Mean intensities of pTrkB do not increase compared to the WT group (*TrkB*^{+/+}: ****, $P < 0.0001$; $n = 47-52$ cells and *TrkB*^{-/-}: $n = 34-37$ cells, 1 experiment). In TrkB KO motoneurons, TrkB is hardly detected and not enhanced upon BDNF stimulation (*TrkB*^{+/+}: ****, $P < 0.0001$; $n = 47-52$ cells and *TrkB*^{-/-}: $n = 34-37$ cells, 1 experiment). Statistical analysis: two-tailed Mann Whitney test. Data are shown in scatter dot plot with mean \pm SEM.



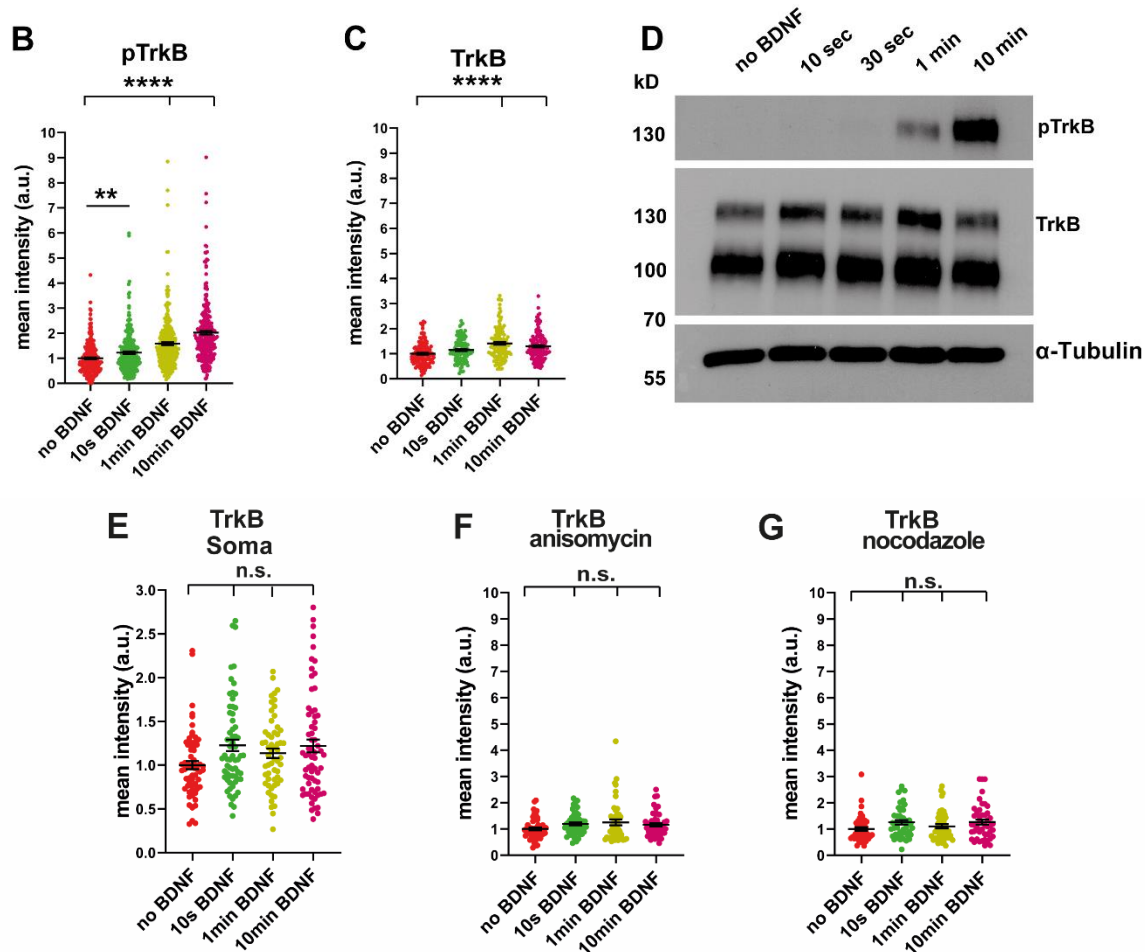
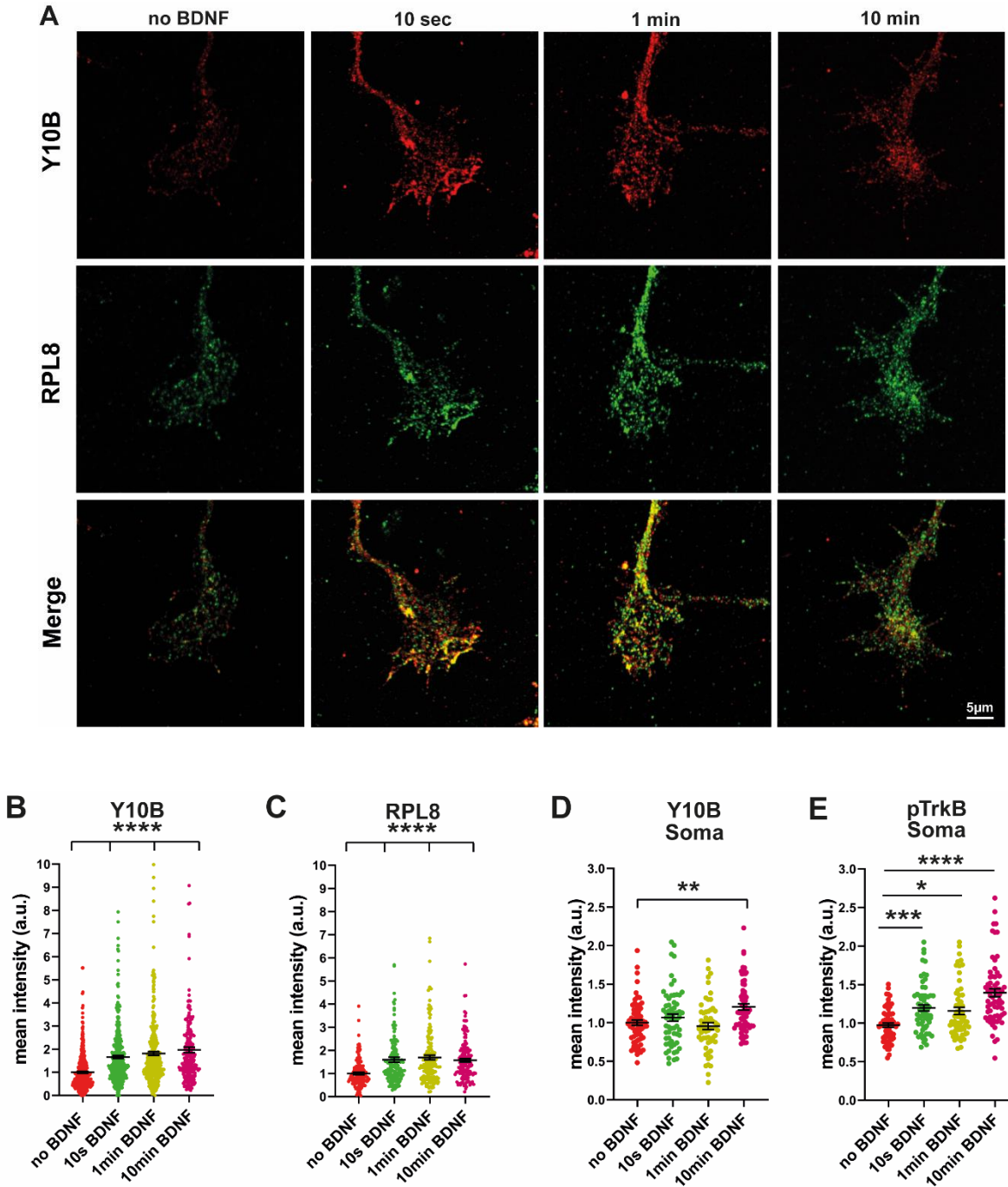


Figure 5.4.2 Extracellular BDNF stimulates TrkB activation on a time scale of seconds in cultured motoneurons. (A) Cultured motoneurons were fixed and immunostained with antibodies against pTrkB and TrkB after extracellular BDNF stimulation for 10 sec, 1 min, and 10 min. White outlines mark the ROIs of growth cones. (B) Quantification of mean intensity of pTrkB in growth cones shows that pTrkB levels are significantly enhanced upon 10 sec BDNF stimulation (**, $P=0.0063$; $n=265-267$ cells, 8 independent experiments), as well as 1 min and 10 min (****, $P<0.0001$; $n=265-267$ cells, 8 independent experiments). (C) Mean intensity of TrkB in growth cones increases after 1 min and 10 min BDNF stimulation (****, $P<0.0001$; $n=120$ - cells, 4 independent experiments). (D) WB of total lysates obtained from cultured motoneurons was probed against pTrkB and TrkB. α -Tubulin was used as a control. Western blot shows an obvious detection of pTrkB only after 1 min BDNF stimulation. (E) Quantification of mean intensity of TrkB in Soma does not show a significant increase after BDNF stimulation (n.s., $P\geq 0.1208$; $n=57-66$ cells, 3 independent experiments). (F and G) Increased mean intensity of TrkB in growth cones is inhibited upon treatment with anisomycin or nocodazole (n.s., $P\geq 0.0893$; $n=45-54$ cells, 2 independent experiments). Statistical analysis: one-way ANOVA with Dunn's post-test. Data are shown in scatter dot plot with mean \pm SEM.

During development, fast and precise regulation of translation in axons ensures the rapid response to different extracellular cues (Willis, van Niekerk et al. 2007, Yoon, Zivraj et al.

2009). The kinetics of ribosomal modulation induced by extracellular cues should be different in the growth cone from that in the cell body. To investigate the dynamics of ribosomal remodeling, motoneurons were first stimulated with BDNF and then immunostained with ribosomal markers: Y10B antibody, which binds to ribosomal ribonucleic acid (rRNA) and anti-RPL8 antibody that detects ribosomal protein L8 in the 60S large ribosomal subunits (Fig. 5.4.3 A). Remarkably, immunoreactivity of Y10B and RPL8 underwent an extremely rapid increase upon 10 sec BDNF stimulation (Fig. 5.4.3 B and C). However, the fast response of ribosomes to BDNF stimulation did not happen in the soma after 1 min BDNF exposure (Fig. 5.4.3 D). Only at a later timepoint of 10 min the immunoreactivity of Y10B increased in the soma, as shown in Fig. 5.4.3 D, even though a BDNF-induced enhancement in immunoreactivity of pTrkB was detectable within 10 sec (Fig. 5.4.3 E). This distinction in ribosomal response to BDNF/TrkB signaling in the growth cone and soma implies that regulatory mechanisms for ribosomal activation or regulation may be different in the soma and growth cones. To the question from where this increase in immunoreactivity of ribosome markers came, there are three major presumptions: transport from axons and soma, local translation of ribosome proteins and ribosomal changes in redistribution and conformation. To scrutinize these possibilities, pharmacological treatments with nocodazole and anisomycin were carried out to disrupt MT-dependent axonal transport and inhibit translation, respectively. As shown in Fig. 5.4.3 F and E, BDNF-induced enhancement in ribosomal immunoreactivity in growth cones was not affected upon nocodazole and anisomycin treatments. These data support that the ribosomal response to BDNF shown above rely neither on MT-dependent axonal transport nor on translation, indicating the third possibility of ribosomal redistribution and conformational change. Interestingly, CytoD treatment that disturbs actin filaments inhibited BDNF-induced ribosomal change completely (Fig. 5.4.3 F and G).

Collectively, these data suggest that BDNF-induced ribosomal change depends on actin. This actin-based ribosomal redistribution and conformational change during ribosome assembly and translating expose epitopes to antibodies, resulting in an enhancement in detection of ribosomes.



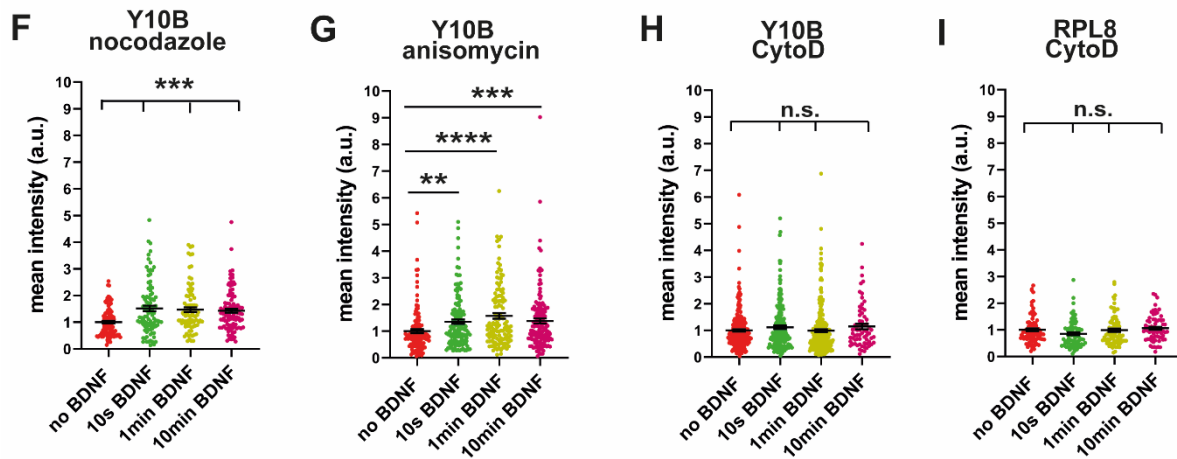


Figure 5.4.3 Redistribution of ribosomes is triggered by BDNF stimulation. (A) Representative images of growth cones of motoneurons fixed after BDNF stimulation and immunostained against ribosomes: rRNA (Y10B) and RPL8. (B and C) Graphs show a remarkable increase in mean intensity of Y10B and RPL8 in growth cones upon 10 sec, 1 min and 10 min BDNF application, compared to those without BDNF stimulation (****, $P < 0.0001$; $n = 138-366$ cells, 4-9 independent experiments). (D) Quantification of mean intensity of Y10B in soma indicates a significant increase after BDNF stimulation, but not earlier than 10 min (**, $P = 0.0042$; $n = 66-67$ cells, 3 independent experiments). (E) Mean intensity of pTrkB in soma shows an increase within 10 sec BDNF stimulation (***, $P = 0.0004$; $n = 63-64$ cells, 3 independent experiments). (F and G) The enhancement in Y10B immunoreactivity is not altered with nocodazole or anisomycin treatment (*, $P = 0.0012$; ***, $P = 0.0008$; ****, $P < 0.0001$; $n = 93-141$ cells, 3-5 independent experiments). (H and I) Treatment using CytoD blocks the increase in mean intensity of Y10B and RPL8 (n.s., $P \geq 0.2256$; $n = 68-252$ cells, 3-5 independent experiments). Statistical analysis: one-way ANOVA with Dunn's post-test. Data are shown in scatter dot plot with mean \pm SEM.

5.5 Extracellular BDNF stimulation induces ribosome assembly and local translation in axonal growth cones of motoneurons

To examine BDNF-induced ribosome change, immunofluorescence staining of motoneurons after 10 sec and 1 min BDNF stimulation was performed and antibodies against ribosomal protein L24 (RPL24), that bind to 60S large ribosomal subunits and ribosomal protein S6 (RPS6), that binds to 40S small ribosomal subunits, were used (Fig. 5.5.1 A). RPL24 and RPS6 connect each other and form a bridge during assembly of large and small ribosomal subunits into 80S ribosomes (Ben-Shem, Garreau de Loubresse et al. 2011). SIM that

achieves a resolution up to 120 nm was used to assess the interaction between RPL24 and RPS6. Quantification of RPL24 and RPS6 co-clusters demonstrates a 3-fold increase in the number of RPL24/RPS6 co-clusters in growth cones upon 10 sec and 1 min BDNF stimulation compared to unstimulated growth cones (Fig. 5.5.1 B). Consistently, the Pearson's Coefficient also shows a significant enhancement in colocalization of RPL24 and RPS6 upon 10 sec and 1 min BDNF pulse (Fig. 5.5.1 C). It is of note that continuous BDNF exposure for 30 min abolished the increase in RPL24/RPS6 co-clusters (Fig. 5.5.1 B) and brought the Pearson's Coefficient value down to the basic level (Fig. 5.5.1 C), implying that this ribosome response to BDNF stimulation is transient in growth cones of motoneurons. CytoD treatment abolished the BDNF-triggered enhancement of RPL24/RPS6 co-clusters completely (Fig. 5.5.1 D), in line with the result in Fig. 5.4.3 H and I. To study whether these fully assembled ribosomes are functional and doing translation, motoneurons were stained against rRNA using Y10B antibody and co-stained against eukaryotic elongation factor 2 (eEF2) using anti-eEF2 antibody (Fig. 5.5.2 A). eEF2 antibody labels actively translating ribosomes and thus allows detection of ribosomes that have entered the translation elongation phase. Similar to the assembly of 80S ribosomes, represented in Fig. 5.5.1 B, we observed an increase in the number of Y10B/eEF2 co-clusters (Fig. 5.5.2 B) as well as the Pearson's Coefficient value (Fig. 5.5.2 C) upon 10 sec BDNF stimulation, providing the proof that these newly assembled ribosomes are doing translation.

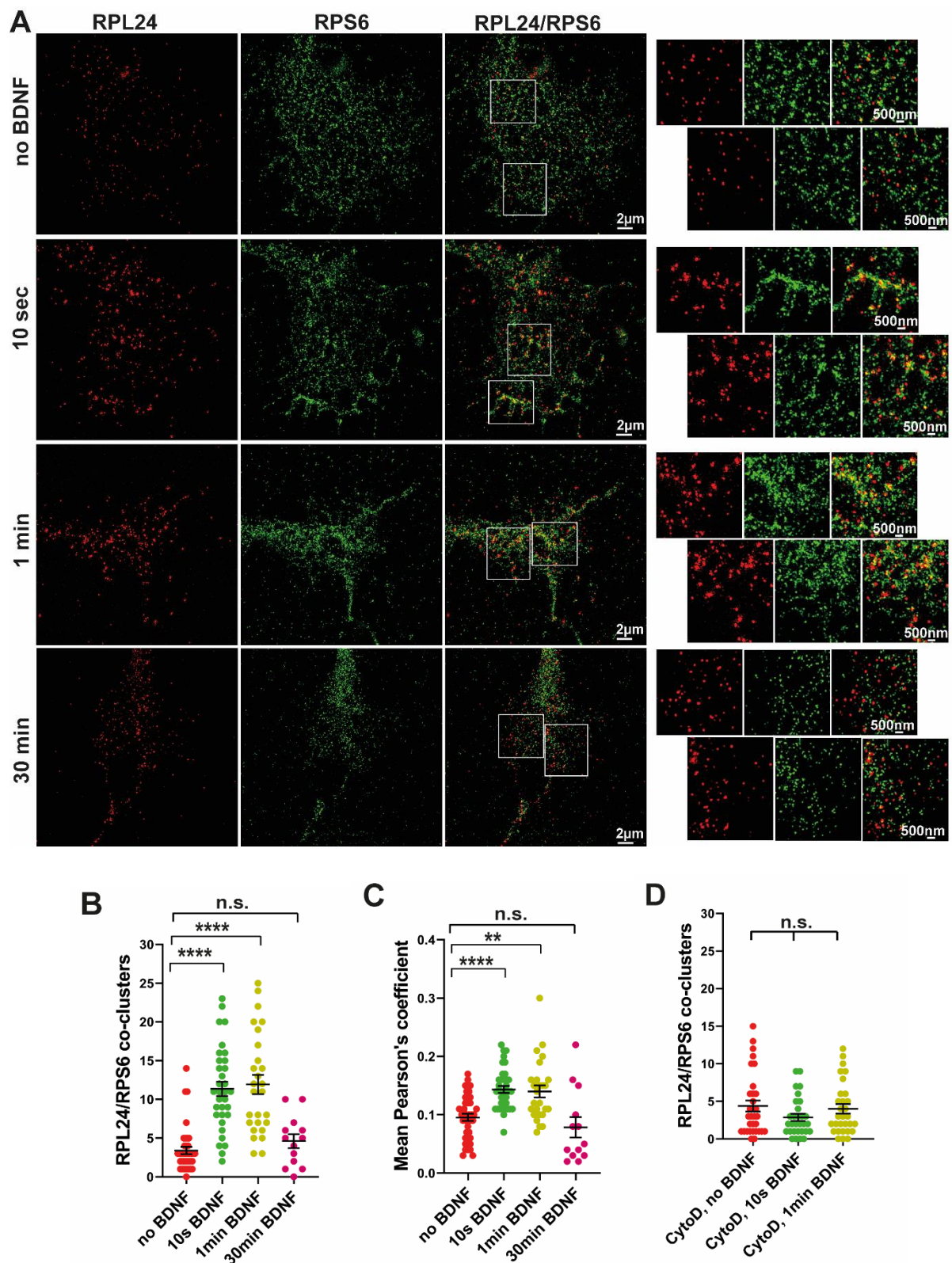


Figure 5.5.1 A short exposure to BDNF triggers ribosome assembly in growth cones of motoneurons. (A) Cultured motoneurons were fixed and immunostained against ribosomal proteins: RPL24 and RPS6. Immunostained growth cones were imaged using SIM. Magnified ROIs marked by white squares illustrate co-

clusters of RPL24 and RPS6. (B) Quantification of RPL24/RPS6 co-clusters demonstrates an increase after 10 sec and 1 min BDNF stimulation, compared to that without BDNF stimulation (****, $P < 0.0001$; $n = 27-33$ cells, 3 independent experiments), while 30 min continuous BDNF application brings the number of RPL24/RPS6 co-clusters back to the basic level (n.s., $P > 0.99$). (C) Quantification of Pearson's correlation coefficient using ImageJ shows enhanced colocalization of RPL24 and RPS6 after 10 s and 1 min BDNF stimulation (**, $P = 0.0002$; *, $P = 0.015$; $n = 26-36$ cells, 3 independent experiments), but not 30 min (n.s. $P \geq 0.99$). (D) Graph depicts that CytoD treatment blocks the increase in RPL24-RPS6 co-clusters induced by BDNF (n.s., $P = 0.616$; $n = 30-32$, 3 independent experiments). Statistical analysis: one-way ANOVA with Dunn's post-test. Data are shown in scatter dot plot with mean \pm SEM.

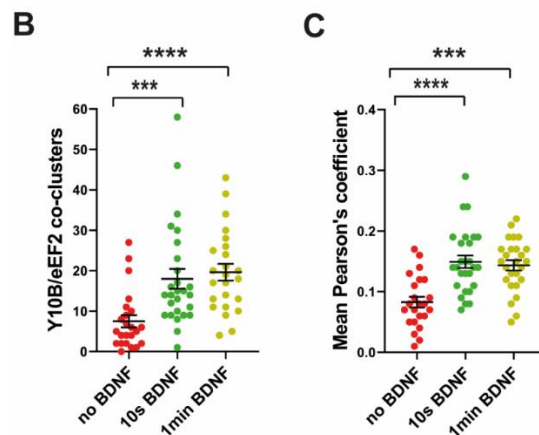
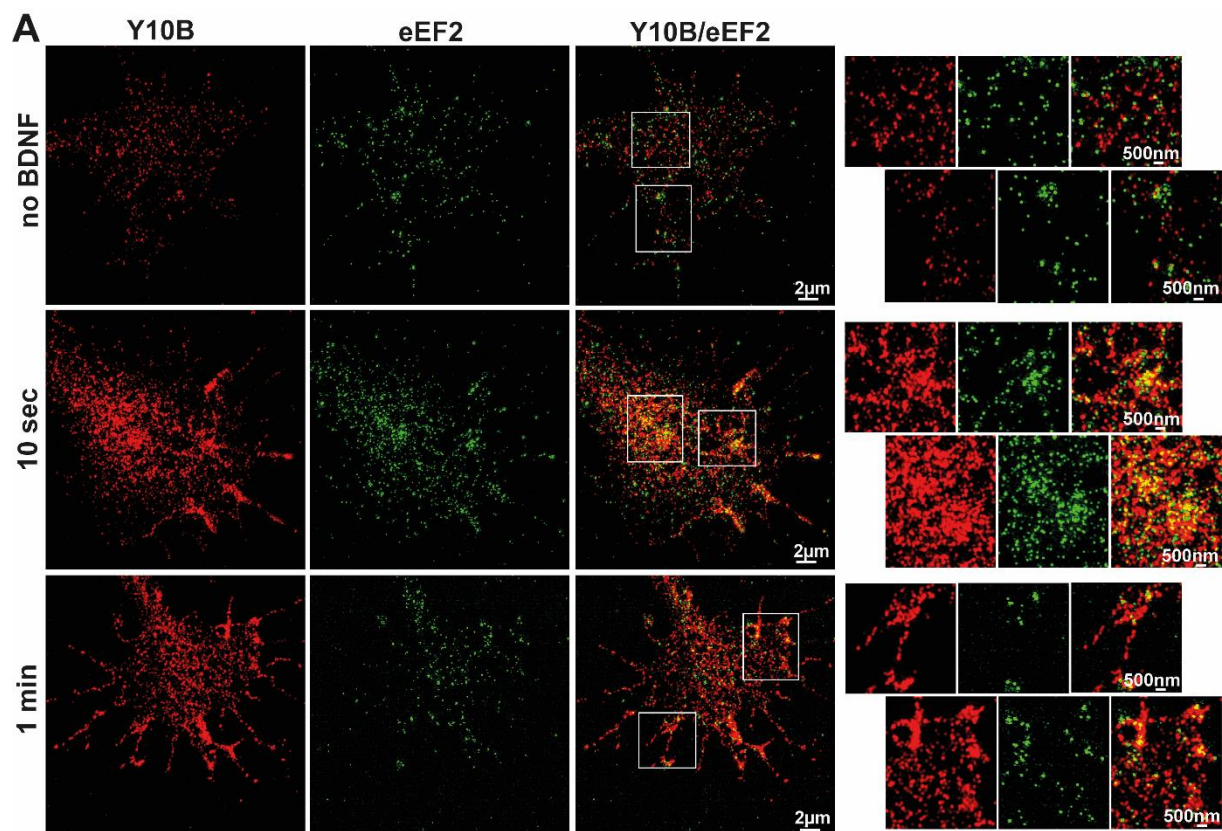


Figure 5.5.2 BDNF promotes ribosomes in growth cone of motoneurons into the stage of elongation. (A) Representative SIM images of growth cones of motoneurons immunostained against rRNA (Y10B antibody) and eukaryotic elongation factor 2 (eEF2). Enlarged images of ROIs marked by white boxes show Y10B/eEF2 co-clusters. (B and C) Graphs demonstrate a notable increment of Y10B/eEF2 co-clusters induced by 10 sec and 1 min BDNF stimulation (***, $P=0.0007$; ****, $P<0.0001$; $n=27-33$ cells, 3 independent experiments), and also a significant rise in mean Pearson's coefficient (****, $P<0.0001$; ***, $P=0.0001$; $n=23-27$ cells, 3 independent experiments). Statistical analysis: one-way ANOVA with Dunn's post-test. Data are shown in scatter dot plot with mean \pm SEM.

Given that BDNF activates its receptor TrkB within seconds and during these seconds, ribosomes have already been assembled and stepped into the elongation stage, BDNF/TrkB could be required for ribosome activation and translation. To confirm this point, motoneurons obtained from TrkB KO mice (Rohrer, Korenbrot et al. 1999) were cultured, fixed after 10 s BDNF exposure and then immunostained with Y10B antibody (Fig. 5.4.3 A). Fig. 5.4.3 B illustrates that ribosomes do not respond to extracellular BDNF stimulation after loss of TrkB, compared to WT (*TrkB*^{+/+}) neurons.

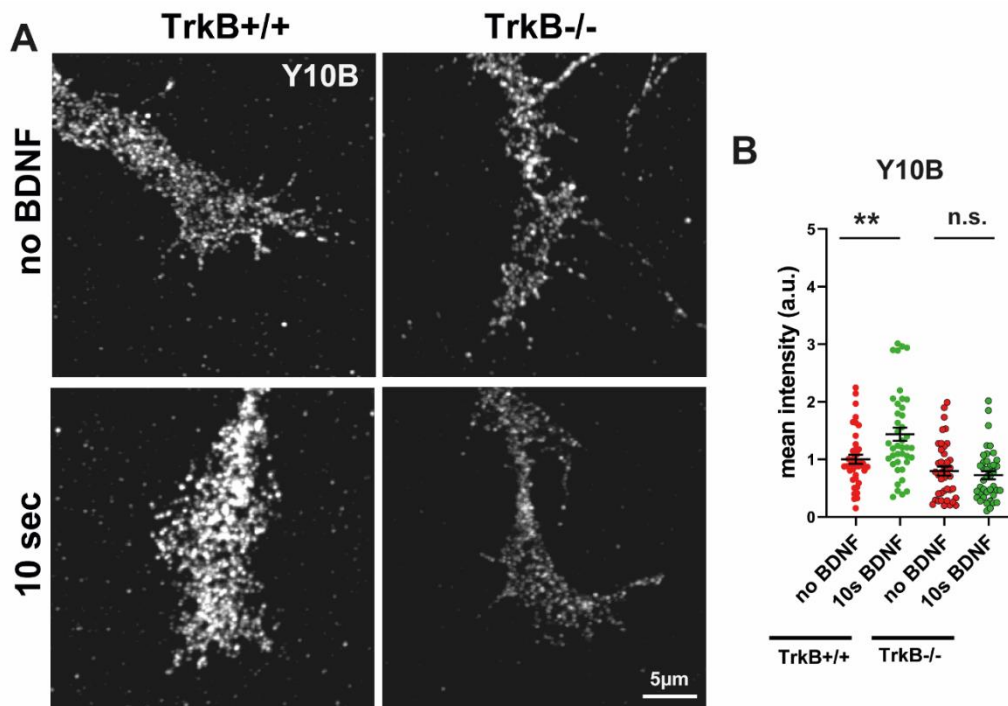


Figure 5.5.3 Loss of TrkB reveals BDNF-induced increase in Y10B immunoreactivity in growth cones of motoneurons. (A) WT (*TrkB*^{+/+}) and TrkB KO (*TrkB*^{-/-}) motoneurons were fixed after 10 sec BDNF pulse and immunostained with Y10B antibody. Images were acquired using confocal microscope. (B) Quantification of mean intensity of Y10B in growth cones shows that the noticeable augmentation in mean intensity of Y10B that happens in WT cells (**, $P=0.0025$; $n=41$ cells, 2 independent experiments) does not appear when TrkB is lost (n.s., $P=0.6019$; $n=40$ cells, 2 independent experiments). Statistical analysis: two-tailed Mann Whitney test. Data are shown in scatter dot plot with mean \pm SEM.

5.6 Extracellular BDNF stimulation rapidly induces protein translation in growth cones of motoneurons

Translation of target proteins should be induced as a consequence of BDNF-triggered ribosome activation. First, puromycin incorporation assay was performed parallel with BDNF stimulation to assess the rate of global protein synthesis (Fig. 5.6.1 A). Puromycin used at the concentration of 10 $\mu\text{g/ml}$ resembles the 3' end of aminoacylated transfer ribonucleic acids (tRNAs) and incorporates into the C-terminus of elongating nascent amino acid chains (Aviner 2020). Anti-puromycin antibody was used to detect puromycin that incorporates into newly synthesized proteins. In growth cones of motoneurons that were omitted from puromycin but immunostained using puromycin antibody, no fluorescent signal was detected (Fig. 5.6.1 B). Puromycin incorporation assay showed that immunoreactivity of incorporated puromycin in growth cones is notably enhanced with 1 min BDNF stimulation (Fig. 5.6.1 C). This was, however, inhibited by anisomycin treatment (Fig. 5.6.1 D) but not by nocodazole (Fig. 5.6.1 E), providing the evidence that BDNF induces local translation at a rapid rate. On the other hand, BDNF stimulation in this puromycin incorporation assay did not result in increased levels of puromycin signal in soma (Fig. 5.6.2 A), supporting again the distinct translational kinetics in soma and distal axonal compartments.

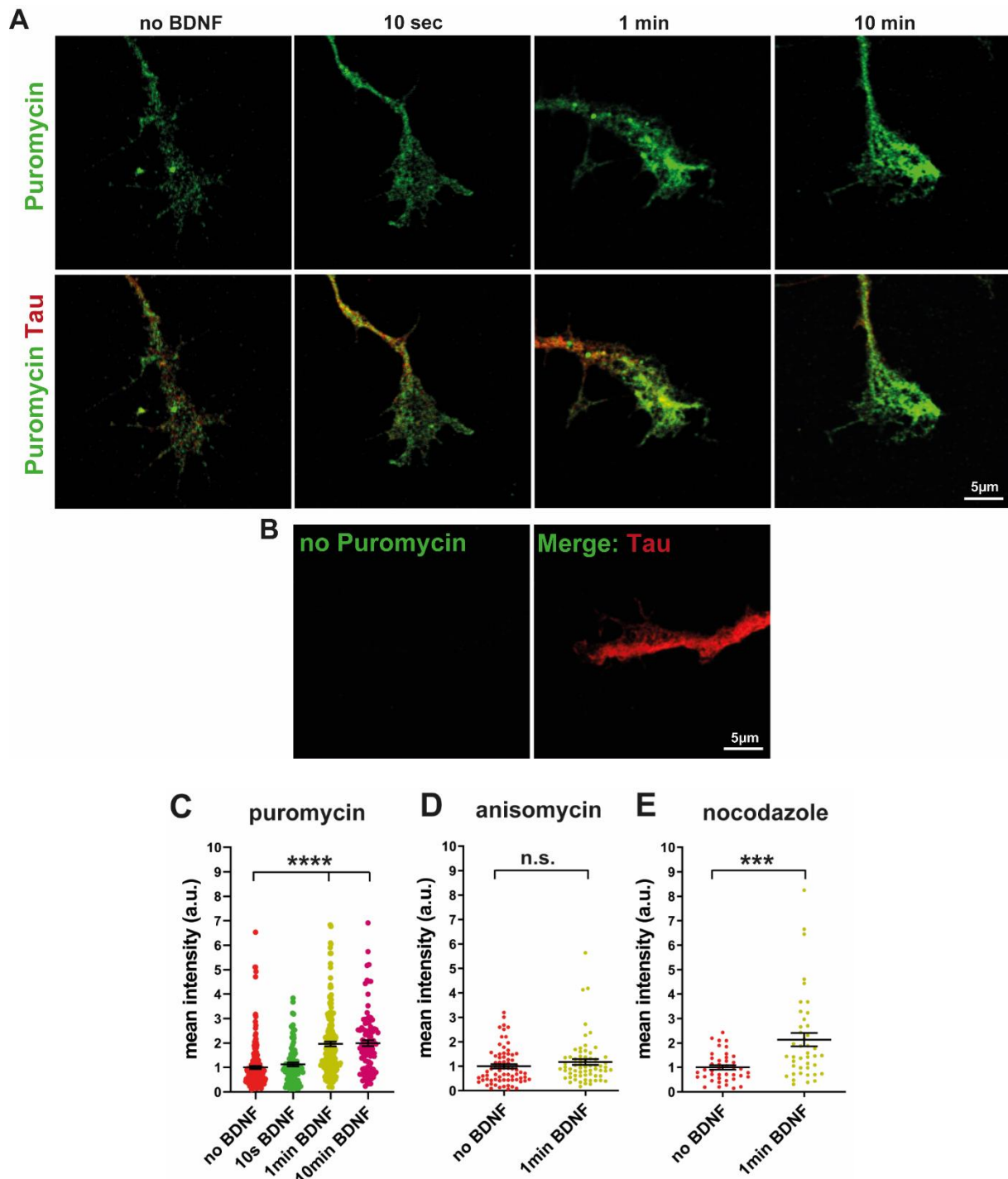


Figure 5.6.1 Puromycin assay reveals increased global protein synthesis in growth cones within 1 min BDNF stimulation. (A) Motoneurons that were incubated with puromycin received 10 sec, 1 min or 10 min BDNF pulse and were then immunostained against puromycin and tau. (B) As negative control, neurons were not incubated with puromycin, but immunostained using puromycin antibody. Almost no puromycin signal was detectable. (C) Mean intensity of puromycin was significantly enhanced within 1 min and 10 min BDNF pulse (****, $P < 0.0001$; $n = 103-218$ cells, 3-6 independent experiments). (D and E) Anisomycin (n.s., $P = 0.1796$; $n = 65-73$ cells, 2 independent experiments) but not nocodazole (****, $P = 0.0002$; $n = 42$ cells, 2 independent

experiments) blocks BDNF-induced mean intensity of puromycin in growth cones after 1 min BDNF stimulation. Statistical analysis: one-way ANOVA with Dunn's post-test in C and Mann Whitney test in D and E. Shown are scatter plot dots with mean \pm SEM.

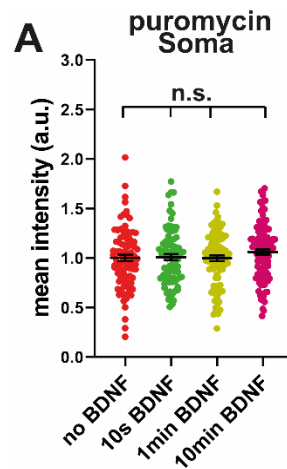


Figure 5.6.2 No obvious increase in immunoreactivity of puromycin in soma of motoneurons is observable in the puromycin assay. (A) Graph shows that mean intensity of puromycin in soma of BDNF-stimulated motoneurons is not notably altered, compared to that of unstimulated neurons (n.s., $P \geq 0.7006$; $n=83-112$ cells, 3 independent experiments). Statistical analysis: one-way ANOVA with Dunn's post-test. Data are shown in scatter plot dots with mean \pm SEM.

Since BDNF triggers the global translation in growth cones, translation of specific proteins was investigated as the next step. There are two major compartments for protein synthesis: the ER and cytosol (Reid and Nicchitta 2015). Secretory and integral membrane proteins are translated on ER attached ribosomes (Siekevitz and Palade 1960, Palade 1975), while cytosolic protein-encoding mRNAs are partially translated on free ribosomes (Reid and Nicchitta 2015). Here, the transmembrane protein α -1 β subunits of the N-type Ca^{2+} channels (Cav2.2) and the cytosolic protein β -actin were studied. Motoneurons were fixed after a series of BDNF stimulation: 10 sec, 1 min and 10 min and then immunostained against Cav2.2 (Fig. 5.6.3 A) or β -actin (Fig. 5.6.4 A). Neurons were marked by anti-Tau antibody. Notably, BDNF stimulation for 1 min results in an increase in fluorescence intensity of both Cav2.2 (Fig. 5.6.3 B) and β -actin (Fig. 5.6.4 B) and the increase in both cases was eradicated due to

anisomycin treatment to inhibit translation (Fig. 5.6.3 C and Fig. 5.6.4 C). With the aim of excluding the possibility of axonal transport from somatic compartment, nocodazole treatment was performed to disturb the MT-dependent axonal transport. As Fig. 5.6.3 D and Fig. 5.6.4 D show, disruption of MT-dependent fast axonal transport did not affect the enhancement in Cav2.2 and β -actin immunosignals. Altogether, BDNF is capable of ribosome activation in growth cones of motoneurons on a timescale of seconds and results in proteomic changes at a rapid speed.

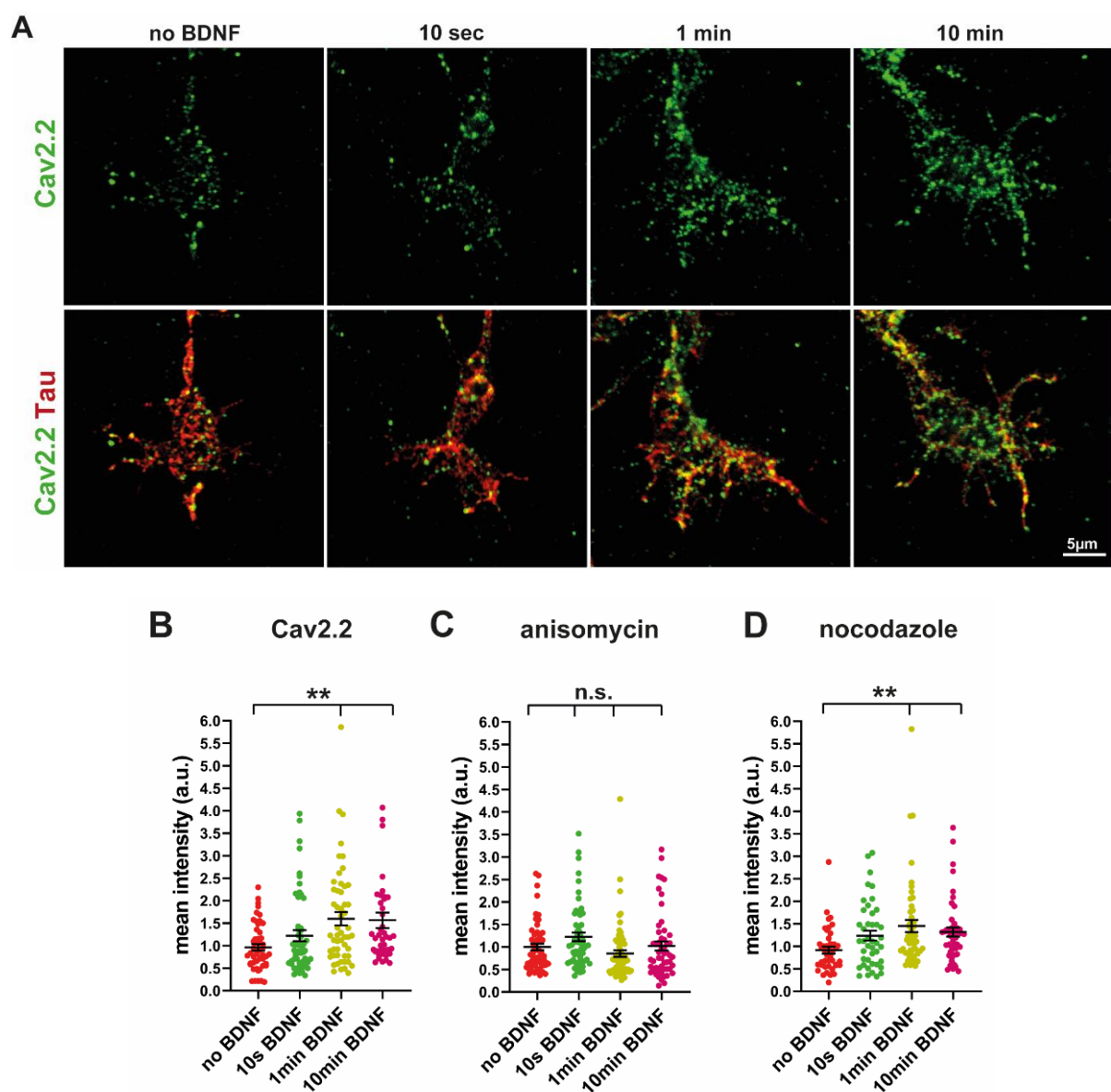


Figure 5.6.3 BDNF stimulation triggers translation of the transmembrane protein Cav2.2. (A) Representative images of growth cones immunostained against Cav2.2 and tau after BDNF application. Tau was

stained to mark neurons (B) Quantification of mean intensity of Cav2.2 in growth cones shows a significant increase after 1 min and 10 min BDNF stimulation (**, $P < 0.0057$; $n = 50-54$ cells, 3 independent experiments). (C) Translation inhibitor anisomycin blocks the BDNF-induced increase in Cav2.2 in growth cones (n.s., $P = 0.26$; $n = 53-67$ cells, 3 independent experiments). (D) Nocodazole treatment did not abolish the enhancement in Cav2.2 induced by BDNF stimulation (**, $P < 0.0099$; $n = 43-50$ cells, 3 independent experiments). Statistical analysis: one-way ANOVA with Dunn's post-test. Data are shown in scatter plot dots with mean \pm SEM.

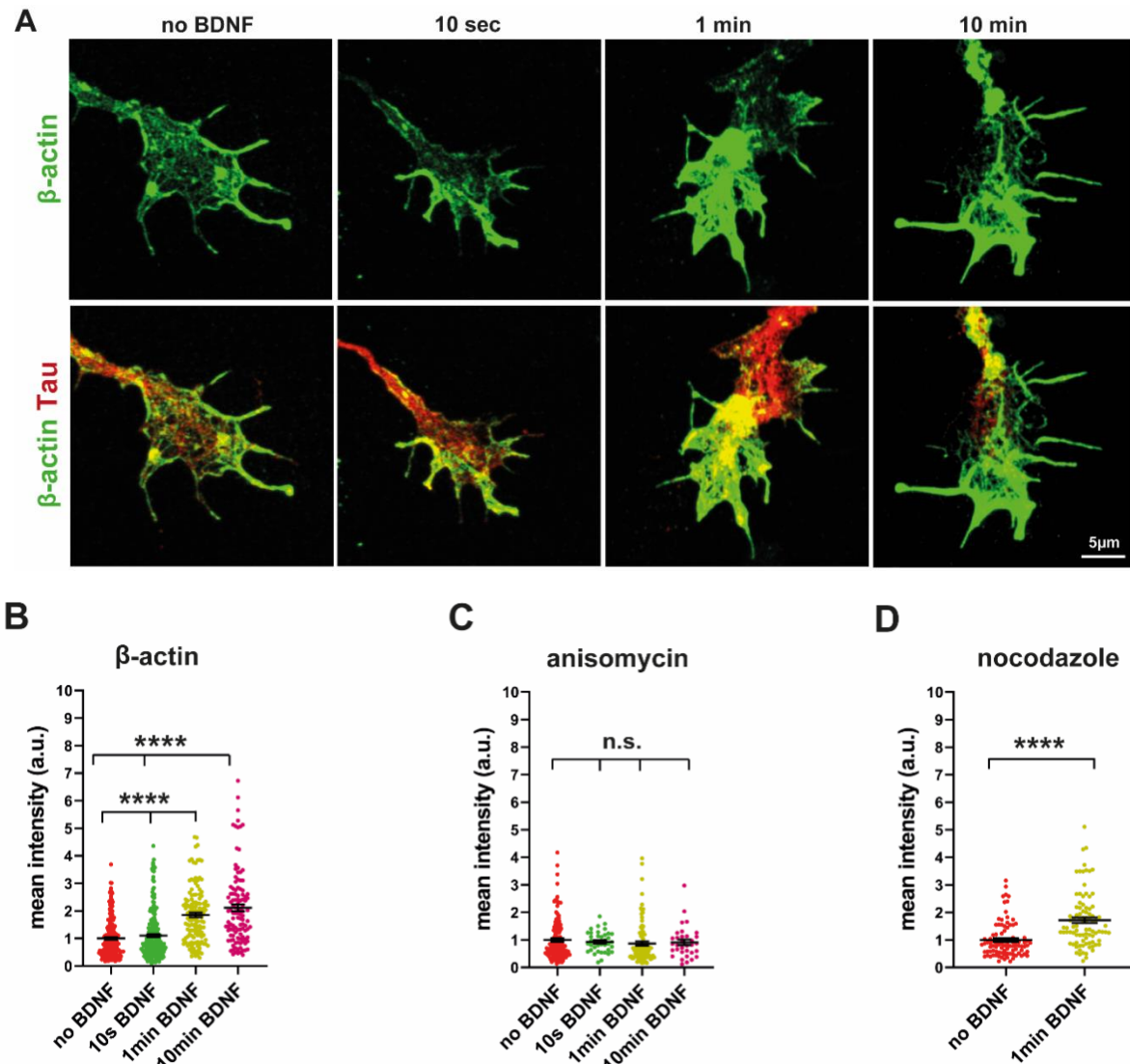


Figure 5.6.4 Translation of cytosolic protein β -actin in growth cones is induced by extracellular BDNF. (A) Representative images of growth cones of motoneurons stimulated by BDNF for 10 sec, 1 min and 10 min, followed by immunostaining against β -actin and Tau. (B) Graph shows that 1 min and 10 min BDNF application both increase mean intensity of β -actin in growth cones (****, $P < 0.0001$; $n = 114-202$ cells, 4 independent experiments). (C and D) Graphs show that the BDNF induced enhancement in mean intensity of β -actin in growth cones is abolished by anisomycin treatment (n.s., $P \geq 0.293$; $n = 33-127$ cells, 2-3 independent

experiments), but not nocodazole (****, $P < 0.0001$; $n = 91-95$ cells, 3 independent experiments). Statistical analysis: one-way ANOVA with Dunn's post-test in B and C, and Mann Whitney test in D. Data are shown in scatter plot dots with mean \pm SEM.

5.7 Activated ribosomes induced by BDNF attach to ER, contributing to protein synthesis in the distal axonal compartment

Observations that BDNF induces fast protein synthesis including the transmembrane protein Cav2.2 and the cytosolic protein β -actin in distal axonal compartments via activating ribosomes raised up the question whether RER in growth cones of motoneurons plays an essential role in BDNF-induced protein synthesis, since ER-bound ribosomes are major sites for protein translation. Even though, ultrastructural approaches revealed only SER in axons (Tsukita and Ishikawa 1976) and RER in dendrites (Farah, Liazoghli et al. 2005). mRNAs encoding transmembrane proteins and ion channels were detected in axons (Merianda, Lin et al. 2009), supporting the possible existence of a RER in axons. To confirm this assumption, motoneurons expressing mCherry-ER were fixed after a series of BDNF stimulation and then immunostained with antibodies against RPL24 and RPS6 to visualize fully assembled 80S ribosomes as well as ER (Fig. 5.7.1 A). SIM microscope was employed to acquire the images. Remarkably, both 10 sec and 1 min BDNF stimulation elevated the number of fully assembled ribosomes, which were attached to the ER (Fig. 5.7.1 B). However, this increase disappeared with continuous exposure to BDNF for 30 min (Fig. 5.7.1 B). Also, CytoD treatment repealed this effect of BDNF on ER-associated ribosomes (Fig. 5.7.1 C), pointing towards the conclusion that the effect of BDNF on ribosome activation and RER formation is transient and this process relies on the actin cytoskeleton.

Afterwards, ER-bound ribosomes at the elongation phase were also investigated by immunofluorescence staining of motoneurons expressing mCherry-ER with antibodies against rRNA and eEF2 (Fig. 5.7.2 A). Consistent with the attachment of fully assembled ribosomes

to ER, BDNF stimulation for 10 sec and 1min both increased the number of ER-attached translating ribosomes in presynaptic compartments (Fig. 5.7.2 B), suggesting that BDNF triggers ribosomes in this compartment rapidly into translational elongation phase and these translating ribosomes are bound to ER.

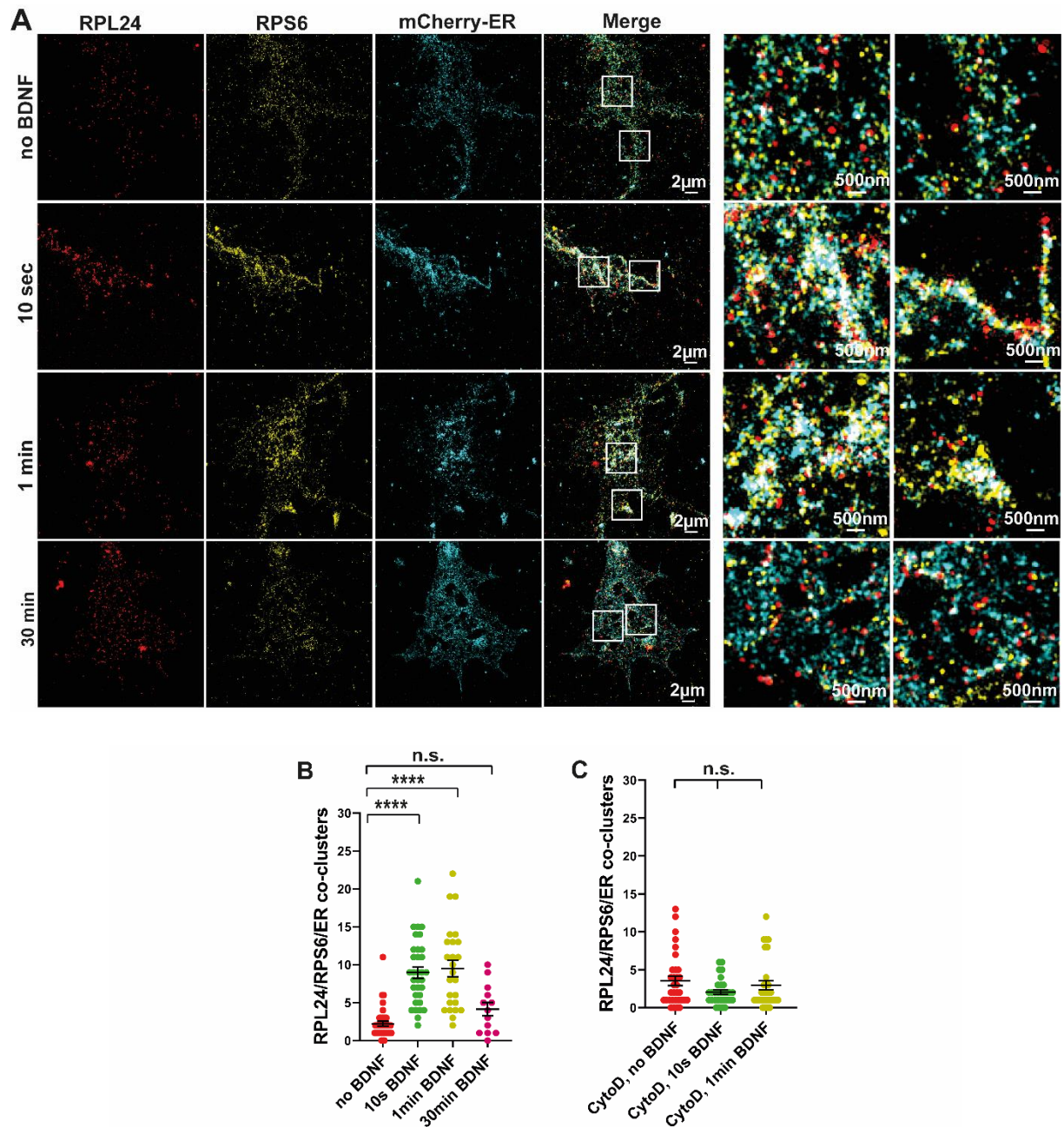


Figure 5.7.1 Increased number of fully assembled ribosomes attach to ER as a result of extracellular BDNF stimulation. (A) Representative SIM images of growth cones of motoneurons transduced with lentiviruses expressing mCherry-ER and stained against RPL24 and RPS6 after 10 sec and 1 min BDNF stimulation. Magnified images indicated by white square boxes illustrate distribution of RPL24 and RPS6. (B)

Quantification of ER-bound RPL24/RPS6 co-clusters demonstrates a significant increase after 10 sec and 1 min BDNF application (****, $P < 0.00001$; $n = 25-33$ cells, 3 independent experiments) and the increase is abolished with 30 min continuous BDNF application (n.s., $P = 0.598$; $n = 13$ cells, 2 independent experiments). (C) CytoD application blocks the effect of BDNF stimulation on ER-bound ribosomes (n.s., $P = 0.728$; $n = 30-32$ cells, 3 independent experiments). Statistical analysis: one-way ANOVA with Dunn's post-test. Data are shown as scatter dot plot with mean \pm SEM.

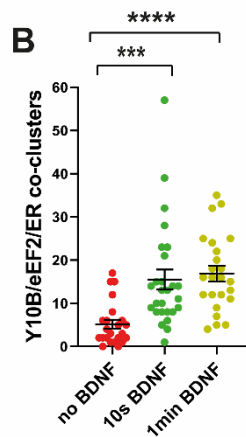
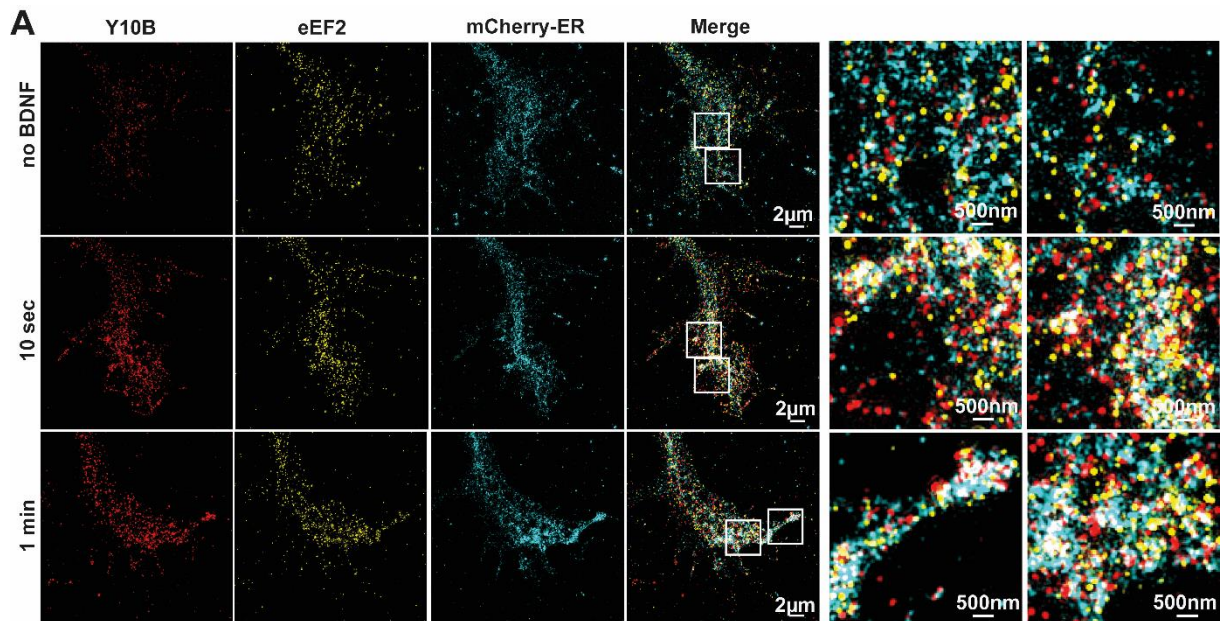


Figure 5.7.2 BDNF-induced ribosomes at the elongation stage are associated with ER in axonal growth cones of motoneurons. (A) mCherry-ER expressing motoneurons were fixed and stained against Y10B and eEF2 after a series of BDNF stimulation. Images were acquired by SIM. (B) Graph demonstrates increased number of co-clusters of Y10B/eEF2/ER upon 10 sec and 1 min BDNF exposure (***, $P = 0.0003$; ****, $P < 0.00001$; $n = 23-27$ cells, 3 independent experiments). Statistical analysis: one-way ANOVA with Dunn's post-test. Data are shown as scatter dot plot with mean \pm SEM.

5.8 Dynamics of ER in axonal growth cones are defective in *Smn*-deficient

motoneurons

Abnormal distribution and dysfunction of ER are associated with diverse neurodegenerative diseases. It was previously shown that F-actin levels are reduced at the NMJs obtained from a SMA mouse model, compared to those from the control group (Ackermann, Kröber et al. 2013). Since it was uncovered that ER dynamic movements in growth cones of cultured motoneurons depend on actin filaments and MTs and especially, filopodia ER movements rely on actin filaments and myosin VI, it was questioned whether ER dynamics in growth cone filopodia is disturbed when SMN is deficient. In my study, a mouse model was used to resemble the severe type I SMA disease and *Smn*^{-/-} with two copies of *SMN2* gene (*Smn*^{-/-}*SMN2**tg*) was regarded as the SMA disease group, while *Smn*^{+/+} with two copies of *SMN2* gene (*Smn*^{+/+}*SMN2**tg*) was considered as the control group (Monani, Sendtner et al. 2000). To investigate ER dynamics in *Smn*-deficient motoneurons, cells obtained from *Smn*^{-/-}; *SMN2**tg* and *Smn*^{+/+}; *SMN2**tg* groups were transduced with lentiviral particles expressing mCherry-ER to visualize ER and live images were captured at intervals of 2 sec for 15 min after DMSO treatment as a control (Fig. 5.8.1 A and Fig. 5.8.2 A) and CytoD treatment to destroy actin filaments. ER dynamics in growth cone filopodia were significantly reduced in *Smn*-deficient motoneurons (Fig. 5.8.1 B and Fig. 5.8.2 B). CytoD treatment reduces ER dynamics in filopodia and core of *Smn*^{+/+}; *SMN2**tg* group, compared to DMSO treated *Smn*^{+/+}; *SMN2**tg* group (Fig. 5.8.1 B and Fig. 5.8.2 B). However, CytoD treatment does not further significantly reduce ER dynamics in filopodia and core of *Smn*^{-/-}; *SMN2**tg* group, compared to DMSO treated *Smn*^{-/-}; *SMN2**tg* group (Fig. 5.8.1 B and Fig. 5.8.2 B). These findings indicate an impairment in ER dynamics that might be due to defects in actin dynamics in SMA.

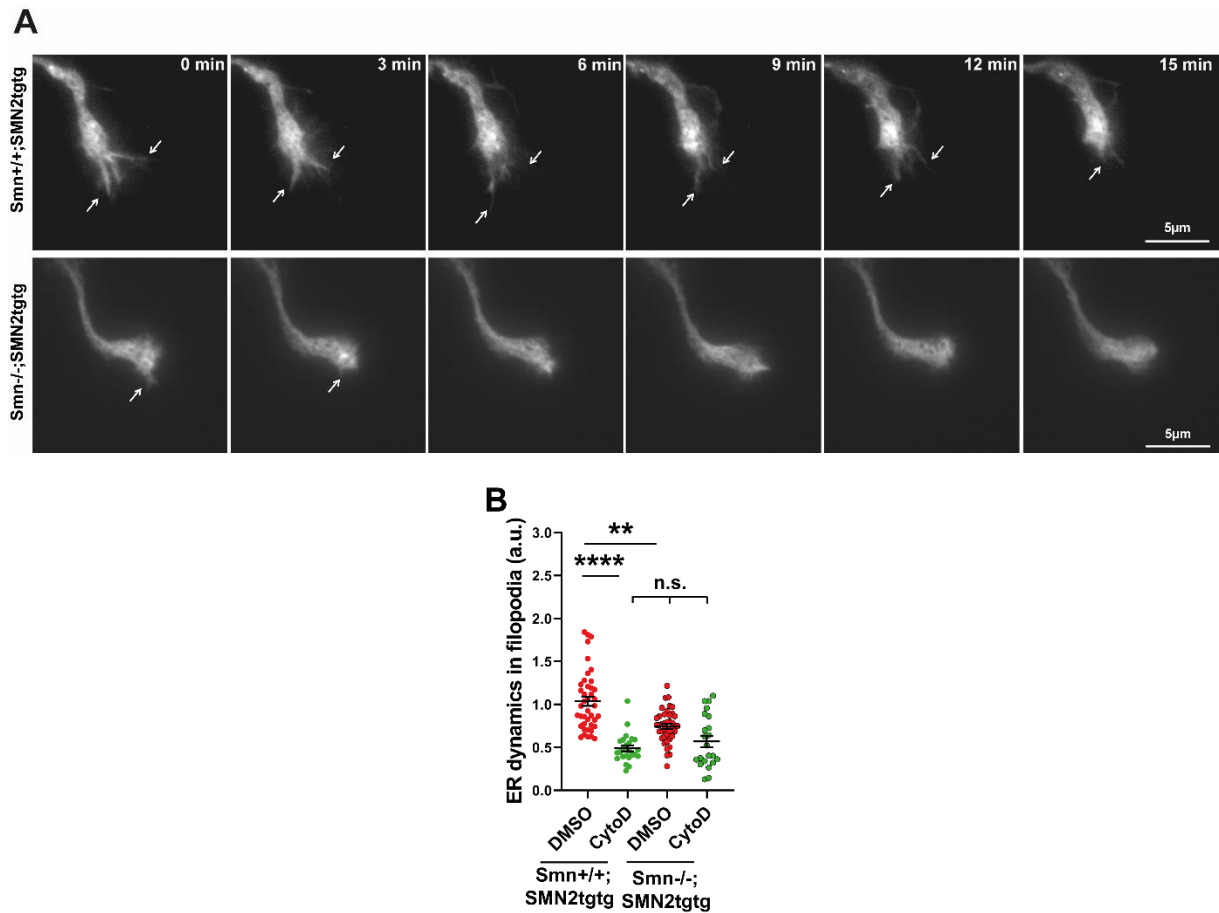


Figure 5.8.1 In *Snn*-deficient motoneurons, ER dynamics in growth cone filopodia are reduced. (A) *Snn*^{+/+}; *SMN2*^{tg}tg (control) and *Snn*^{-/-}; *SMN2*^{tg}tg motoneurons obtained from SMA mice were transduced with a lentivirus expressing mCherry-ER. Representative time-lapse images of mCherry-ER in growth cone filopodia of DMSO treated cells are shown and white arrows indicate movements of filopodia ER. (B) ICS analysis of filopodia ER dynamics demonstrates a significant reduction in DMSO treated *Snn*-deficient motoneurons, compared to the DMSO treated control group (**, $P=0.0077$; $n=41$ cells, 6 independent experiments). CytoD treatment causes significant reduction in filopodia ER dynamics in *Snn*^{+/+}; *SMN2*^{tg}tg motoneurons compared to *Snn*^{-/-}; *SMN2*^{tg}tg motoneurons (****, $P < 0.0001$). However, CytoD treated *Snn*^{-/-}; *SMN2*^{tg}tg motoneurons show similar ER dynamics with DMSO-treated *Snn*^{-/-}; *SMN2*^{tg}tg motoneurons (n.s., $P = 0.1025$; $n=22-41$ cells, 3 independent experiments). Statistical analysis: two-tailed Mann Whitney test. Data are shown as scatter dot plot with mean \pm SEM.

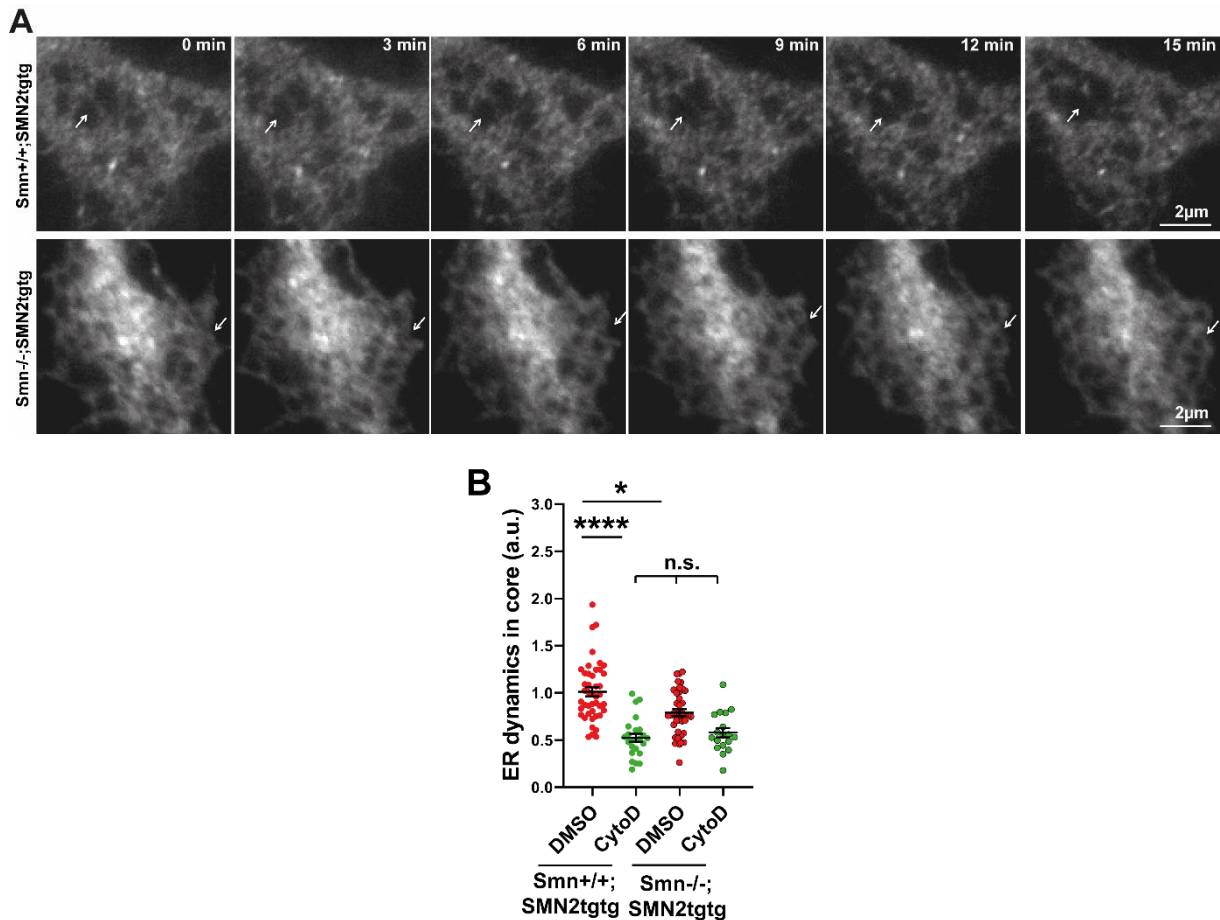


Figure 5.8.2 ER in the growth cone core of *Smn*-deficient motoneurons shows reduced dynamics compared to that in the control group. (A) Representative time-lapse images of ER movements in growth cone cores of DMSO treated *Smn*^{+/+}; *SMN2**tg**tg* (control) and *Smn*^{-/-}; *SMN2**tg**tg* motoneurons transduced with lentiviral particles expressing mCherry-ER. White arrows show changes in ER morphology in growth cone cores. (B) ICS analysis of ER in growth cone cores reveals that *Smn*-deficiency and CytoD treatment both lead to a decrease in ER dynamics in growth cone core compared to DMSO treated *Smn*^{+/+}; *SMN2**tg**tg* motoneurons (*, $P=0.020$; ****, $P < 0.0001$; $n=24-44$ cells, 3-6 independent experiments). CytoD treatment of *Smn*^{-/-}; *SMN2**tg**tg* motoneurons results in a slight but not significant reduction in ER dynamics in core compared to DMSO treated *Smn*^{-/-}; *SMN2**tg**tg* motoneurons (n.s., $P=0.057$; $n=18-40$ cells, 3 independent experiments). Statistical analysis: two-tailed Mann Whitney test. Data are shown in scatter dot plot with mean \pm SEM.

As a next step, immunofluorescence staining of motoneurons transduced with lentiviruses expressing mCherry-ER was performed using antibodies against mCherry-ER and F-actin (Alexa 647-Phalloidin) and images were captured using SIM.

To further study the association between ER and F-actin in growth cones of *Smn*-deficient motoneurons, *Smn*^{-/-}; *SMN2**tg**tg* and *Smn*^{+/+}; *SMN2**tg**tg* cells transduced with lentiviruses expressing mCherry-ER were immunostained against F-actin (Alexa647 Phalloidin) and mCherry-ER. Images were captured using SIM microscope to evaluate the distribution of these proteins in growth cone cores (Fig. 5.8.3 A) and filopodia (Fig. 5.8.4 A). Line scan analysis from growth cone core and filopodia in *Smn*^{-/-}; *SMN2**tg**tg* and *Smn*^{+/+}; *SMN2**tg**tg* neurons show that SMN deficiency causes a defect in overlapping of mCherry-ER and F-actin (Fig. 5.8.3 and Fig. 5.8.4). To exclude an overlap by chance, ER channel was rotated by 90°, and only a partial overlapping was detectable (Fig. 5.8.3 and Fig. 5.8.4).

Overall, ER dynamic movements in growth cones of cultured motoneurons are disturbed in *Smn*-deficient motoneurons that could be due to the reduced level of F-actin and abnormal association of ER with F-actin.

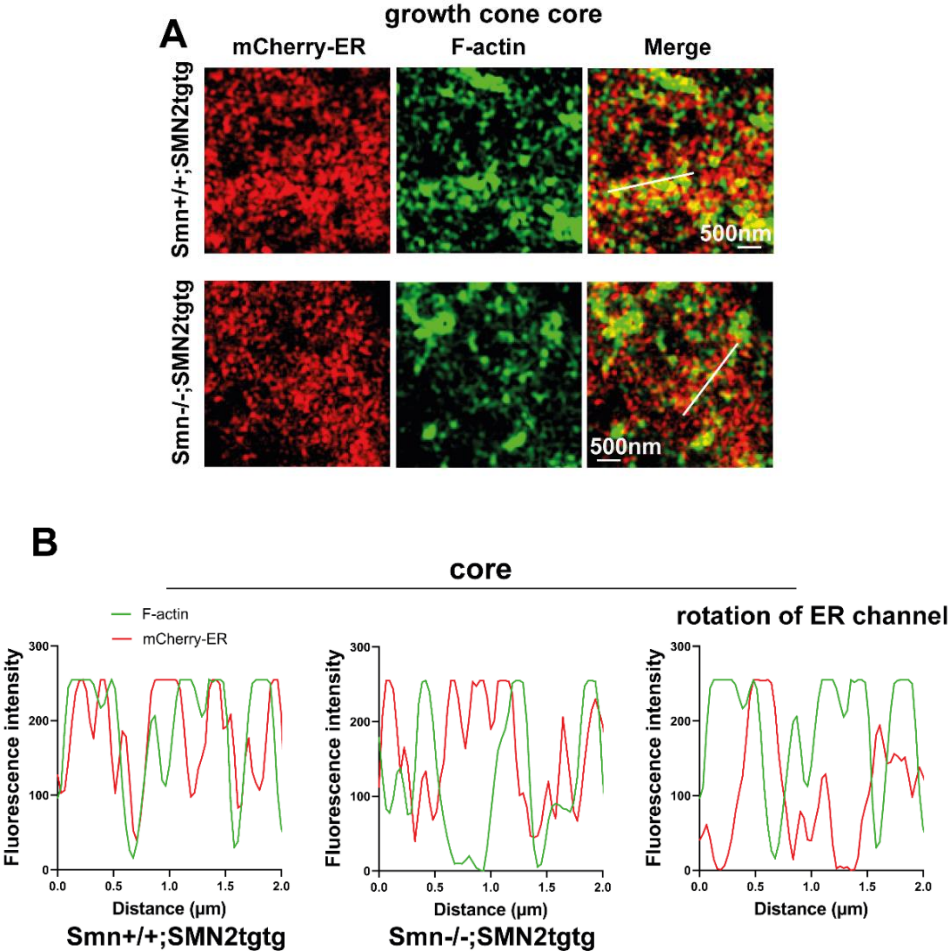


Figure 5.8.3 Association between ER and F-actin in growth cone cores of *Smn*-deficient motoneurons. (A) Motoneurons isolated from *Smn*^{+/+}; *SMN2*^{tg} (control) and *Smn*^{-/-}; *SMN2*^{tg} mice were transduced with lentiviruses expressing mCherry-ER before seeding onto coverslips. At DIV6, neurons were fixed and immunostained against F-actin and mCherry-ER. Images were captured by SIM to assess the interaction between ER and F-actin. Representative images of the growth cone core in control and *Smn*-deficient cells. (B) Line scan analysis shows that ER mostly overlaps with F-actin in control cells but not in *Smn*-deficient neurons. As a control, ER channel was rotated by 90° and only a partial overlapping was detectable.

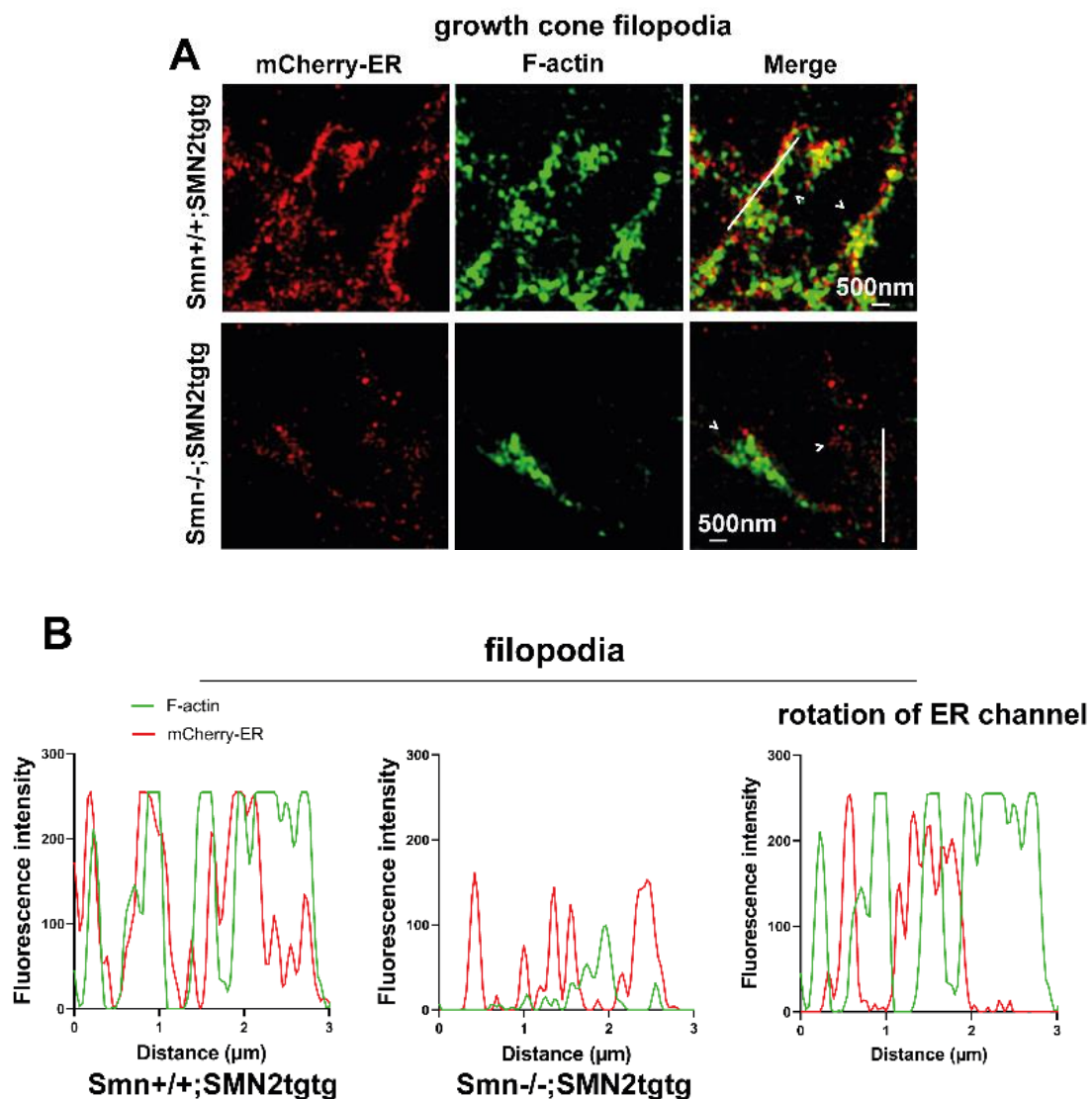


Figure 5.8.4 Overlap of ER with F-actin in growth cone filopodia is altered when SMN is deficient. (A) Representative SIM images of mCherry-ER expressing motoneurons from *Smn*^{+/+}; *SMN2*^{tg} and *Smn*^{-/-}; *SMN2*^{tg} groups immunostained with antibodies anti-mCherry-ER and phalloidin. (B) Line scan analysis indicates overlapping of mCherry-ER and F-actin in *Smn*^{+/+}; *SMN2*^{tg} group. In *Smn*-deficient group, this

overlap between ER and F-actin in growth cones is defected. Rotation of ER channel by 90° results in only a partial overlapping.

5.9 Deficiency in SMN protein abolishes the effects of BDNF on ribosome activation and local translation in axon terminals

Since ER dynamic movements in growth cones are disturbed in *Smn*-deficient motoneurons and ribosomes are induced to assemble and attach to ER by BDNF stimulation that is dependent on actin, the question was raised up whether BDNF-stimulated ribosome dynamics and local translation could also be disrupted upon SMN deficiency. To answer this question, immunofluorescence staining with antibody Y10B against rRNA (Fig. 5.9.1 A) and puromycin incorporation assay (Fig. 5.9.1 B) were carried out with *Smn*^{-/-}; *SMN2**tg**tg* and *Smn*^{+/+}; *SMN2**tg**tg* motoneurons after a series of BDNF stimulation. Noteworthy, the remarkable increase in immunoreactivity of Y10B in growth cones of the *Smn*^{+/+}; *SMN2**tg**tg* control neurons that occurred upon BDNF stimulation was not detected in *Smn*-deficient cells in the whole series of BDNF stimulation (Fig. 5.9.1 B). In line with other studies in which it was shown that translation is impaired in SMA (Bernabò, Tebaldi et al. 2017, Moradi, Sivadasan et al. 2017), puromycin incorporation assay after BDNF stimulation (Fig. 5.9.2 A) in my study also confirms a disturbed global translation in growth cones of *Smn*-deficient motoneurons (Fig. 5.9.2 B). These data indicate that BDNF stimulation do not elevate the levels of newly synthesized proteins in *Smn*^{-/-}; *SMN2**tg**tg* neurons compared to unstimulated *Smn*^{-/-}; *SMN2**tg**tg*.

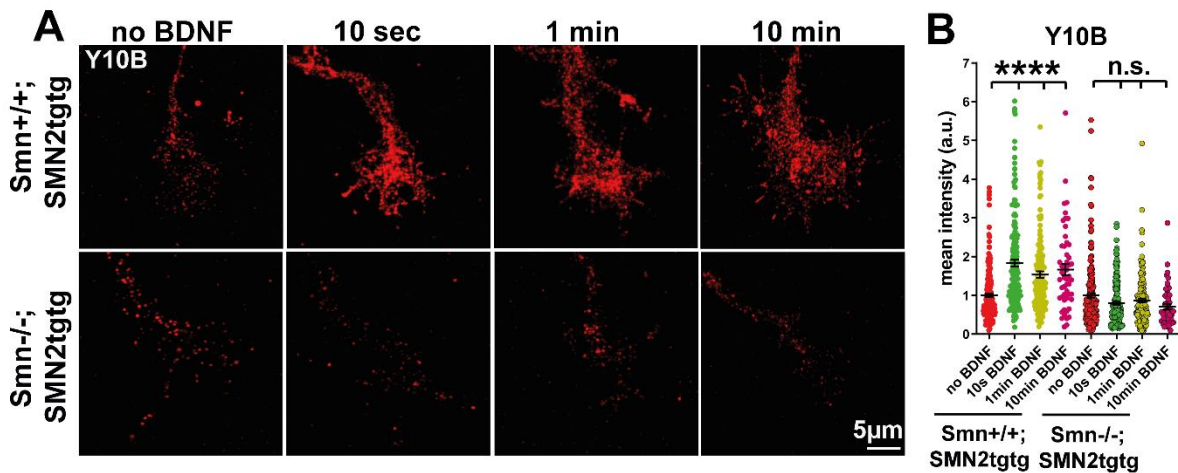


Figure 5.9.1 Ribosomal response to BDNF is altered in axonal growth cones of *Snn*-deficient motoneurons. (A) Representative images of growth cones stained with Y10B antibody in *Snn*-deficient and control motoneurons after BDNF stimulation. (B) Graph shows that the increased immunoreactivity of Y10B induced by BDNF in control cells (****, $P < 0.0001$; $n = 52$ -214 cells, 3 independent experiments) did not happen in *Snn*-deficient motoneurons (n.s., $P \geq 0.0774$; $n = 51$ -220 cells, 3-5 independent experiments). Statistical analysis: one-way ANOVA with Dunn's post-test. Data are shown in Scatter dot plot, mean \pm SEM.

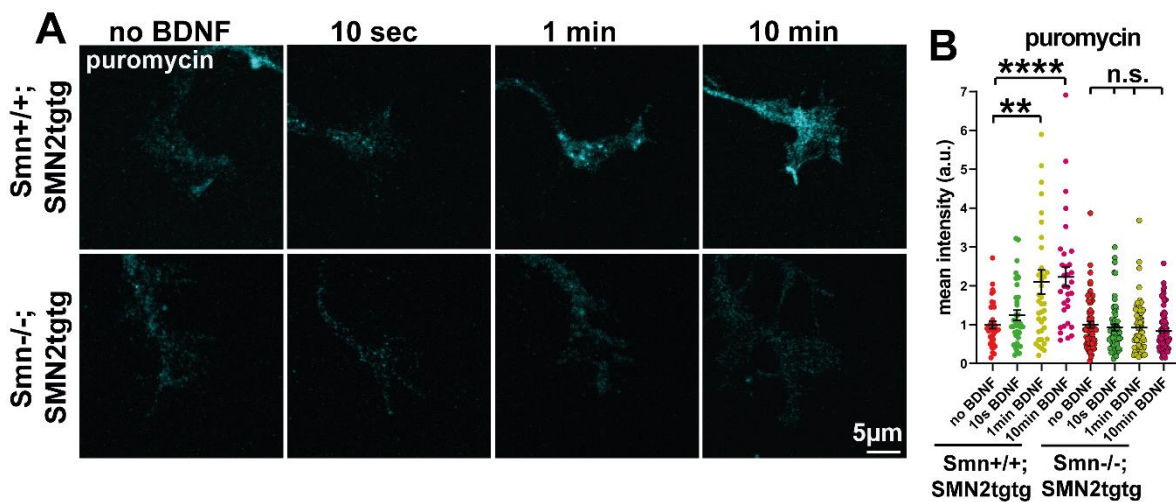


Figure 5.9.2 Global protein synthesis stimulated by BDNF is not detectable in growth cones of *Snn*-deficient motoneurons using puromycin incorporation assay. (A) Representative images of growth cones of *Snn*^{+/+}; *SMN2tggtg* and *Snn*^{-/-}; *SMN2tggtg* motoneurons immunostained with anti-puromycin antibody in puromycin incorporation assay. (B) Graph representing the mean intensity of puromycin immunoreactivity in a series of BDNF stimulation shows an increase in puromycin immunoreactivity in *Snn*^{+/+}; *SMN2tggtg* cells (**, $P = 0.0061$; ****, $P < 0.0001$; $n = 32$ -83 cells, 2 independent experiments) but not in *Snn*^{-/-}; *SMN2tggtg* group (n.s.,

P>0.9999; n=61-68 cells, 3 independent experiments). Statistical analysis: one-way ANOVA with Dunn's post-test. Graphs were shown in scatter dot plot with mean \pm SEM.

5.10 BDNF-induced active ribosomes and their association with ER are disturbed in axonal growth cones of cultured SMA motoneurons.

In axonal growth cones of Smn-deficient motoneurons, BDNF-stimulated rapid changes in rRNA levels were disturbed, which indicates that kinetics of ribosomes induced by BDNF could be impaired. To confirm this, ribosome assembly and actively translating ribosomes, as well as their association with ER after a series of BDNF stimulation were investigated in Smn-deficient motoneurons. Cultured control and Smn-deficient motoneurons transduced with lentiviral particles expressing mCherry-KDEL were fixed after a series of BDNF stimulation and immunostained against ribosomes with antibodies anti-RPL24 and anti-RPS6 (Fig. 5.10.1 A and B), as well as against ribosomes in the phase of elongation with antibodies anti-rRNA (Y10B) and anti-eEF2 (Fig. 5.10.2 A and B). Co-clusters were quantified using JACoP plugin of ImageJ. BDNF application did not elevated the number of fully assembled ribosomes indicated by RPL24/RPS6 co-clusters in the axonal growth cone of Smn-deficient motoneurons which has been shown in control cells (Fig. 5.10.1 C). We also could not detect an increase in the number of ER-associated 80S ribosomes in Smn-deficient neurons (Fig. 5.10.1 D). In line with that, the number of actively translating ribosomes indicated by Y10B/eEF2 co-clusters was not increasingly induced by BDNF stimulation in Smn-deficient motoneurons (Fig. 5.10.2 C), neither was the number of translating ribosomes attached to ER enhanced (Fig. 5.10.2 D). In conclusion, SMN deficiency leads to impaired ribosomal assembly and translating as well as its association with ER in growth cones of motoneurons in response to BDNF stimulation.

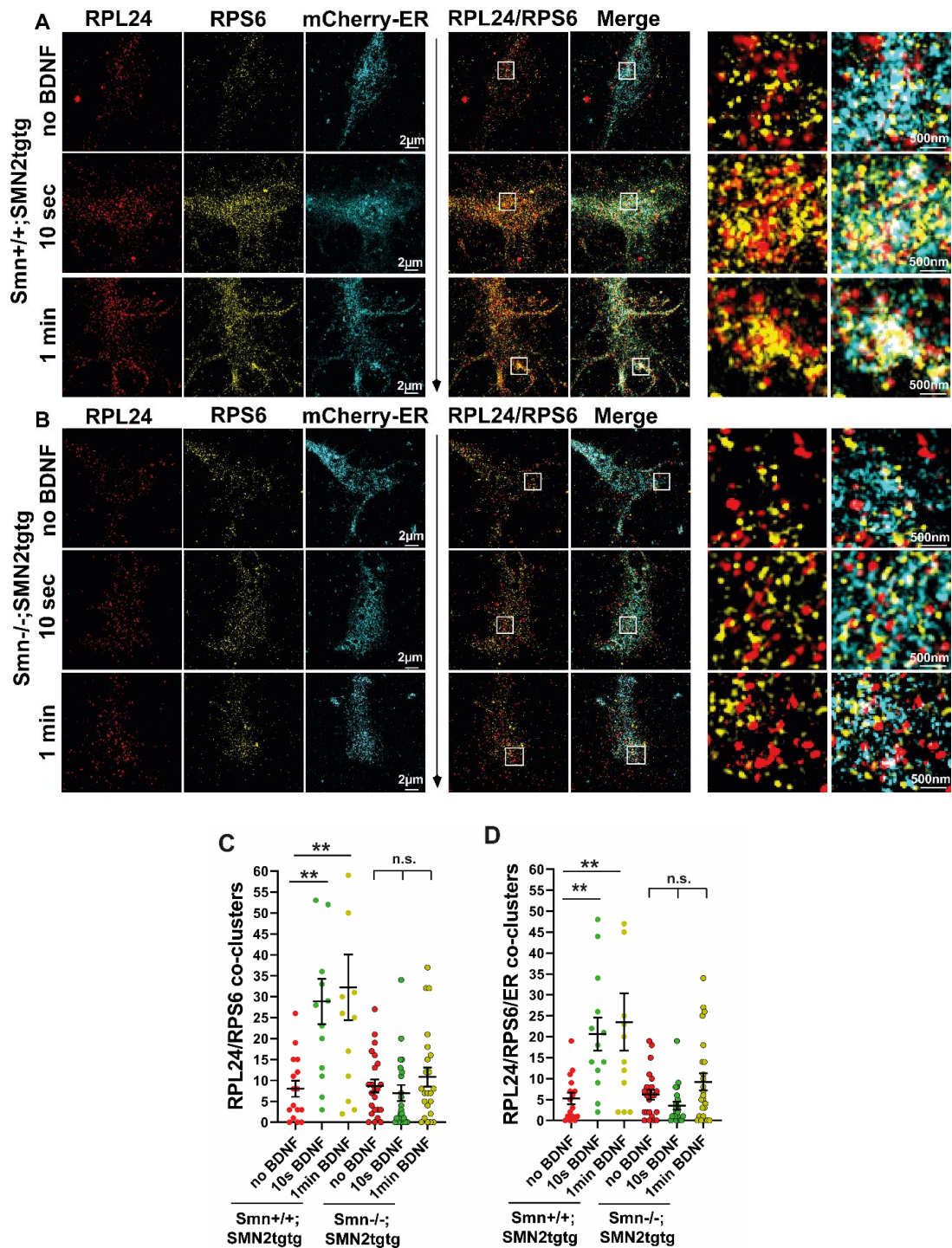


Figure 5.10.1 BDNF-induced assembly of ribosomes and their association with ER in growth cones of **Smn-deficient motoneurons**. (A and B) Representative SIM images of growth cones of *Smn*^{+/+}; *SMN2*^{tg} and *Smn*^{-/-}; *SMN2*^{tg} motoneurons expressing mCherry-ER and immunostained against RPL24 and RPS6. Enlarged images of ROIs marked by white square boxes show the association between RPL24, RPS6 and ER. (C) Graph shows that the number of RPL24/RPS6 co-clusters is enhanced in the control group upon BDNF stimulation (**, $P=0.0047$; $P=0.0095$; $n=13-16$ cells, 3 independent experiments), but not increased in *Smn*-deficient motoneurons (n.s., $P>0.9999$; $n=21-23$ cells, 3 independent experiments). (D) The increase in number of ER-

associated RPL24/RPS6 co-clusters induced by 10 sec and 1 min BDNF stimulation that happens in the control group (**, $P=0.0022$; $P=0.0088$; $n=13-16$ cells, 3 independent experiments) does not occur in *Smn*-deficient cells (n.s., $P>0.9999$; $n=21-23$ cells, 3 independent experiments). Statistical analysis: one-way ANOVA with Dunn's post-test. Graphs were shown in scatter dot plot with mean \pm SEM.

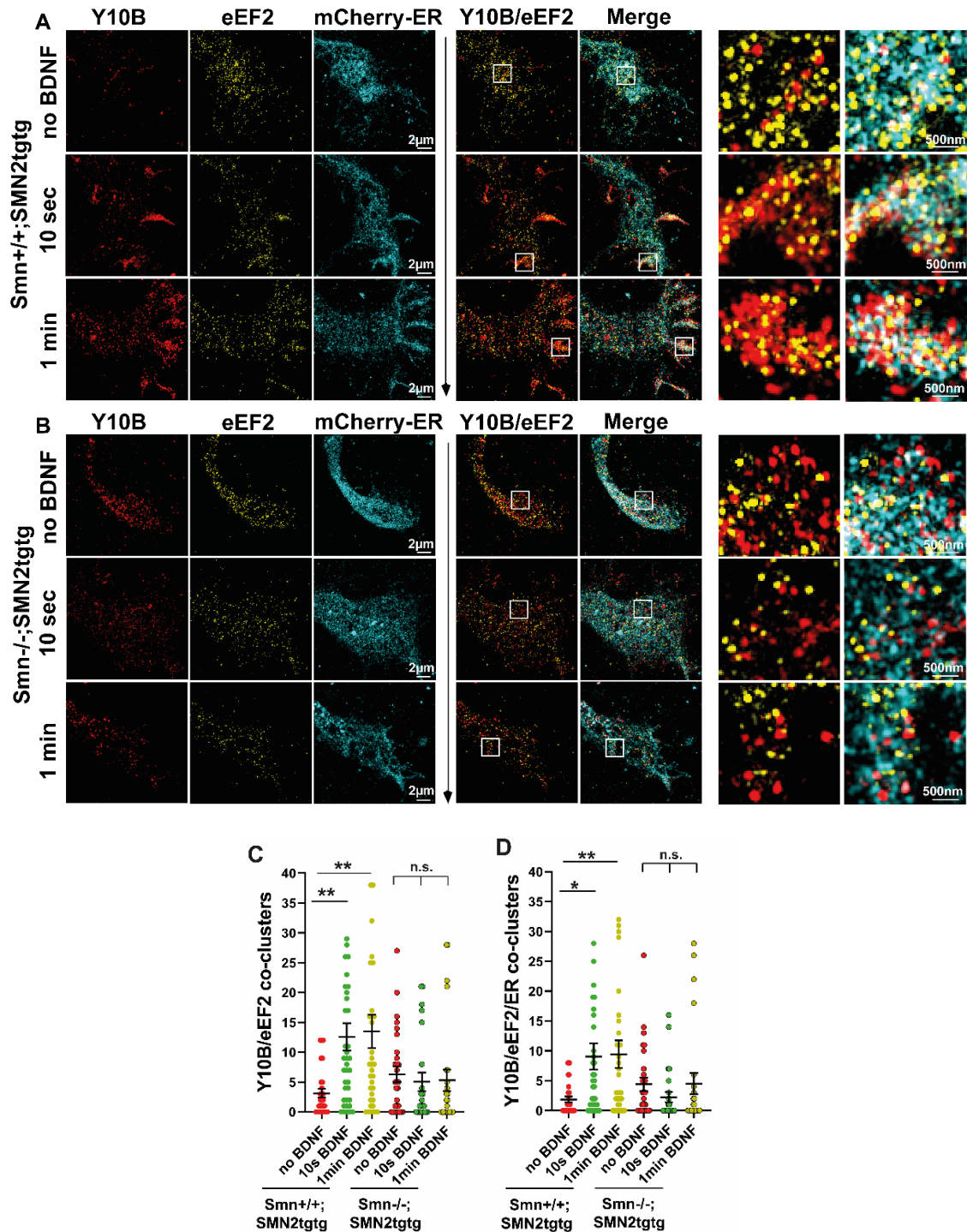


Figure 5.10.2 In *Smn*-deficient motoneurons, ribosomes and ER tethering is impaired during translation elongation phase. (A and B) Representative SIM images of growth cones of *Smn*^{+/+}; *SMN2tg/tg* (A) and *Smn*^{-/-}

; *SMN2tggtg* (B) Motoneurons expressing mCherry-ER that were immunostained against rRNA (Y10B), eEF2 and mCherry-ER after 10 sec and 1 min BDNF stimulation to visualize the kinetics of translating ribosomes. Magnified images were marked by white square boxes. (C) Graph demonstrates that SMN deficiency abolishes the BDNF-induced increase of Y10B/eEF2 co-clusters (n.s., $P > 0.9999$; $n = 23-29$ cells, 3 independent experiments), that is shown in the control group (**, $P = 0.0022$; **, $P = 0.0053$; $n = 28-38$ cells, 3 independent experiments). (D) Quantification of Y10B/eEF2/ER co-clusters also indicates that loss of SMN results in blockage of an increased number of Y10B/eEF2 associated with ER (*, $P = 0.0101$; **, $P = 0.0066$; $n = 28-38$ cells, 3 independent experiments), compared to the control group (n.s., $P = 0.5647$; $n = 23-29$ cells, 3 independent experiments). Statistical analysis: one-way ANOVA with Dunn's post-test. Data are shown as scatter dot plot with mean \pm SEM.

5.11 Basic TrkB levels are comparable in growth cones of Snn-deficient and control motoneurons

As shown above that in Snn-deficient motoneurons, BDNF-stimulated ribosomal activation and protein synthesis in growth cones were affected and BDNF-induced ribosome change depends on TrkB. BDNF binds to its receptor TrkB and activates signaling pathways to regulate protein production (Takei, Kawamura et al. 2001, Santos, Comprido et al. 2010). Hence, it was assessed whether TrkB levels in motoneurons could be altered by deficiency of SMN protein. First, WB of the whole lysates from cultured *Snn*^{-/-}; *SMN2tggtg* and *Snn*^{+/+}; *SMN2tggtg* motoneurons without BDNF stimulation that describes the basic level of TrkB did not show an obvious difference in TrkB levels in the whole lysates from Snn-deficient and control neurons (Fig. 5.11.1 A). Immunofluorescence staining of TrkB showed similar TrkB levels in the soma of unstimulated *Snn*^{-/-}; *SMN2tggtg* and *Snn*^{+/+}; *SMN2tggtg* motoneurons (Fig. 5.11.1 B and C) as well as in growth cones (Fig. 5.11.1 D and E). Furthermore, surface TrkB level was unchanged in growth cones of unstimulated *Snn*^{-/-}; *SMN2tggtg* motoneurons, compared to unstimulated *Snn*^{+/+}; *SMN2tggtg* cells (Fig. 5.11.2). Results of WB and immunocytochemistry revealed that basal levels of TrkB in unstimulated *Snn*^{-/-}; *SMN2tggtg* and *Snn*^{+/+}; *SMN2tggtg* motoneurons are similar.

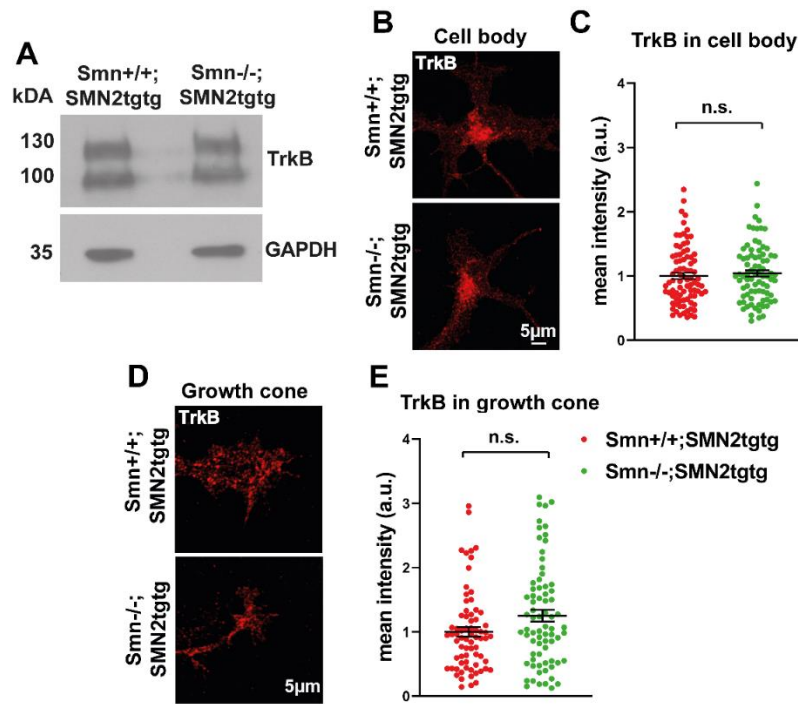


Figure 5.11.1 Total TrkB level of *Smn*-deficient motoneurons is similar with the control group. (A) WB of lysates from cultured motoneurons without BDNF stimulation probed against TrkB and GAPDH (control) shows similar TrkB protein levels under basal conditions. (B) Representative images of soma from *Smn*^{+/+}; *SMN2tgtg* and *Smn*^{-/-}; *SMN2tgtg* motoneurons immunostained against TrkB. (C) Mean intensities of TrkB show a comparable level of TrkB protein in soma of *Smn*^{+/+}; *SMN2tgtg* and *Smn*^{-/-}; *SMN2tgtg* motoneurons (n.s., $P=0.0512$; $n=71-85$ cells, 4 independent experiments). (D) Representative images of growth cones of *Smn*^{+/+}; *SMN2tgtg* and *Smn*^{-/-}; *SMN2tgtg* motoneurons immunostained against TrkB. (E) Graph shows that mean intensities of TrkB in growth cones of control and *Smn*-deficient neurons are not significantly different (n.s., $P=0.4546$; $n=71-85$ cells, 4 independent experiments). Statistical analysis: two-tailed Mann Whitney test. Data are shown as scatter dot plot with mean \pm SEM.

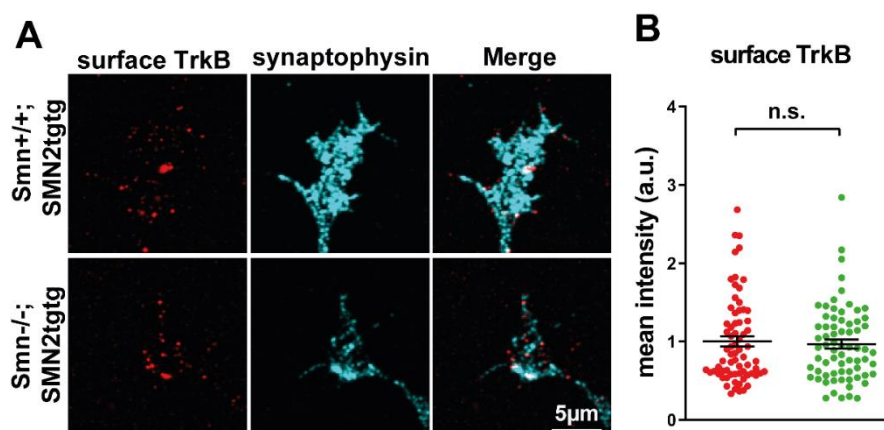


Figure 5.11.2 TrkB levels on the surface of growth cones of *Smn*-deficient motoneurons are comparable to the control. (A) Representative images of surface TrkB labeling in growth cones of unstimulated of *Smn*^{+/+}; *SMN2^{tg}tg* and *Smn*^{-/-}; *SMN2^{tg}tg* motoneurons. Synaptophysin staining was used to outline the growth cones. (B) Graph does not show an obvious difference in mean intensity of surface TrkB in growth cones of unstimulated *Smn*^{+/+}; *SMN2^{tg}tg* and *Smn*^{-/-}; *SMN2^{tg}tg* motoneurons (n.s., P=0.999; n=70 cells, 3 independent experiments). Statistical analysis: two-tailed Mann Whitney test. Data are shown as scatter dot plot with mean ± SEM.

5.12 BDNF induced TrkB activation is altered in axon terminals of *Smn*-deficient motoneurons

Since total TrkB level in the whole cells and surface TrkB level in growth cones are not altered when SMN is deficient, it could be the activation of TrkB induced by BDNF that contributes to the impaired ribosome activation and local translation. First, WB of lysates from the whole neurons showed that in *Smn*-deficient motoneurons, TrkB receptors can be successfully activated by BDNF, same as in control cells (Fig. 5.12.1 A). Immunoreactivity of BDNF-induced pTrkB in soma of *Smn*-deficient motoneurons is also similar to that of control neurons (Fig. 5.12.1 B and C). Then the immunoreactivity of pTrkB and TrkB in growth cones of BDNF-stimulated *Smn*-deficient motoneurons was studied with the purpose of confirmation whether this activation of TrkB could be only affected in subregions such as growth cones (Fig. 5.12.2 A and B). It is of note that BDNF did not induce increased level of pTrkB and TrkB in growth cones of *Smn*-deficient motoneurons, which happened in control cells (Fig. 5.12.2 C and D).

Collectively, BDNF induced TrkB activation is impaired in growth cones of *Smn*-deficient motoneurons but not in soma. This disturbed BDNF/TrkB signaling contributes to disrupted BDNF-induced ribosome activation and local translation.

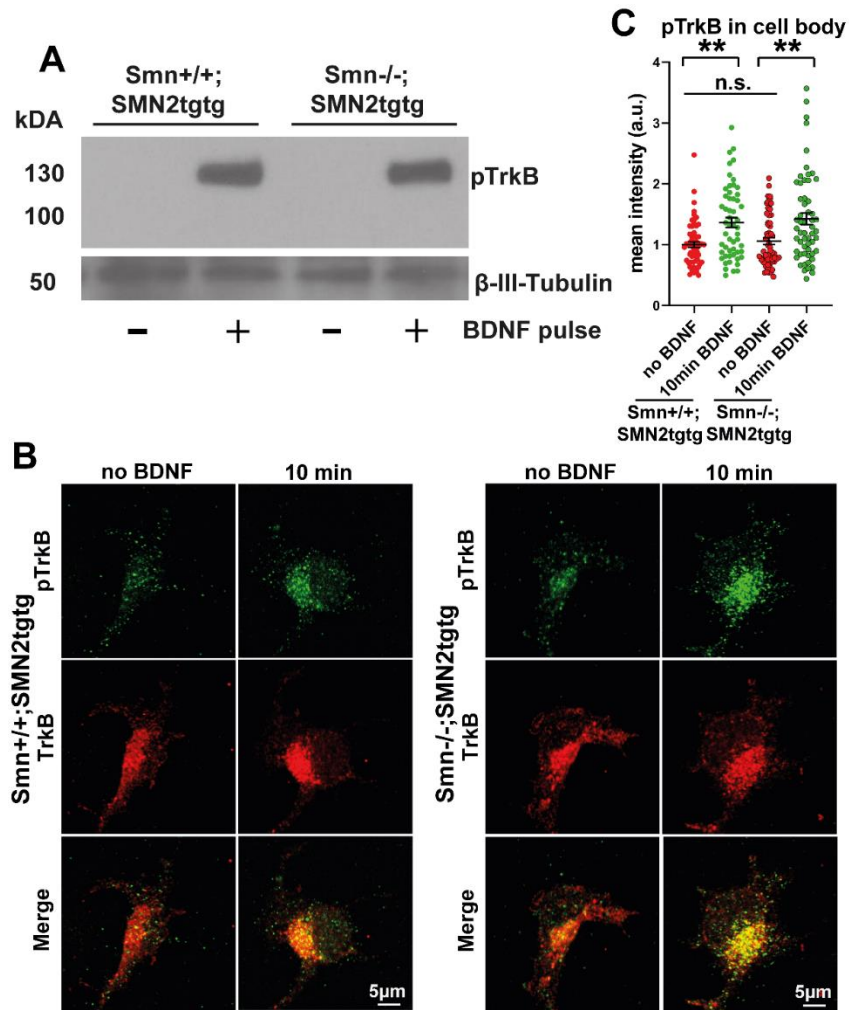


Figure 5.12.1 BDNF can stimulate activation of TrkB in Smn-deficient motoneurons. (A) Representative WB of whole cell lysates from BDNF-stimulated *Smn*^{+/+}; *SMN2tggtg* and *Smn*^{-/-}; *SMN2tggtg* motoneurons probed against pTrkB. β-III-Tubulin was used as loading control. (B) Representative images of cell bodies of *Smn*^{+/+}; *SMN2tggtg* and *Smn*^{-/-}; *SMN2tggtg* motoneurons immunostained against pTrkB and TrkB after 10 min BDNF stimulation. (C) Mean intensity of pTrkB in soma of Smn-deficient motoneurons is increased after BDNF stimulation (**, $P < 0.0011$; $n = 61-98$ cells, 3 independent experiments), similar to the control group (**, $P < 0.0036$; $n = 59$ cells, 3 independent experiments). Statistical analysis: two-tailed Mann Whitney test. Data are shown as scatter dot plot with mean \pm SEM.

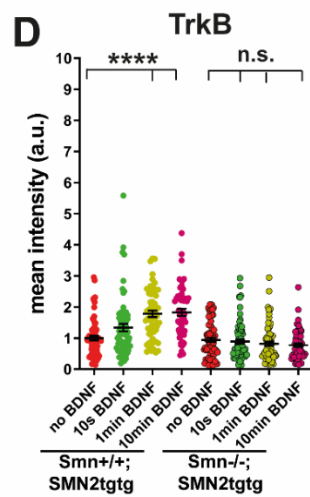
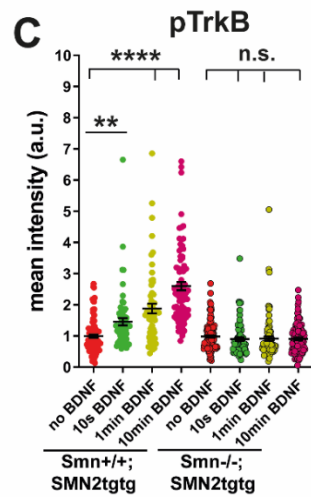
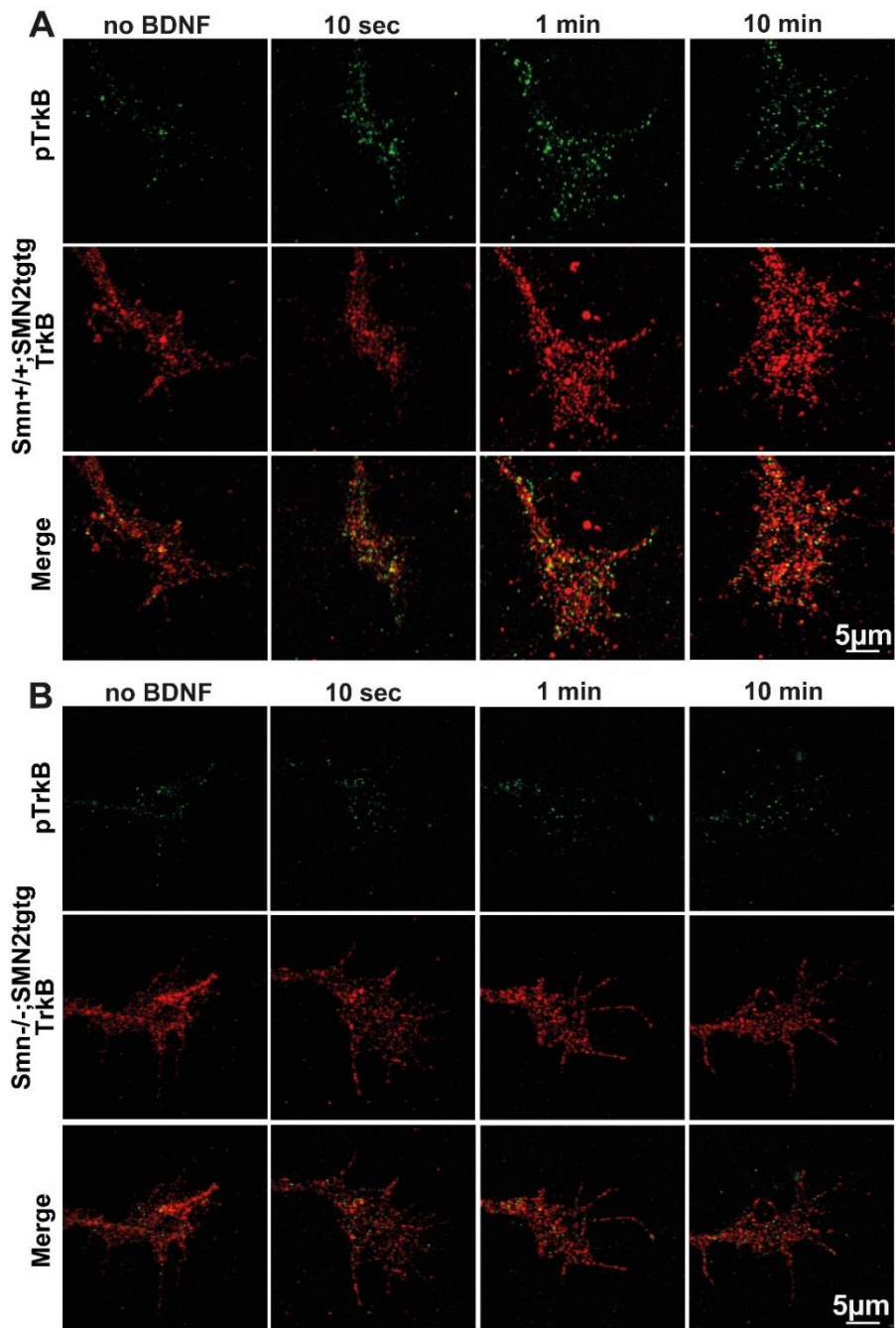


Figure 5.12.2 BDNF does not trigger phosphorylation of TrkB receptor in growth cones of Smn-deficient motoneurons. (A and B) Representative confocal images of growth cones from control and Smn-deficient motoneurons stained against pTrkB and TrkB after 10 sec, 1 min and 10 min BDNF stimulation. (C and D) Mean intensities of pTrkB and TrkB in growth cones of Smn-deficient motoneurons do not increase after BDNF stimulation (n.s., $P \geq 0.6078$; $n=65-76$ cells), while in control neurons, pTrkB and TrkB levels increase significantly after BDNF pulse (****, $P < 0.0001$; $n=54-76$ cells, 4 independent experiments). Statistical analysis: one-way ANOVA with Dunn's post-test. Data are shown as scatter dot plot with mean \pm SEM.

6. Discussion

6.1 ER dynamics depend on drebrin A-mediated actin/microtubule crosstalk in axonal growth cones in motoneurons.

ER is a physically continuous organelle, that is highly dynamic and distributes throughout all eukaryotic cells including neurons. As a type of extremely polarized cells, neurons face the challenges of maintaining and dynamic remodeling of these physical structures as well as regulation of biological functions in dendrites and long axons that can have a length of up to 1 meter. Recent studies on mechanisms underlying regulation of axonal ER dynamics and its functions have brought greater attention to these aspects (Summerville, Faust et al. 2016, De Gregorio, Delgado et al. 2017, Lindhout, Cao et al. 2019). As one type of cytoskeleton filaments, MTs have been found closely connected with ER remodeling in animal cells including neurons (Waterman-Storer and Salmon 1998, Farías, Fréal et al. 2019, Pavez, Thompson et al. 2019), while the interaction between ER and another type of cytoskeleton filaments, actin filaments, has not been clearly studied in detail, particularly in axons and presynaptic compartments of neurons. Here, I focused on the interaction between ER and cytoskeletal actin and MTs in sub-regions of cultured motoneurons: growth cone filopodia and core.

Axonal growth cones consist of different domains: growth cone core and membrane protrusions. Growth cone core localizes in the central region and seems relatively more stable and membrane protrusions, also called filopodia and lamellipodia, are highly dynamic (Dent and Gertler 2003). While in the central region MTs are abundant, filopodia and lamellipodia are enriched in actin and mostly lack MTs. These filopodia structures can exceed core region (Mallavarapu and Mitchison 1999). Interestingly, live cell imaging and analysis of ER dynamics in growth cones of cultured motoneurons revealed significantly higher ER dynamics in filopodia where actin is abundant and slower ER movements in core that is enriched in MTs. Further, actin and MTs are found both important for ER movements in the growth cone core and actin is particularly required for ER dynamics in growth cone filopodia. Disruption of actin filaments by cytochalasin D treatment resulted in failed ER movements in filopodia of 80% of observed motoneurons. Tracking of GFP-actin and ER simultaneously revealed co-movements of actin and ER in some of the growth cone filopodia, while in some filopodia, ER retracts and extends without actin movements. These results show the direct interaction between actin and ER dynamic remodeling and integrity in distal axons of motoneurons for the first time. ER extension into filopodia supposes a membrane contact between ER and the PM (Wu, Whiteus et al. 2017) and this physical contact could be involved in surface delivery of locally synthesized products such as receptors, membrane proteins and receptors. Actin-based motors such as myosin Va that transports ER into dendritic spines of Purkinje neurons (Wagner, Brenowitz et al. 2011) might also contribute to the regulation of axonal ER dynamic movements in filopodia. However, my study found that actin-based motor proteins myosin V and VI are both involved in ER dynamics in growth cones of motoneurons. In particular, pharmacological inhibition of myosin VI affects ER dynamics in filopodia to the greatest extent.

It has been shown that ER movement along MTs is mediated by TAC in a way that a complex of STIM1 and EB1 connects ER and MT plus end and thus driving the movement of ER

together with the MT, or by MT motor proteins such as kinesin and dynein-based sliding (Waterman-Storer and Salmon 1998, Friedman, Webster et al. 2010). On the other hand, investigations have observed that disruption of MTs with nocodazole treatment does not cause immediately retraction of peripheral ER (Terasaki, Chen et al. 1986) and in the absence of MTs, cultured cells can still form ER tubules (Dreier and Rapoport 2000, Voeltz, Prinz et al. 2006, Wang, Romano et al. 2013). In my study, nocodazole treatment caused a decrease in ER movements in both growth cone filopodia and core. Previously published studies have shown that actin and MT interaction with each other is mediated by macromolecules such as drebrin E through connecting F-actin with MT plus end binding proteins (Zhao, Meka et al. 2017, Dogterom and Koenderink 2019). My data implicated that, albeit mRNA levels of drebrin isoforms: drebrin A and E are similar in cultured motoneurons, only knockdown of drebrin A decreases ER dynamics in growth cone core and filopodia, while additional knockdown of drebrin E does not further reduce ER dynamics. These data point to a specific function of drebrin A in actin and MT crosstalk during regulation of ER dynamic movements.

6.2 ER associates with active ribosomes and contributes to protein synthesis including transmembrane proteins in axonal growth cones of cultured motoneurons

Protein degradation and production take place constantly. Subcellular localization of transcripts and local protein synthesis ensure spatial and temporal regulation of the proteomics in subcellular compartments, thus controlling the axonal growth, synapse differentiation and plasticity (Holt, Martin et al. 2019). ER and cytosol are two major compartments for protein synthesis (Reid and Nicchitta 2015). Transcripts encoding membrane and secreted proteins are detectable in axonal compartment (Willis, van Niekerk et al. 2007, Saal, Briese et al. 2014, Pouloupoulos, Murphy et al. 2019) and de novo synthesis of these types of proteins require rough ER and Golgi apparatus for glycosylation. Even though

so far, no direct evidence supports that ER is enriched in ribosomes and as a hot spot for protein synthesis in the axonal compartment (Tsukita and Ishikawa 1976, Krijnse-Locker, Parton et al. 1995, Horton and Ehlers 2003), Golgi components have been found in DRG axons and at postsynapses of hippocampal neurons (Hanus and Ehlers 2008, Merianda, Lin et al. 2009). In dendrites, an unconventional secretory pathway bypassing the Golgi apparatus has been observed for GluA2-containing glutamate receptors (Hanus, Geptin et al. 2016). Results from my study provide evidence for a function of ER in growth cones in local protein synthesis of membrane proteins such as N-type Ca^{2+} channel.

BDNF-activated signaling pathways are involved in protein synthesis in neurons via regulation of translation initiation and elongation (Takei, Inamura et al. 2004, Manadas, Santos et al. 2009, Esvald, Tuvikene et al. 2020). We used super-resolution microscopy and showed that, extracellular BDNF application triggers assembly of ribosomes on a time scale of seconds and increases the number of ribosomes at the stage of elongation in growth cones of motoneurons. These active ribosomes tether to ER in growth cones in response to BDNF. On the contrary, BDNF-induced ribosomal response in soma happened much slower than that in distal axonal compartment, even though the activation of TrkB was detectable upon 10 s BDNF stimulation in both compartments. These differences in dynamics of BDNF-induced ribosomal activation in soma and growth cones could be due to distinct signaling pathways such as the second messenger cyclic adenosine monophosphate (cAMP) (Ming, Song et al. 1997).

Furthermore, it was shown in my study that extracellular BDNF induces the global protein synthesis and the local translation of the specific transmembrane protein α -1 β subunits of N-type Ca^{2+} channels as well as cytosolic protein β -actin that can be detected upon 1 min stimulation. Fast association of ribosomes onto ER could support the existence of RER and its function in providing the sites for post-translational process of locally synthesized proteins induced by extracellular stimuli. However, 30 min continuous BDNF exposure abolishes the

effect on activation of ribosomes and their attachment with ER. This fast and transient extracellular stimuli-induced ribosomal response could be the reason for the failed detection of RER in axon terminals in previously published studies, indicating that without specific and proper stimulation, RER could not be detected. Taken together, my data have provided evidence for a novel function of ER in BDNF-induced local translation of proteins including transmembrane protein α -1 β subunits of N-type Ca^{2+} channels in distal axonal compartment of cultured motoneurons.

6.3 ER dynamics are impaired in growth cones of SMA motoneurons

Disturbance of ER organization, morphology and dynamic remodeling is closely correlated with its dysfunction and with neurodegenerative diseases (Elden, Kim et al. 2010, Sharoar, Shi et al. 2016, Parodi, Coarelli et al. 2018). For example, HSPs are associated with mutations in different ER-shaping proteins including spastin, REEP, atlastin and RTN2 (Park, Zhu et al. 2010, Boutry, Morais et al. 2019). VAPA and VAPB proteins are involved in maintaining proper ER morphology and in regulating SV cycling (Elden, Kim et al. 2010, Lindhout, Cao et al. 2019). These proteins are required for connecting membranes of opposite organelles at the site of MCSs (Teuling, Ahmed et al. 2007), and are mutated in ALS (Elden, Kim et al. 2010, Lindhout, Cao et al. 2019). AD patients and AD mouse models harbor mis-localization and accumulation of tubular ER in the brain (Sharoar, Shi et al. 2016). Mutations in Rab10 that influences ER morphology were identified in AD patients (Shim, Wang et al. 2008, Ridge, Karch et al. 2018). Therefore, mutations in genes encoding these proteins disrupt functions of ER as well as the functions of MCSs associated organelles such as mitochondria (Öztürk, O'Kane et al. 2020). One of my interesting findings is that low expression level of SMN protein correlates with impaired ER dynamics in growth cones of cultured motoneurons and disruption of actin polymerization does not further decrease the ER dynamics in growth cones of Smn-deficient motoneurons. These data suggest that disturbed ER movements in

Smn-deficient motoneurons are associated with impairment of actin dynamics. In accordance with this indication, SIM images and line scan analysis of immunostained growth cones demonstrate a defective colocalization of F-actin and ER in the growth cone of *Smn*-deficient motoneurons. Under basal conditions without BDNF stimulation, TrkB levels in the whole motoneurons and in sub-compartments such as soma, axonal growth cones and on the surface of growth cones are comparable in *Smn*-deficient and WT neurons, indicating that the activable TrkB receptors are not defective when SMN is lost. These data exclude the possibility that less TrkB contributes to impaired ER dynamics and thus, actin impairment is responsible for defective ER dynamic remodeling.

In addition, other studies also have given hints for actin impairment in the context of SMA mouse models and SMA patients. For instance, in cultured motoneurons, loss of SMN protein results in disturbed localization of transcripts in axons and defective local synthesis of actin isoforms Act α and Act β , consequently leading to damaged polymerization of F-actin in the growth cone (Moradi, Sivadasan et al. 2017). So far, there is no evidence that shows the direct interaction between SMN protein and F-actin. But actin-associated proteins have been identified to connect with SMN. As an example, profilin2 as a regulator of actin dynamics has been proved to be expressed mainly in nerve tissues and connect to SMN protein directly (Giesemann, Schwarz et al. 2003, Nölle, Zeug et al. 2011). Less SMN interacting with profilin2 permits profilin2 release that leads to more binding of profilin2 to monomer actin and thus decreases polymerization of actin (Sharma, Lambrechts et al. 2005). Overexpression of PLS3, an actin related protein that regulates its turnover, has been shown to rescue the defective axonal length and outgrowth caused by loss of SMN protein (Oprea, Kröber et al. 2008).

6.4 BDNF/TrkB induced dynamics of translational machinery is defected in SMA.

SMN is required for the assembly of snRNPs, which is essential for pre-mRNA splicing and loss of SMN causes mis-localization of transcripts in axons (Sanchez, Dury et al. 2013, Bernabo, Tebaldi et al. 2017, Moradi, Sivadasan et al. 2017). Furthermore, SMN has also been shown to interact directly with actively translating ribosomes in the spinal cord and brain tissues as well as cultured cells (Bechade, Rostaing et al. 1999, Lauria, Bernabo et al. 2020). In my study, it was found that activation of ribosomes in response to extracellular BDNF stimulation was impaired and the number of fully assembled ribosomes attached to ER was not increased in growth cones of Smn-deficient motoneurons. Interestingly, the total level of TrkB in Smn-deficient motoneurons is similar with that in control cells, and the basic levels of TrkB in sub-compartments including soma and growth cones of unstimulated Smn-deficient motoneurons are also comparable to that of unstimulated control cells, indicating that TrkB receptors that are ready for activation under basal condition are not impaired when SMN is deficient. But the enhancement in TrkB levels, that appears within 1 min and 10 min in the growth cone of control motoneurons is abolished when SMN is deficient. This increased level of TrkB is considered essential for its translocation to cell surface in order to increase the BDNF/TrkB signaling (Andreska, Lüningschrör et al. 2020). Combining a published study that showed TrkB transport to cell membrane was blocked by CytoD application to destroy actin filaments (Zhao, Sheng et al. 2009) with our observation that CytoD treatment inhibits BDNF induced ribosomal assembly and activation, it is suggested that translocation of ribosomes to ER upon BDNF stimulation might be actin dependent and this actin dependent movements of ribosomes, TrkB receptors and ER dynamics could be the underlying mechanisms for axonopathies in SMA.

7. References

Ackermann, B., S. Kröber, L. Torres-Benito, A. Borgmann, M. Peters, S. M. Hosseini Barkoöie, R. Tejero, M. Jakubik, J. Schreml, J. Milbradt, T. F. Wunderlich, M. Riessland, L. Tabares and B. Wirth (2013). "Plastin 3 ameliorates spinal muscular atrophy via delayed axon pruning and improves neuromuscular junction functionality." *Human Molecular Genetics* **22**(7): 1328-1347.

Allison, R., J. R. Edgar, G. Pearson, T. Rizo, T. Newton, S. Günther, F. Berner, J. Hague, J. W. Connell, J. Winkler, J. Lippincott-Schwartz, C. Beetz, B. Winner and E. Reid (2017). "Defects in ER-endosome contacts impact lysosome function in hereditary spastic paraplegia." *J Cell Biol* **216**(5): 1337-1355.

Alvarez-Fischer, D., J. Fuchs, F. Castagner, O. Stettler, O. Massiani-Beaudoin, K. L. Moya, C. Bouillot, W. H. Oertel, A. Lombès, W. Faigle, R. L. Joshi, A. Hartmann and A. Prochiantz (2011). "Engrailed protects mouse midbrain dopaminergic neurons against mitochondrial complex I insults." *Nat Neurosci* **14**(10): 1260-1266.

Andreassi, C., C. Zimmermann, R. Mitter, S. Fusco, S. De Vita, A. Saiardi and A. Riccio (2010). "An NGF-responsive element targets myo-inositol monophosphatase-1 mRNA to sympathetic neuron axons." *Nat Neurosci* **13**(3): 291-301.

Andreska, T., P. Lüningschrör and M. Sendtner (2020). "Regulation of TrkB cell surface expression-a mechanism for modulation of neuronal responsiveness to brain-derived neurotrophic factor." *Cell Tissue Res* **382**(1): 5-14.

Aschrafi, A., A. D. Schwechter, M. G. Mameza, O. Natera-Naranjo, A. E. Gioio and B. B. Kaplan (2008). "MicroRNA-338 regulates local cytochrome c oxidase IV mRNA levels and oxidative phosphorylation in the axons of sympathetic neurons." *J Neurosci* **28**(47): 12581-12590.

Aviner, R. (2020). "The science of puromycin: From studies of ribosome function to applications in biotechnology." *Comput Struct Biotechnol J* **18**: 1074-1083.

Bassell, G. J., H. Zhang, A. L. Byrd, A. M. Femino, R. H. Singer, K. L. Taneja, L. M. Lifshitz, I. M. Herman and K. S. Kosik (1998). "Sorting of β -Actin mRNA and Protein to Neurites and Growth Cones in Culture." *The Journal of Neuroscience* **18**(1): 251-265.

Bechade, C., P. Rostaing, C. Cisterni, R. Kalisch, V. La Bella, B. Pettmann and A. Triller (1999). "Subcellular distribution of survival motor neuron (SMN) protein: possible involvement in nucleocytoplasmic and dendritic transport." *Eur J Neurosci* **11**(1): 293-304.

Beetz, C., R. Schüle, T. Deconinck, K. N. Tran-Viet, H. Zhu, B. P. Kremer, S. G. Frints, W. A. van Zelst-Stams, P. Byrne, S. Otto, A. O. Nygren, J. Baets, K. Smets, B. Ceulemans, B. Dan, N. Nagan, J. Kassubek, S. Klimpe, T. Klopstock, H. Stolze, H. J. Smeets, C. T. Schrandt-Stumpel, M. Hutchinson, B. P. van de Warrenburg, C. Braastad, T. Deufel, M. Pericak-Vance, L. Schöls, P. de Jonghe and S. Züchner (2008). "REEP1 mutation spectrum and genotype/phenotype correlation in hereditary spastic paraplegia type 31." *Brain* **131**(Pt 4): 1078-1086.

Bellofatto, M., G. De Michele, A. Iovino, A. Filla and F. M. Santorelli (2019). "Management of Hereditary Spastic Paraplegia: A Systematic Review of the Literature." *Frontiers in Neurology* **10**(3).

Ben-Shem, A., N. Garreau de Loubresse, S. Melnikov, L. Jenner, G. Yusupova and M. Yusupov (2011). "The structure of the eukaryotic ribosome at 3.0 Å resolution." *Science* **334**(6062): 1524-1529.

Bernabo, P., T. Tebaldi, E. J. N. Groen, F. M. Lane, E. Perenthaler, F. Mattedi, H. J. Newbery, H. Zhou, P. Zuccotti, V. Potrich, H. K. Shorrock, F. Muntoni, A. Quattrone, T. H. Gillingwater and G. Viero (2017). "In Vivo Translatome Profiling in Spinal Muscular Atrophy Reveals a Role for SMN Protein in Ribosome Biology." *Cell Rep* **21**(4): 953-965.

Bernabò, P., T. Tebaldi, E. J. N. Groen, F. M. Lane, E. Perenthaler, F. Mattedi, H. J. Newbery, H. Zhou, P. Zuccotti, V. Potrich, H. K. Shorrock, F. Muntoni, A. Quattrone, T. H. Gillingwater and G. Viero (2017). "In Vivo Translatome Profiling in Spinal Muscular Atrophy Reveals a Role for SMN Protein in Ribosome Biology." *Cell Reports* **21**(4): 953-965.

Bernard-Marissal, N., R. Chrast and B. L. Schneider (2018). "Endoplasmic reticulum and mitochondria in diseases of motor and sensory neurons: a broken relationship?" *Cell Death & Disease* **9**(3): 333.

Bernard-Marissal, N., J. J. Médard, H. Azzedine and R. Chrast (2015). "Dysfunction in endoplasmic reticulum-mitochondria crosstalk underlies SIGMAR1 loss of function mediated motor neuron degeneration." *Brain* **138**(Pt 4): 875-890.

Bernhard, W. and C. Rouiller (1956). "Close topographical relationship between mitochondria and ergastoplasm of liver cells in a definite phase of cellular activity." J Biophys Biochem Cytol **2**(4 Suppl): 73-78.

Biever, A., C. Glock, G. Tushev, E. Ciirdaeva, T. Dalmay, J. D. Langer and E. M. Schuman (2020). "Monosomes actively translate synaptic mRNAs in neuronal processes." Science **367**(6477).

Blackstone, C., C. J. O'Kane and E. Reid (2011). "Hereditary spastic paraplegias: membrane traffic and the motor pathway." Nat Rev Neurosci **12**(1): 31-42.

Bobinac, Y., C. Marcaillou, X. Morin and A. Debec (2003). "Dynamics of the endoplasmic reticulum during early development of *Drosophila melanogaster*." Cell Motil Cytoskeleton **54**(3): 217-225.

Böckler, S. and B. Westermann (2014). "Mitochondrial ER contacts are crucial for mitophagy in yeast." Dev Cell **28**(4): 450-458.

Boutry, M., S. Morais and G. Stevanin (2019). "Update on the Genetics of Spastic Paraplegias." Curr Neurol Neurosci Rep **19**(4): 18.

Brady, J. P., J. K. Claridge, P. G. Smith and J. R. Schnell (2015). "A conserved amphipathic helix is required for membrane tubule formation by Yop1p." Proceedings of the National Academy of Sciences **112**(7): E639-E648.

Briese, M., L. Saal, S. Appenzeller, M. Moradi, A. Baluapuri and M. Sendtner (2016). "Whole transcriptome profiling reveals the RNA content of motor axons." Nucleic Acids Res **44**(4): e33.

Bunge, M. B. (1973). "Fine structure of nerve fibers and growth cones of isolated sympathetic neurons in culture." J Cell Biol **56**(3): 713-735.

Burchell, A., B. B. Allan and R. Hume (1994). "Glucose-6-phosphatase proteins of the endoplasmic reticulum." Mol Membr Biol **11**(4): 217-227.

Burghes, A. H. M. and C. E. Beattie (2009). "Spinal muscular atrophy: why do low levels of survival motor neuron protein make motor neurons sick?" Nature reviews. Neuroscience **10**(8): 597-609.

Cajigas, I. J., G. Tushev, T. J. Will, S. tom Dieck, N. Fuerst and E. M. Schuman (2012). "The local transcriptome in the synaptic neuropil revealed by deep sequencing and high-resolution imaging." Neuron **74**(3): 453-466.

Campbell, D. S. and C. E. Holt (2001). "Chemotropic responses of retinal growth cones mediated by rapid local protein synthesis and degradation." Neuron **32**(6): 1013-1026.

Capell, B. C. and F. S. Collins (2006). "Human laminopathies: nuclei gone genetically awry." Nat Rev Genet **7**(12): 940-952.

Casadio, A., K. C. Martin, M. Giustetto, H. Zhu, M. Chen, D. Bartsch, C. H. Bailey and E. R. Kandel (1999). "A transient, neuron-wide form of CREB-mediated long-term facilitation can be stabilized at specific synapses by local protein synthesis." Cell **99**(2): 221-237.

Chang, J., S. Lee and C. Blackstone (2013). "Protrudin binds atlastins and endoplasmic reticulum-shaping proteins and regulates network formation." Proceedings of the National Academy of Sciences **110**(37): 14954-14959.

Chao, J. A., Y. Patskovsky, V. Patel, M. Levy, S. C. Almo and R. H. Singer (2010). "ZBP1 recognition of beta-actin zipcode induces RNA looping." Genes Dev **24**(2): 148-158.

Chen, S., P. Novick and S. Ferro-Novick (2012). "ER network formation requires a balance of the dynamin-like GTPase Sey1p and the Lunapark family member Lnp1p." Nat Cell Biol **14**(7): 707-716.

Clapham, D. E. (2007). "Calcium signaling." Cell **131**(6): 1047-1058.

Cox, L. J., U. Hengst, N. G. Gurskaya, K. A. Lukyanov and S. R. Jaffrey (2008). "Intra-axonal translation and retrograde trafficking of CREB promotes neuronal survival." Nat Cell Biol **10**(2): 149-159.

Crawford, T. O. and C. A. Pardo (1996). "The neurobiology of childhood spinal muscular atrophy." Neurobiol Dis **3**(2): 97-110.

Dahm, R., M. Zeitelhofer, B. Götze, M. A. Kiebler and P. Macchi (2008). Visualizing mRNA Localization and Local Protein Translation in Neurons. Methods in Cell Biology, Academic Press. **85**: 293-327.

Dailey, M. and P. Bridgman (1989). "Dynamics of the endoplasmic reticulum and other membranous organelles in growth cones of cultured neurons." The Journal of Neuroscience **9**(6): 1897-1909.

Dailey, M. E. and P. C. Bridgman (1989). "Dynamics of the endoplasmic reticulum and other membranous organelles in growth cones of cultured neurons." J Neurosci **9**(6): 1897-1909.

de Brito, O. M. and L. Scorrano (2008). "Mitofusin 2 tethers endoplasmic reticulum to mitochondria." Nature **456**(7222): 605-610.

De Gregorio, C., R. Delgado, A. Ibacache, J. Sierralta and A. Couve (2017). "Drosophila Atlastin in motor neurons is required for locomotion and presynaptic function." J Cell Sci **130**(20): 3507-3516.

de Juan-Sanz, J., G. T. Holt, E. R. Schreiter, F. de Juan, D. S. Kim and T. A. Ryan (2017). "Axonal Endoplasmic Reticulum Ca(2+) Content Controls Release Probability in CNS Nerve Terminals." Neuron **93**(4): 867-881.e866.

del Castillo, U., M. M. Gnazzo, C. G. Sorensen Turpin, K. C. Q. Nguyen, E. Semaya, Y. Lam, M. A. de Cruz, J. N. Bembenek, D. H. Hall, B. Riggs, V. I. Gelfand and A. R. Skop (2019). "Conserved role for Ataxin-2 in mediating endoplasmic reticulum dynamics." Traffic **20**(6): 436-447.

Dent, E. W. and F. B. Gertler (2003). "Cytoskeletal dynamics and transport in growth cone motility and axon guidance." Neuron **40**(2): 209-227.

Denton, K. R., L. Lei, J. Grenier, V. Rodionov, C. Blackstone and X. J. Li (2014). "Loss of spastin function results in disease-specific axonal defects in human pluripotent stem cell-based models of hereditary spastic paraplegia." Stem Cells **32**(2): 414-423.

Dogterom, M. and G. H. Koenderink (2019). "Actin-microtubule crosstalk in cell biology." Nat Rev Mol Cell Biol **20**(1): 38-54.

Dong, R., Y. Saheki, S. Swarup, L. Lucast, J. W. Harper and P. De Camilli (2016). "Endosome-ER Contacts Control Actin Nucleation and Retromer Function through VAP-Dependent Regulation of PI4P." Cell **166**(2): 408-423.

Dong, R., T. Zhu, L. Benedetti, S. Gowrishankar, H. Deng, Y. Cai, X. Wang, K. Shen and P. De Camilli (2018). "The inositol 5-phosphatase INPP5K participates in the fine control of ER organization." J Cell Biol **217**(10): 3577-3592.

Dreier, L. and T. A. Rapoport (2000). "In vitro formation of the endoplasmic reticulum occurs independently of microtubules by a controlled fusion reaction." J Cell Biol **148**(5): 883-898.

Du, Y., S. Ferro-Novick and P. Novick (2004). "Dynamics and inheritance of the endoplasmic reticulum." Journal of Cell Science **117**(14): 2871-2878.

DuBoff, B., M. Feany and J. Götz (2013). "Why size matters - balancing mitochondrial dynamics in Alzheimer's disease." Trends Neurosci **36**(6): 325-335.

Dull, T., R. Zufferey, M. Kelly, R. J. Mandel, M. Nguyen, D. Trono and L. Naldini (1998). "A third-generation lentivirus vector with a conditional packaging system." J Virol **72**(11): 8463-8471.

Eden, E. R. (2016). "The formation and function of ER-endosome membrane contact sites." Biochim Biophys Acta **1861**(8 Pt B): 874-879.

Eggert, C., A. Chari, B. Laggenbauer and U. Fischer (2006). "Spinal muscular atrophy: the RNP connection." Trends in Molecular Medicine **12**(3): 113-121.

Elden, A. C., H. J. Kim, M. P. Hart, A. S. Chen-Plotkin, B. S. Johnson, X. Fang, M. Armakola, F. Geser, R. Greene, M. M. Lu, A. Padmanabhan, D. Clay-Falcone, L. McCluskey, L. Elman, D. Juhr, P. J. Gruber, U. Rüb, G. Auburger, J. Q. Trojanowski, V. M. Lee, V. M. Van Deerlin, N. M. Bonini and A. D. Gitler (2010). "Ataxin-2 intermediate-length polyglutamine expansions are associated with increased risk for ALS." Nature **466**(7310): 1069-1075.

English, A. R. and G. K. Voeltz (2013). "Rab10 GTPase regulates ER dynamics and morphology." Nat Cell Biol **15**(2): 169-178.

Espadas, J., D. Pendin, R. Bocanegra, A. Escalada, G. Misticoni, T. Trevisan, A. Velasco Del Olmo, A. Montagna, S. Bova, B. Ibarra, P. I. Kuzmin, P. V. Bashkirov, A. V. Shnyrova, V. A. Frolov and A. Daga (2019). "Dynamic constriction and fission of endoplasmic reticulum membranes by reticulon." Nat Commun **10**(1): 5327.

Esteves, T., A. Durr, E. Mundwiller, J. L. Loureiro, M. Boutry, M. A. Gonzalez, J. Gauthier, K. H. El-Hachimi, C. Depienne, M. P. Muriel, R. F. Acosta Lebrigio, M. Gausson, A. Noreau, F. Speziani, A. Dionne-Laporte, J. F. Deleuze, P. Dion, P. Coutinho, G. A. Rouleau, S. Zuchner, A. Brice, G. Stevanin and F. Darios (2014). "Loss of association of REEP2 with membranes leads to hereditary spastic paraplegia." Am J Hum Genet **94**(2): 268-277.

Estrada, P., J. Kim, J. Coleman, L. Walker, B. Dunn, P. Takizawa, P. Novick and S. Ferro-Novick (2003). "Myo4p and She3p are required for cortical ER inheritance in *Saccharomyces cerevisiae*." J Cell Biol **163**(6): 1255-1266.

Esvald, E.-E., J. Tuvikene, A. Sirp, S. Patil, C. R. Bramham and T. Timmusk (2020). "CREB Family Transcription Factors Are Major Mediators of BDNF Transcriptional Autoregulation in Cortical Neurons." The Journal of Neuroscience **40**(7): 1405-1426.

Fagone, P. and S. Jackowski (2009). "Membrane phospholipid synthesis and endoplasmic reticulum function." J Lipid Res **50 Suppl**(Suppl): S311-316.

Fallini, C., G. J. Bassell and W. Rossoll (2012). "Spinal muscular atrophy: the role of SMN in axonal mRNA regulation." Brain Res **1462**: 81-92.

Farah, C. A., D. Liazoghli, S. Perreault, M. Desjardins, A. Guimont, A. Anton, M. Lauzon, G. Kreibich, J. Paiement and N. Leclerc (2005). "Interaction of microtubule-associated protein-2 and p63: a new link between microtubules and rough endoplasmic reticulum membranes in neurons." J Biol Chem **280**(10): 9439-9449.

Farias, G. G., A. Freal, E. Tortosa, R. Stucchi, X. Pan, S. Portegies, L. Will, M. Altelaar and C. C. Hoogenraad (2019). "Feedback-Driven Mechanisms between Microtubules and the Endoplasmic Reticulum Instruct Neuronal Polarity." Neuron **102**(1): 184-201 e188.

Farías, G. G., A. Fréal, E. Tortosa, R. Stucchi, X. Pan, S. Portegies, L. Will, M. Altelaar and C. C. Hoogenraad (2019). "Feedback-Driven Mechanisms between Microtubules and the Endoplasmic Reticulum Instruct Neuronal Polarity." Neuron **102**(1): 184-201.e188.

Fox, M. A., J. R. Sanes, D. B. Borza, V. P. Eswarakumar, R. Fässler, B. G. Hudson, S. W. John, Y. Ninomiya, V. Pedchenko, S. L. Pfaff, M. N. Rheault, Y. Sado, Y. Segal, M. J. Werle and H. Umemori (2007). "Distinct target-derived signals organize formation, maturation, and maintenance of motor nerve terminals." Cell **129**(1): 179-193.

Fox, P. D., C. J. Haberkorn, E. J. Akin, P. J. Seel, D. Krapf and M. M. Tamkun (2015). "Induction of stable ER-plasma-membrane junctions by Kv2.1 potassium channels." J Cell Sci **128**(11): 2096-2105.

Friedman, J. R., L. L. Lackner, M. West, J. R. DiBenedetto, J. Nunnari and G. K. Voeltz (2011). "ER tubules mark sites of mitochondrial division." Science **334**(6054): 358-362.

Friedman, J. R., B. M. Webster, D. N. Mastronarde, K. J. Verhey and G. K. Voeltz (2010). "ER sliding dynamics and ER-mitochondrial contacts occur on acetylated microtubules." J Cell Biol **190**(3): 363-375.

Gardiol, A., C. Racca and A. Triller (1999). "Dendritic and postsynaptic protein synthetic machinery." J Neurosci **19**(1): 168-179.

Gautreau, A., K. Oguievetskaia and C. Ungermann (2014). "Function and regulation of the endosomal fusion and fission machineries." Cold Spring Harb Perspect Biol **6**(3).

Genç, Ö., D. K. Dickman, W. Ma, A. Tong, R. D. Fetter and G. W. Davis (2017). "MCTP is an ER-resident calcium sensor that stabilizes synaptic transmission and homeostatic plasticity." Elife **6**.

Geraldo, S. and P. R. Gordon-Weeks (2009). "Cytoskeletal dynamics in growth-cone steering." J Cell Sci **122**(Pt 20): 3595-3604.

Geraldo, S., U. K. Khanzada, M. Parsons, J. K. Chilton and P. R. Gordon-Weeks (2008). "Targeting of the F-actin-binding protein drebrin by the microtubule plus-tip protein EB3 is required for neuritegenesis." Nature Cell Biology **10**(10): 1181-1189.

Gerondopoulos, A., R. N. Bastos, S.-i. Yoshimura, R. Anderson, S. Carpanini, I. Aligianis, M. T. Handley and F. A. Barr (2014). "Rab18 and a Rab18 GEF complex are required for normal ER structure." Journal of Cell Biology **205**(5): 707-720.

Giesemann, T., G. Schwarz, R. Nawrothki, K. Berhorster, M. Rothkegel, K. Schluter, N. Schrader, H. Schindelin, R. R. Mendel, J. Kirsch and B. M. Jockusch (2003). "Complex formation between the postsynaptic scaffolding protein gephyrin, profilin, and Mena: a possible link to the microfilament system." J Neurosci **23**(23): 8330-8339.

Gioio, A. E., M. Eyman, H. Zhang, Z. S. Lavina, A. Giuditta and B. B. Kaplan (2001). "Local synthesis of nuclear-encoded mitochondrial proteins in the presynaptic nerve terminal." J Neurosci Res **64**(5): 447-453.

Goldstein, B. and I. G. Macara (2007). "The PAR proteins: fundamental players in animal cell polarization." *Dev Cell* **13**(5): 609-622.

Gómez-Suaga, P., B. G. Pérez-Nievas, E. B. Glennon, D. H. W. Lau, S. Paillusson, G. M. Mórotz, T. Cali, P. Pizzo, W. Noble and C. C. J. Miller (2019). "The VAPB-PTPIP51 endoplasmic reticulum-mitochondria tethering proteins are present in neuronal synapses and regulate synaptic activity." *Acta Neuropathologica Communications* **7**(1): 35.

Gomez, T. M. and P. C. Letourneau (2014). "Actin dynamics in growth cone motility and navigation." *J Neurochem* **129**(2): 221-234.

Gonzalez, A., G. Moya-Alvarado, C. Gonzalez-Billaut and F. C. Bronfman (2016). "Cellular and molecular mechanisms regulating neuronal growth by brain-derived neurotrophic factor." *Cytoskeleton* **73**(10): 612-628.

González, C., J. Cánovas, J. Fresno, E. Couve, F. A. Court and A. Couve (2016). "Axons provide the secretory machinery for trafficking of voltage-gated sodium channels in peripheral nerve." *Proceedings of the National Academy of Sciences* **113**(7): 1823-1828.

Gould, R. M., H. Pant, H. Gainer and M. Tytell (1983). "Phospholipid synthesis in the squid giant axon: incorporation of lipid precursors." *J Neurochem* **40**(5): 1293-1299.

Grigoriev, I., S. M. Gouveia, B. van der Vaart, J. Demmers, J. T. Smyth, S. Honnappa, D. Splinter, M. O. Steinmetz, J. W. Putney, Jr., C. C. Hoogenraad and A. Akhmanova (2008). "STIM1 is a MT-plus-end-tracking protein involved in remodeling of the ER." *Curr Biol* **18**(3): 177-182.

Gumy, L. F., C. L. Tan and J. W. Fawcett (2010). "The role of local protein synthesis and degradation in axon regeneration." *Exp Neurol* **223**(1): 28-37.

Gumy, L. F., G. S. Yeo, Y. C. Tung, K. H. Zivraj, D. Willis, G. Coppola, B. Y. Lam, J. L. Twiss, C. E. Holt and J. W. Fawcett (2011). "Transcriptome analysis of embryonic and adult sensory axons reveals changes in mRNA repertoire localization." *Rna* **17**(1): 85-98.

Hafner, A.-S., P. G. Donlin-Asp, B. Leitch, E. Herzog and E. M. Schuman (2019). "Local protein synthesis is a ubiquitous feature of neuronal pre- and postsynaptic compartments." *Science* **364**(6441): eaau3644.

Hanson, J. E. and D. V. Madison (2007). "Presynaptic FMR1 genotype influences the degree of synaptic connectivity in a mosaic mouse model of fragile X syndrome." *J Neurosci* **27**(15): 4014-4018.

Hanus, C. and M. D. Ehlers (2008). "Secretory outposts for the local processing of membrane cargo in neuronal dendrites." *Traffic* **9**(9): 1437-1445.

Hanus, C., H. Geptin, G. Tushev, S. Garg, B. Alvarez-Castelao, S. Sambandan, L. Kochen, A.-S. Hafner, J. D. Langer and E. M. Schuman (2016). "Unconventional secretory processing diversifies neuronal ion channel properties." *eLife* **5**: e20609.

Hayashi, T. and T. P. Su (2007). "Sigma-1 receptor chaperones at the ER-mitochondrion interface regulate Ca(2+) signaling and cell survival." *Cell* **131**(3): 596-610.

Helle, S. C., G. Kanfer, K. Kolar, A. Lang, A. H. Michel and B. Kornmann (2013). "Organization and function of membrane contact sites." *Biochim Biophys Acta* **1833**(11): 2526-2541.

Hengst, U., A. Deglincerti, H. J. Kim, N. L. Jeon and S. R. Jaffrey (2009). "Axonal elongation triggered by stimulus-induced local translation of a polarity complex protein." *Nature Cell Biology* **11**(8): 1024-1030.

Hensel, N. and P. Claus (2017). "The Actin Cytoskeleton in SMA and ALS: How Does It Contribute to Motoneuron Degeneration?" *The Neuroscientist* **24**(1): 54-72.

Hernández, M. V., M. G. Sala, J. Balsamo, J. Lilien and C. O. Arregui (2006). "ER-bound PTP1B is targeted to newly forming cell-matrix adhesions." *J Cell Sci* **119**(Pt 7): 1233-1243.

Herrera-Cruz, M. S. and T. Simmen (2017). "Of yeast, mice and men: MAMs come in two flavors." *Biol Direct* **12**(1): 3.

Hillefors, M., A. E. Gioio, M. G. Mameza and B. B. Kaplan (2007). "Axon viability and mitochondrial function are dependent on local protein synthesis in sympathetic neurons." *Cell Mol Neurobiol* **27**(6): 701-716.

Hirabayashi, Y., S. K. Kwon, H. Paek, W. M. Pernice, M. A. Paul, J. Lee, P. Erfani, A. Raczowski, D. S. Petrey, L. A. Pon and F. Polleux (2017). "ER-mitochondria tethering by PDZD8 regulates Ca(2+) dynamics in mammalian neurons." *Science* **358**(6363): 623-630.

Holt, C. E., K. C. Martin and E. M. Schuman (2019). "Local translation in neurons: visualization and function." *Nat Struct Mol Biol* **26**(7): 557-566.

Hoppins, S., L. Lackner and J. Nunnari (2007). "The machines that divide and fuse mitochondria." *Annu Rev Biochem* **76**: 751-780.

Horton, A. C. and M. D. Ehlers (2003). "Dual modes of endoplasmic reticulum-to-Golgi transport in dendrites revealed by live-cell imaging." *J Neurosci* **23**(15): 6188-6199.

Hosseini-barkoobe, S., M. Peters, L. Torres-Benito, R. H. Rastetter, K. Hupperich, A. Hoffmann, N. Mendoza-Ferreira, A. Kaczmarek, E. Janzen, J. Milbradt, T. Lamkemeyer, F. Rigo, C. F. Bennett, C. Guschlbauer, A. Büschges, M. Hammerschmidt, M. Riessland, M. J. Kye, C. S. Clemen and B. Wirth (2016). "The Power of Human Protective Modifiers: PLS3 and CORO1C Unravel Impaired Endocytosis in Spinal Muscular Atrophy and Rescue SMA Phenotype." *Am J Hum Genet* **99**(3): 647-665.

Huotari, J. and A. Helenius (2011). "Endosome maturation." *Embo j* **30**(17): 3481-3500.

Hüttelmaier, S., D. Zenklusen, M. Lederer, J. Dichtenberg, M. Lorenz, X. Meng, G. J. Bassell, J. Condeelis and R. H. Singer (2005). "Spatial regulation of beta-actin translation by Src-dependent phosphorylation of ZBP1." *Nature* **438**(7067): 512-515.

Inamura, N., H. Nawa and N. Takei (2005). "Enhancement of translation elongation in neurons by brain-derived neurotrophic factor: implications for mammalian target of rapamycin signaling." *J Neurochem* **95**(5): 1438-1445.

Ivanov, A., M. Esclapez, C. Pellegrino, T. Shirao and L. Ferhat (2009). "Drebrin A regulates dendritic spine plasticity and synaptic function in mature cultured hippocampal neurons." *J Cell Sci* **122**(Pt 4): 524-534.

Jablonka, S., M. Beck, B. D. Lechner, C. Mayer and M. Sendtner (2007). "Defective Ca²⁺ channel clustering in axon terminals disturbs excitability in motoneurons in spinal muscular atrophy." *Journal of Cell Biology* **179**(1): 139-149.

Jablonka, S. and M. Sendtner (2003). "Molecular and cellular basis of spinal muscular atrophy." *Amyotroph Lateral Scler Other Motor Neuron Disord* **4**(3): 144-149.

Jacquemyn, J., A. Cascalho and R. E. Goodchild (2017). "The ins and outs of endoplasmic reticulum-controlled lipid biosynthesis." *EMBO Rep* **18**(11): 1905-1921.

Jan, C. H., C. C. Williams and J. S. Weissman (2014). "Principles of ER cotranslational translocation revealed by proximity-specific ribosome profiling." *Science* **346**(6210): 1257521.

Je, H. S., Y. Ji, Y. Wang, F. Yang, W. Wu and B. Lu (2011). "Presynaptic protein synthesis required for NT-3-induced long-term synaptic modulation." *Molecular Brain* **4**(1): 1.

Jirikowski, G. F., P. P. Sanna and F. E. Bloom (1990). "mRNA coding for oxytocin is present in axons of the hypothalamo-neurohypophysial tract." *Proc Natl Acad Sci U S A* **87**(19): 7400-7404.

Jung, H., B. C. Yoon and C. E. Holt (2012). "Axonal mRNA localization and local protein synthesis in nervous system assembly, maintenance and repair." *Nature Reviews Neuroscience* **13**(5): 308-324.

Kalinski, A. L., R. Sachdeva, C. Gomes, S. J. Lee, Z. Shah, J. D. Houle and J. L. Twiss (2015). "mRNAs and Protein Synthetic Machinery Localize into Regenerating Spinal Cord Axons When They Are Provided a Substrate That Supports Growth." *The Journal of Neuroscience* **35**(28): 10357-10370.

Kiebler, M. A. and G. J. Bassell (2006). "Neuronal RNA granules: movers and makers." *Neuron* **51**(6): 685-690.

Kim, S. and P. A. Coulombe (2010). "Emerging role for the cytoskeleton as an organizer and regulator of translation." *Nat Rev Mol Cell Biol* **11**(1): 75-81.

Kim, S. and K. C. Martin (2015). "Neuron-wide RNA transport combines with netrin-mediated local translation to spatially regulate the synaptic proteome." *Elife* **4**.

Kirmiz, M., S. Palacio, P. Thapa, A. N. King, J. T. Sack and J. S. Trimmer (2018). "Remodeling neuronal ER-PM junctions is a conserved nonconducting function of Kv2 plasma membrane ion channels." *Mol Biol Cell* **29**(20): 2410-2432.

Koenig, E., R. Martin, M. Titmus and J. R. Sotelo-Silveira (2000). "Cryptic Peripheral Ribosomal Domains Distributed Intermittently along Mammalian Myelinated Axons." The Journal of Neuroscience **20**(22): 8390-8400.

Krijnse-Locker, J., R. G. Parton, S. D. Fuller, G. Griffiths and C. G. Dotti (1995). "The organization of the endoplasmic reticulum and the intermediate compartment in cultured rat hippocampal neurons." Mol Biol Cell **6**(10): 1315-1332.

Kumar, N., M. Leonzino, W. Hancock-Cerutti, F. A. Horenkamp, P. Li, J. A. Lees, H. Wheeler, K. M. Reinisch and P. De Camilli (2018). "VPS13A and VPS13C are lipid transport proteins differentially localized at ER contact sites." J Cell Biol **217**(10): 3625-3639.

Kun, A., L. Otero, J. R. Sotelo-Silveira and J. R. Sotelo (2007). "Ribosomal distributions in axons of mammalian myelinated fibers." J Neurosci Res **85**(10): 2087-2098.

Kye, M. J., E. D. Niederst, M. H. Wertz, I. d. C. G. Gonçalves, B. Akten, K. Z. Dover, M. Peters, M. Riessland, P. Neveu, B. Wirth, K. S. Kosik, S. P. Sardi, U. R. Monani, M. A. Passini and M. Sahin (2014). "SMN regulates axonal local translation via miR-183/mTOR pathway." Human molecular genetics **23**(23): 6318-6331.

Lahiri, S., A. Toulmay and W. A. Prinz (2015). "Membrane contact sites, gateways for lipid homeostasis." Curr Opin Cell Biol **33**: 82-87.

Lasek, R. J., C. Dabrowski and R. Nordlander (1973). "Analysis of Axoplasmic RNA from Invertebrate Giant Axons." Nature New Biology **244**(136): 162-165.

Lauria, F., P. Bernabo, T. Tebaldi, E. J. N. Groen, E. Perenthaler, F. Maniscalco, A. Rossi, D. Donzel, M. Clamer, M. Marchioretto, N. Omersa, J. Orri, M. Dalla Serra, G. Anderluh, A. Quattrone, A. Inga, T. H. Gillingwater and G. Viero (2020). "SMN-primed ribosomes modulate the translation of transcripts related to spinal muscular atrophy." Nat Cell Biol **22**(10): 1239-1251.

Lauwers, E., R. Goodchild and P. Verstreken (2016). "Membrane Lipids in Presynaptic Function and Disease." Neuron **90**(1): 11-25.

Lee, C. and L. B. Chen (1988). "Dynamic behavior of endoplasmic reticulum in living cells." Cell **54**(1): 37-46.

Lee, J. E., P. I. Cathey, H. Wu, R. Parker and G. K. Voeltz (2020). "Endoplasmic reticulum contact sites regulate the dynamics of membraneless organelles." Science **367**(6477).

Leung, K. M., F. P. van Horck, A. C. Lin, R. Allison, N. Standart and C. E. Holt (2006). "Asymmetrical beta-actin mRNA translation in growth cones mediates attractive turning to netrin-1." Nat Neurosci **9**(10): 1247-1256.

Lim, Y., I. T. Cho, L. J. Schoel, G. Cho and J. A. Golden (2015). "Hereditary spastic paraplegia-linked REEP1 modulates endoplasmic reticulum/mitochondria contacts." Ann Neurol **78**(5): 679-696.

Lindhout, F. W., Y. Cao, J. T. Kevenaar, A. Bodzeta, R. Stucchi, M. M. Boumpoutsari, E. A. Katrukha, M. Altelaar, H. D. MacGillavry and C. C. Hoogenraad (2019). "VAP-SCRN1 interaction regulates dynamic endoplasmic reticulum remodeling and presynaptic function." EMBO J **38**(20): e101345.

Liu, Q., U. Fischer, F. Wang and G. Dreyfuss (1997). "The Spinal Muscular Atrophy Disease Gene Product, SMN, and Its Associated Protein SIP1 Are in a Complex with Spliceosomal snRNP Proteins." Cell **90**(6): 1013-1021.

Liu, X., X. Guo, L. Niu, X. Li, F. Sun, J. Hu, X. Wang and K. Shen (2019). "Atlastin-1 regulates morphology and function of endoplasmic reticulum in dendrites." Nature Communications **10**(1): 568.

Lohof, A. M., N. Y. Ip and M. M. Poo (1993). "Potentiation of developing neuromuscular synapses by the neurotrophins NT-3 and BDNF." Nature **363**(6427): 350-353.

Lyles, V., Y. Zhao and K. C. Martin (2006). "Synapse Formation and mRNA Localization in Cultured Aplysia Neurons." Neuron **49**(3): 349-356.

Maday, S., A. E. Twelvetrees, A. J. Moughamian and E. L. Holzbaur (2014). "Axonal transport: cargo-specific mechanisms of motility and regulation." Neuron **84**(2): 292-309.

Mallavarapu, A. and T. Mitchison (1999). "Regulated actin cytoskeleton assembly at filopodium tips controls their extension and retraction." J Cell Biol **146**(5): 1097-1106.

Manadas, B., A. R. Santos, K. Szabadfi, J. R. Gomes, S. D. Garbis, M. Fountoulakis and C. B. Duarte (2009). "BDNF-Induced Changes in the Expression of the Translation Machinery in Hippocampal Neurons: Protein Levels and Dendritic mRNA." *Journal of Proteome Research* **8**(10): 4536-4552.

Mandikian, D., E. Bocksteins, L. K. Parajuli, H. I. Bishop, O. Cerda, R. Shigemoto and J. S. Trimmer (2014). "Cell type-specific spatial and functional coupling between mammalian brain Kv2.1 K⁺ channels and ryanodine receptors." *J Comp Neurol* **522**(15): 3555-3574.

Marongiu, R., B. Spencer, L. Crews, A. Adame, C. Patrick, M. Trejo, B. Dallapiccola, E. M. Valente and E. Masliah (2009). "Mutant Pink1 induces mitochondrial dysfunction in a neuronal cell model of Parkinson's disease by disturbing calcium flux." *J Neurochem* **108**(6): 1561-1574.

Martin, K. C., A. Casadio, H. Zhu, E. Yaping, J. C. Rose, M. Chen, C. H. Bailey and E. R. Kandel (1997). "Synapse-specific, long-term facilitation of aplysia sensory to motor synapses: a function for local protein synthesis in memory storage." *Cell* **91**(7): 927-938.

Maxfield, F. R. and T. E. McGraw (2004). "Endocytic recycling." *Nature Reviews Molecular Cell Biology* **5**(2): 121-132.

Medeiros, N. A., D. T. Burnette and P. Forscher (2006). "Myosin II functions in actin-bundle turnover in neuronal growth cones." *Nat Cell Biol* **8**(3): 215-226.

Melia, K. R., A. Trembleau, R. Oddi, P. P. Sanna and F. E. Bloom (1994). "Detection and regulation of tyrosine hydroxylase mRNA in catecholaminergic terminal fields: possible axonal compartmentalization." *Exp Neurol* **130**(2): 394-406.

Melko, M. and B. Bardoni (2010). "The role of G-quadruplex in RNA metabolism: Involvement of FMRP and FMR2P." *Biochimie* **92**(8): 919-926.

Merianda, T. and J. Twiss (2013). "Peripheral nerve axons contain machinery for co-translational secretion of axonally-generated proteins." *Neurosci Bull* **29**(4): 493-500.

Merianda, T. T., A. C. Lin, J. S. Lam, D. Vuppalanchi, D. E. Willis, N. Karin, C. E. Holt and J. L. Twiss (2009). "A functional equivalent of endoplasmic reticulum and Golgi in axons for secretion of locally synthesized proteins." *Mol Cell Neurosci* **40**(2): 128-142.

Miller, M., E. Bower, P. Levitt, D. Li and P. D. Chantler (1992). "Myosin II distribution in neurons is consistent with a role in growth cone motility but not synaptic vesicle mobilization." *Neuron* **8**(1): 25-44.

Ming, G.-l., S. T. Wong, J. Henley, X.-b. Yuan, H.-j. Song, N. C. Spitzer and M.-m. Poo (2002). "Adaptation in the chemotactic guidance of nerve growth cones." *Nature* **417**(6887): 411-418.

Ming, G. L., H. J. Song, B. Berninger, C. E. Holt, M. Tessier-Lavigne and M. M. Poo (1997). "cAMP-dependent growth cone guidance by netrin-1." *Neuron* **19**(6): 1225-1235.

Misko, A. L., Y. Sasaki, E. Tuck, J. Milbrandt and R. H. Baloh (2012). "Mitofusin2 mutations disrupt axonal mitochondrial positioning and promote axon degeneration." *J Neurosci* **32**(12): 4145-4155.

Mitchell, C. B., R. J. Gasperini, D. H. Small and L. Foa (2012). "STIM1 is necessary for store-operated calcium entry in turning growth cones." *Journal of Neurochemistry* **122**(6): 1155-1166.

Mohr, E., S. Fehr and D. Richter (1991). "Axonal transport of neuropeptide encoding mRNAs within the hypothalamo-hypophyseal tract of rats." *Embo j* **10**(9): 2419-2424.

Monani, U. R., M. Sendtner, D. D. Covert, D. W. Parsons, C. Andreassi, T. T. Le, S. Jablonka, B. Schrank, W. Rossol, T. W. Prior, G. E. Morris and A. H. M. Burghes (2000). "The human centromeric survival motor neuron gene (SMN2) rescues embryonic lethality in Smn^{-/-} mice and results in a mouse with spinal muscular atrophy." *Human Molecular Genetics* **9**(3): 333-339.

Monani, U. R., M. Sendtner, D. D. Covert, D. W. Parsons, C. Andreassi, T. T. Le, S. Jablonka, B. Schrank, W. Rossol, T. W. Prior, G. E. Morris and A. H. Burghes (2000). "The human centromeric survival motor neuron gene (SMN2) rescues embryonic lethality in Smn^(-/-) mice and results in a mouse with spinal muscular atrophy." *Hum Mol Genet* **9**(3): 333-339.

Moradi, M., R. Sivadasan, L. Saal, P. Luningschrör, B. Dombert, R. J. Rathod, D. C. Dieterich, R. Blum and M. Sendtner (2017). "Differential roles of alpha-, beta-, and gamma-actin in axon growth and collateral branch formation in motoneurons." *J Cell Biol* **216**(3): 793-814.

Moradi, M., R. Sivadasan, L. Saal, P. Lüningschrör, B. Dombert, R. J. Rathod, D. C. Dieterich, R. Blum and M. Sendtner (2017). "Differential roles of α -, β -, and γ -actin in axon growth and collateral branch formation in motoneurons." *J Cell Biol* **216**(3): 793-814.

Muallem, S., W. Y. Chung, A. Jha and M. Ahuja (2017). "Lipids at membrane contact sites: cell signaling and ion transport." *EMBO Rep* **18**(11): 1893-1904.

Müller, M. S., M. Fouyssac and C. W. Taylor (2018). "Effective Glucose Uptake by Human Astrocytes Requires Its Sequestration in the Endoplasmic Reticulum by Glucose-6-Phosphatase- β ." *Curr Biol* **28**(21): 3481-3486.e3484.

Nakajima, K., H. Hirose, M. Taniguchi, H. Kurashina, K. Arasaki, M. Nagahama, K. Tani, A. Yamamoto and M. Tagaya (2004). "Involvement of BNIP1 in apoptosis and endoplasmic reticulum membrane fusion." *Embo j* **23**(16): 3216-3226.

Narayanan, U., V. Nalavadi, M. Nakamoto, G. Thomas, S. Ceman, G. J. Bassell and S. T. Warren (2008). "S6K1 phosphorylates and regulates fragile X mental retardation protein (FMRP) with the neuronal protein synthesis-dependent mammalian target of rapamycin (mTOR) signaling cascade." *J Biol Chem* **283**(27): 18478-18482.

Nishimura, A. L., M. Mitne-Neto, H. C. Silva, A. Richieri-Costa, S. Middleton, D. Cascio, F. Kok, J. R. Oliveira, T. Gillingwater, J. Webb, P. Skehel and M. Zatz (2004). "A mutation in the vesicle-trafficking protein VAPB causes late-onset spinal muscular atrophy and amyotrophic lateral sclerosis." *Am J Hum Genet* **75**(5): 822-831.

Nölle, A., A. Zeug, J. van Bergeijk, L. Tönges, R. Gerhard, H. Brinkmann, S. Al Rayes, N. Hensel, Y. Schill, D. Apkhazava, S. Jablonka, J. O'Mer, R. K. Srivastav, A. Baasner, P. Lingor, B. Wirth, E. Ponimaskin, R. Niedenthal, C. Grothe and P. Claus (2011). "The spinal muscular atrophy disease protein SMN is linked to the Rho-kinase pathway via profilin." *Hum Mol Genet* **20**(24): 4865-4878.

Novarino, G., A. G. Fenstermaker, M. S. Zaki, M. Hofree, J. L. Silhavy, A. D. Heiberg, M. Abdellateef, B. Rosti, E. Scott, L. Mansour, A. Masri, H. Kayserili, J. Y. Al-Aama, G. M. H. Abdel-Salam, A. Karminejad, M. Kara, B. Kara, B. Bozorgmehri, T. Ben-Omran, F. Mojahedi, I. G. El Din Mahmoud, N. Bouslam, A. Bouhouche, A. Benomar, S. Hanein, L. Raymond, S. Forlani, M. Mascaro, L. Selim, N. Shehata, N. Al-Allawi, P. S. Bindu, M. Azam, M. Gunel, A. Caglayan, K. Bilguvar, A. Tolun, M. Y. Issa, J. Schroth, E. G. Spencer, R. O. Rosti, N. Akizu, K. K. Vaux, A. Johansen, A. A. Koh, H. Megahed, A. Durr, A. Brice, G. Stevanin, S. B. Gabriel, T. Ideker and J. G. Gleeson (2014). "Exome sequencing links corticospinal motor neuron disease to common neurodegenerative disorders." *Science* **343**(6170): 506-511.

Ogawa-Goto, K., K. Tanaka, T. Ueno, K. Tanaka, T. Kurata, T. Sata and S. Irie (2007). "p180 is involved in the interaction between the endoplasmic reticulum and microtubules through a novel microtubule-binding and bundling domain." *Mol Biol Cell* **18**(10): 3741-3751.

Oprea, G. E., S. Kröber, M. L. McWhorter, W. Rossoll, S. Müller, M. Krawczak, G. J. Bassell, C. E. Beattie and B. Wirth (2008). "Plastin 3 is a protective modifier of autosomal recessive spinal muscular atrophy." *Science* **320**(5875): 524-527.

Orso, G., D. Pendin, S. Liu, J. Tosetto, T. J. Moss, J. E. Faust, M. Micaroni, A. Egorova, A. Martinuzzi, J. A. McNew and A. Daga (2009). "Homotypic fusion of ER membranes requires the dynamin-like GTPase Atlastin." *Nature* **460**(7258): 978-983.

Osterweil, E., D. G. Wells and M. S. Mooseker (2005). "A role for myosin VI in postsynaptic structure and glutamate receptor endocytosis." *J Cell Biol* **168**(2): 329-338.

Öztürk, Z., C. J. O'Kane and J. J. Pérez-Moreno (2020). "Axonal Endoplasmic Reticulum Dynamics and Its Roles in Neurodegeneration." *Front Neurosci* **14**: 48.

Paillasson, S., P. Gomez-Suaga, R. Stoica, D. Little, P. Gissen, M. J. Devine, W. Noble, D. P. Hanger and C. C. J. Miller (2017). " α -Synuclein binds to the ER-mitochondria tethering protein VAPB to disrupt Ca(2+) homeostasis and mitochondrial ATP production." *Acta Neuropathol* **134**(1): 129-149.

Palade, G. (1975). "Intracellular aspects of the process of protein synthesis." *Science* **189**(4200): 347-358.

Pareyson, D. and C. Marchesi (2009). "Diagnosis, natural history, and management of Charcot-Marie-Tooth disease." *Lancet Neurol* **8**(7): 654-667.

Park, S. H., P. P. Zhu, R. L. Parker and C. Blackstone (2010). "Hereditary spastic paraplegia proteins REEP1, spastin, and atlastin-1 coordinate microtubule interactions with the tubular ER network." J Clin Invest **120**(4): 1097-1110.

Parodi, L., G. Coarelli, G. Stevanin, A. Brice and A. Durr (2018). "Hereditary ataxias and paraparesias: clinical and genetic update." Curr Opin Neurol **31**(4): 462-471.

Paushkin, S., A. K. Gubitz, S. Massenet and G. Dreyfuss (2002). "The SMN complex, an assemblysome of ribonucleoproteins." Current Opinion in Cell Biology **14**(3): 305-312.

Pavez, M., A. C. Thompson, H. J. Arnott, C. B. Mitchell, I. D'Atri, E. K. Don, J. K. Chilton, E. K. Scott, J. Y. Lin, K. M. Young, R. J. Gasperini and L. Foa (2019). "STIM1 Is Required for Remodeling of the Endoplasmic Reticulum and Microtubule Cytoskeleton in Steering Growth Cones." J Neurosci **39**(26): 5095-5114.

Pavlov, D., A. Muhrad, J. Cooper, M. Wear and E. Reisler (2007). "Actin filament severing by cofilin." J Mol Biol **365**(5): 1350-1358.

Pellizzoni, L., B. Charroux and G. Dreyfuss (1999). "SMN mutants of spinal muscular atrophy patients are defective in binding to snRNP proteins." Proceedings of the National Academy of Sciences **96**(20): 11167-11172.

Pellizzoni, L., J. Yong and G. Dreyfuss (2002). "Essential role for the SMN complex in the specificity of snRNP assembly." Science **298**(5599): 1775-1779.

Piper, M., R. Anderson, A. Dwivedy, C. Weinl, F. van Horck, K. M. Leung, E. Cogill and C. Holt (2006). "Signaling mechanisms underlying Slit2-induced collapse of *Xenopus* retinal growth cones." Neuron **49**(2): 215-228.

Poon, M. M., S. H. Choi, C. A. Jamieson, D. H. Geschwind and K. C. Martin (2006). "Identification of process-localized mRNAs from cultured rodent hippocampal neurons." J Neurosci **26**(51): 13390-13399.

Poulopoulos, A., A. J. Murphy, A. Ozkan, P. Davis, J. Hatch, R. Kirchner and J. D. Macklis (2019). "Subcellular transcriptomes and proteomes of developing axon projections in the cerebral cortex." Nature **565**(7739): 356-360.

Prinz, W. A. (2014). "Bridging the gap: membrane contact sites in signaling, metabolism, and organelle dynamics." J Cell Biol **205**(6): 759-769.

Prior, M., Q. Shi, X. Hu, W. He, A. Levey and R. Yan (2010). "RTN/Nogo in forming Alzheimer's neuritic plaques." Neurosci Biobehav Rev **34**(8): 1201-1206.

Puhka, M., M. Joensuu, H. Vihinen, I. Belevich and E. Jokitalo (2012). "Progressive sheet-to-tubule transformation is a general mechanism for endoplasmic reticulum partitioning in dividing mammalian cells." Molecular biology of the cell **23**(13): 2424-2432.

Puri, R., X.-T. Cheng, M.-Y. Lin, N. Huang and Z.-H. Sheng (2019). "Mul1 restrains Parkin-mediated mitophagy in mature neurons by maintaining ER-mitochondrial contacts." Nature Communications **10**(1): 3645.

Raffaello, A., C. Mammucari, G. Gherardi and R. Rizzuto (2016). "Calcium at the Center of Cell Signaling: Interplay between Endoplasmic Reticulum, Mitochondria, and Lysosomes." Trends Biochem Sci **41**(12): 1035-1049.

Rao, K., M. C. Stone, A. T. Weiner, K. W. Gheres, C. Zhou, D. L. Deitcher, E. S. Levitan and M. M. Rolls (2016). "Spastin, atlastin, and ER relocalization are involved in axon but not dendrite regeneration." Mol Biol Cell **27**(21): 3245-3256.

Rehberg, M., A. Lepier, B. Solchenberger, P. Osten and R. Blum (2008). "A new non-disruptive strategy to target calcium indicator dyes to the endoplasmic reticulum." Cell Calcium **44**(4): 386-399.

Reid, D. W. and C. V. Nicchitta (2015). "Diversity and selectivity in mRNA translation on the endoplasmic reticulum." Nat Rev Mol Cell Biol **16**(4): 221-231.

Ribeiro, C. M., R. R. McKay, E. Hosoki, G. S. Bird and J. W. Putney, Jr. (2000). "Effects of elevated cytoplasmic calcium and protein kinase C on endoplasmic reticulum structure and function in HEK293 cells." Cell Calcium **27**(3): 175-185.

Ridge, P. G., C. M. Karch, S. Hsu, I. Arano, C. C. Teerlink, M. T. W. Ebbert, J. D. G. Murcia, J. M. Farnham, A. R. Damato, M. Allen, X. Wang, O. Harari, V. M. Fernandez, R. Guerreiro, J. Bras, J. Hardy,

R. Munger, M. Norton, C. Sassi, A. Singleton, S. G. Younkin, D. W. Dickson, T. E. Golde, N. D. Price, N. Ertekin-Taner, C. Cruchaga, A. M. Goate, C. Corcoran, J. Tschanz, L. A. Cannon-Albright, J. S. K. Kauwe and I. Alzheimer's Disease Neuroimaging (2018). "Correction to: Linkage, whole genome sequence, and biological data implicate variants in RAB10 in Alzheimer's disease resilience." Genome Med **10**(1): 4.

Rizzuto, R., P. Pinton, W. Carrington, F. S. Fay, K. E. Fogarty, L. M. Lifshitz, R. A. Tuft and T. Pozzan (1998). "Close contacts with the endoplasmic reticulum as determinants of mitochondrial Ca²⁺ responses." Science **280**(5370): 1763-1766.

Rogers, K. (2019). "Rough endoplasmic reticulum. ." Encyclopedia Britannica., from <https://www.britannica.com/science/rough-endoplasmic-reticulum>.

Rogers, R. S. and H. Nishimune (2017). "The role of laminins in the organization and function of neuromuscular junctions." Matrix Biol **57-58**: 86-105.

Rohrer, B., J. I. Korenbrot, M. M. LaVail, L. F. Reichardt and B. Xu (1999). "Role of neurotrophin receptor TrkB in the maturation of rod photoreceptors and establishment of synaptic transmission to the inner retina." J Neurosci **19**(20): 8919-8930.

Ronesi, J. A. and K. M. Huber (2008). "Metabotropic glutamate receptors and fragile x mental retardation protein: partners in translational regulation at the synapse." Sci Signal **1**(5): pe6.

Ross, W. N. (2012). "Understanding calcium waves and sparks in central neurons." Nature Reviews Neuroscience **13**(3): 157-168.

Rossoll, W., S. Jablonka, C. Andreassi, A.-K. Kröning, K. Karle, U. R. Monani and M. Sendtner (2003). "Smn, the spinal muscular atrophy-determining gene product, modulates axon growth and localization of β -actin mRNA in growth cones of motoneurons." Journal of Cell Biology **163**(4): 801-812.

Rowland, Ashley A., Patrick J. Chitwood, Melissa J. Phillips and Gia K. Voeltz (2014). "ER Contact Sites Define the Position and Timing of Endosome Fission." Cell **159**(5): 1027-1041.

Saal, L., M. Briese, S. Kneitz, M. Glinka and M. Sendtner (2014). "Subcellular transcriptome alterations in a cell culture model of spinal muscular atrophy point to widespread defects in axonal growth and presynaptic differentiation." Rna **20**(11): 1789-1802.

Saheki, Y. and P. D. Camilli (2017). "Endoplasmic Reticulum-Plasma Membrane Contact Sites." Annual Review of Biochemistry **86**(1): 659-684.

Sahu, G., R. M. Wazen, P. Colarusso, S. R. W. Chen, G. W. Zamponi and R. W. Turner (2019). "Junctophilin Proteins Tether a Cav1-RyR2-KCa3.1 Tripartite Complex to Regulate Neuronal Excitability." Cell Rep **28**(9): 2427-2442.e2426.

Salinas, S., C. Proukakis, A. Crosby and T. T. Warner (2008). "Hereditary spastic paraplegia: clinical features and pathogenetic mechanisms." The Lancet Neurology **7**(12): 1127-1138.

Samtleben, S., B. Wachter and R. Blum (2015). "Store-operated calcium entry compensates fast ER calcium loss in resting hippocampal neurons." Cell Calcium **58**(2): 147-159.

Sanchez, G., A. Y. Dury, L. M. Murray, O. Biondi, H. Tadesse, R. El Fatimy, R. Kothary, F. Charbonnier, E. W. Khandjian and J. Cote (2013). "A novel function for the survival motoneuron protein as a translational regulator." Hum Mol Genet **22**(4): 668-684.

Santos, A. R., D. Comprido and C. B. Duarte (2010). "Regulation of local translation at the synapse by BDNF." Prog Neurobiol **92**(4): 505-516.

Sanyal, S., C. Consoulas, H. Kuromi, A. Basole, L. Mukai, Y. Kidokoro, K. S. Krishnan and M. Ramaswami (2005). "Analysis of conditional paralytic mutants in *Drosophila* sarco-endoplasmic reticulum calcium ATPase reveals novel mechanisms for regulating membrane excitability." Genetics **169**(2): 737-750.

Sasaki, Y., K. Welshhans, Z. Wen, J. Yao, M. Xu, Y. Goshima, J. Q. Zheng and G. J. Bassell (2010). "Phosphorylation of zipcode binding protein 1 is required for brain-derived neurotrophic factor signaling of local beta-actin synthesis and growth cone turning." J Neurosci **30**(28): 9349-9358.

Savitz, A. J. and D. I. Meyer (1990). "Identification of a ribosome receptor in the rough endoplasmic reticulum." Nature **346**(6284): 540-544.

Schratt, G. M., F. Tuebing, E. A. Nigh, C. G. Kane, M. E. Sabatini, M. Kiebler and M. E. Greenberg (2006). "A brain-specific microRNA regulates dendritic spine development." *Nature* **439**(7074): 283-289.

Schuck, S., W. A. Prinz, K. S. Thorn, C. Voss and P. Walter (2009). "Membrane expansion alleviates endoplasmic reticulum stress independently of the unfolded protein response." *J Cell Biol* **187**(4): 525-536.

Serrano-Pozo, A., M. P. Frosch, E. Masliah and B. T. Hyman (2011). "Neuropathological alterations in Alzheimer disease." *Cold Spring Harb Perspect Med* **1**(1): a006189.

Sharma, A., A. Lambrechts, T. Hao le, T. T. Le, C. A. Sewry, C. Ampe, A. H. Burghes and G. E. Morris (2005). "A role for complexes of survival of motor neurons (SMN) protein with gemins and profilin in neurite-like cytoplasmic extensions of cultured nerve cells." *Exp Cell Res* **309**(1): 185-197.

Sharoar, M. G., Q. Shi, Y. Ge, W. He, X. Hu, G. Perry, X. Zhu and R. Yan (2016). "Dysfunctional tubular endoplasmic reticulum constitutes a pathological feature of Alzheimer's disease." *Mol Psychiatry* **21**(9): 1263-1271.

Shibata, Y., T. Shemesh, W. A. Prinz, A. F. Palazzo, M. M. Kozlov and T. A. Rapoport (2010). "Mechanisms determining the morphology of the peripheral ER." *Cell* **143**(5): 774-788.

Shibata, Y., C. Voss, J. M. Rist, J. Hu, T. A. Rapoport, W. A. Prinz and G. K. Voeltz (2008). "The reticulon and DP1/Yop1p proteins form immobile oligomers in the tubular endoplasmic reticulum." *J Biol Chem* **283**(27): 18892-18904.

Shigeoka, T., H. Jung, J. Jung, B. Turner-Bridger, J. Ohk, J. Q. Lin, P. S. Amieux and C. E. Holt (2016). "Dynamic Axonal Translation in Developing and Mature Visual Circuits." *Cell* **166**(1): 181-192.

Shim, S. Y., J. Wang, N. Asada, G. Neumayer, H. C. Tran, K. Ishiguro, K. Sanada, Y. Nakatani and M. D. Nguyen (2008). "Protein 600 is a microtubule/endoplasmic reticulum-associated protein in CNS neurons." *J Neurosci* **28**(14): 3604-3614.

Shirao, T., K. Hanamura, N. Koganezawa, Y. Ishizuka, H. Yamazaki and Y. Sekino (2017). "The role of drebrin in neurons." *J Neurochem* **141**(6): 819-834.

Siekevitz, P. and G. E. Palade (1960). "A cytochemical study on the pancreas of the guinea pig. 5. In vivo incorporation of leucine-1-C14 into the chymotrypsinogen of various cell fractions." *J Biophys Biochem Cytol* **7**(4): 619-630.

Sivadasan, R., D. Hornburg, C. Drepper, N. Frank, S. Jablonka, A. Hansel, X. Lojewski, J. Sternecker, A. Hermann, P. J. Shaw, P. G. Ince, M. Mann, F. Meissner and M. Sendtner (2016). "C9ORF72 interaction with cofilin modulates actin dynamics in motor neurons." *Nat Neurosci* **19**(12): 1610-1618.

Spillantini, M. G., M. L. Schmidt, V. M. Lee, J. Q. Trojanowski, R. Jakes and M. Goedert (1997). "Alpha-synuclein in Lewy bodies." *Nature* **388**(6645): 839-840.

Steenbergen, R., T. S. Nanowski, A. Beigneux, A. Kulinski, S. G. Young and J. E. Vance (2005). "Disruption of the phosphatidylserine decarboxylase gene in mice causes embryonic lethality and mitochondrial defects." *J Biol Chem* **280**(48): 40032-40040.

Steward, O. and C. Ribak (1986). "Polyribosomes associated with synaptic specializations on axon initial segments: localization of protein-synthetic machinery at inhibitory synapses." *The Journal of Neuroscience* **6**(10): 3079-3085.

Stutzmann, G. E. and M. P. Mattson (2011). "Endoplasmic reticulum Ca(2+) handling in excitable cells in health and disease." *Pharmacol Rev* **63**(3): 700-727.

Subramanian, N., A. Wetzels, B. Dombert, P. Yadav, S. Havlicek, S. Jablonka, M. A. Nassar, R. Blum and M. Sendtner (2012). "Role of Nav1.9 in activity-dependent axon growth in motoneurons." *Human Molecular Genetics* **21**(16): 3655-3667.

Summerville, J. B., J. F. Faust, E. Fan, D. Pendin, A. Daga, J. Formella, M. Stern and J. A. McNew (2016). "The effects of ER morphology on synaptic structure and function in *Drosophila melanogaster*." *J Cell Sci* **129**(8): 1635-1648.

Suter, D. M., F. S. Espindola, C. H. Lin, P. Forscher and M. S. Mooseker (2000). "Localization of unconventional myosins V and VI in neuronal growth cones." *J Neurobiol* **42**(3): 370-382.

Takei, N., N. Inamura, M. Kawamura, H. Namba, K. Hara, K. Yonezawa and H. Nawa (2004). "Brain-derived neurotrophic factor induces mammalian target of rapamycin-dependent local activation of translation machinery and protein synthesis in neuronal dendrites." *J Neurosci* **24**(44): 9760-9769.

Takei, N., M. Kawamura, K. Hara, K. Yonezawa and H. Nawa (2001). "Brain-derived neurotrophic factor enhances neuronal translation by activating multiple initiation processes: comparison with the effects of insulin." *J Biol Chem* **276**(46): 42818-42825.

Takei, N., M. Kawamura, Y. Ishizuka, N. Kakiya, N. Inamura, H. Namba and H. Nawa (2009). "Brain-derived neurotrophic factor enhances the basal rate of protein synthesis by increasing active eukaryotic elongation factor 2 levels and promoting translation elongation in cortical neurons." *J Biol Chem* **284**(39): 26340-26348.

Tanaka, A., M. M. Cleland, S. Xu, D. P. Narendra, D. F. Suen, M. Karbowski and R. J. Youle (2010). "Proteasome and p97 mediate mitophagy and degradation of mitofusins induced by Parkin." *J Cell Biol* **191**(7): 1367-1380.

Tasseva, G., H. D. Bai, M. Davidescu, A. Haromy, E. Michelakis and J. E. Vance (2013). "Phosphatidylethanolamine deficiency in Mammalian mitochondria impairs oxidative phosphorylation and alters mitochondrial morphology." *J Biol Chem* **288**(6): 4158-4173.

Taylor, A. M., N. C. Berchtold, V. M. Perreau, C. H. Tu, N. Li Jeon and C. W. Cotman (2009). "Axonal mRNA in uninjured and regenerating cortical mammalian axons." *J Neurosci* **29**(15): 4697-4707.

Tcherkezian, J., P. A. Brittis, F. Thomas, P. P. Roux and J. G. Flanagan (2010). "Transmembrane receptor DCC associates with protein synthesis machinery and regulates translation." *Cell* **141**(4): 632-644.

Terasaki, M., L. B. Chen and K. Fujiwara (1986). "Microtubules and the endoplasmic reticulum are highly interdependent structures." *J Cell Biol* **103**(4): 1557-1568.

Terasaki, M., N. T. Slater, A. Fein, A. Schmidek and T. S. Reese (1994). "Continuous network of endoplasmic reticulum in cerebellar Purkinje neurons." *Proceedings of the National Academy of Sciences* **91**(16): 7510-7514.

Terenzio, M., S. Koley, N. Samra, I. Rishal, Q. Zhao, P. K. Sahoo, A. Urisman, L. Marvaldi, J. A. Oses-Prieto, C. Forester, C. Gomes, A. L. Kalinski, A. Di Pizio, E. Doron-Mandel, R. B. Perry, I. Koppel, J. L. Twiss, A. L. Burlingame and M. Fainzilber (2018). "Locally translated mTOR controls axonal local translation in nerve injury." *Science* **359**(6382): 1416-1421.

Teuling, E., S. Ahmed, E. Haasdijk, J. Demmers, M. O. Steinmetz, A. Akhmanova, D. Jaarsma and C. C. Hoogenraad (2007). "Motor neuron disease-associated mutant vesicle-associated membrane protein-associated protein (VAP) B recruits wild-type VAPs into endoplasmic reticulum-derived tubular aggregates." *J Neurosci* **27**(36): 9801-9815.

Tobias, G. S. and E. Koenig (1975). "Influence of nerve cell body and neurolemma cell on local axonal protein synthesis following neurotomy." *Experimental Neurology* **49**(1): 235-245.

Trembleau, A., K. R. Melia and F. E. Bloom (1995). "BC1 RNA and vasopressin mRNA in rat neurohypophysis: axonal compartmentalization and differential regulation during dehydration and rehydration." *Eur J Neurosci* **7**(11): 2249-2260.

Trembleau, A., M. Morales and F. E. Bloom (1996). "Differential compartmentalization of vasopressin messenger RNA and neuropeptide within the rat hypothalamo-neurohypophysial axonal tracts: light and electron microscopic evidence." *Neuroscience* **70**(1): 113-125.

Trivedi, N., D. R. Stabley, B. Cain, D. Howell, C. Laumonnerie, J. S. Ramahi, J. Temirov, R. A. Kerekes, P. R. Gordon-Weeks and D. J. Solecki (2017). "Drebrin-mediated microtubule-actomyosin coupling steers cerebellar granule neuron nucleokinesis and migration pathway selection." *Nature Communications* **8**(1): 14484.

Tsukita, S. and H. Ishikawa (1976). "Three-dimensional distribution of smooth endoplasmic reticulum in myelinated axons." *J Electron Microsc (Tokyo)* **25**(3): 141-149.

Valadas, J. S., G. Esposito, D. Vandekerkhove, K. Miskiewicz, L. Deaulmerie, S. Raitano, P. Seibler, C. Klein and P. Verstreken (2018). "ER Lipid Defects in Neuropeptidergic Neurons Impair Sleep Patterns in Parkinson's Disease." *Neuron* **98**(6): 1155-1169.e1156.

Vance, J. E. (2014). "MAM (mitochondria-associated membranes) in mammalian cells: lipids and beyond." *Biochim Biophys Acta* **1841**(4): 595-609.

Vedrenne, C., D. R. Klopfenstein and H. P. Hauri (2005). "Phosphorylation controls CLIMP-63-mediated anchoring of the endoplasmic reticulum to microtubules." *Mol Biol Cell* **16**(4): 1928-1937.

Villegas, R., N. W. Martinez, J. Lillo, P. Pihan, D. Hernandez, J. L. Twiss and F. A. Court (2014). "Calcium release from intra-axonal endoplasmic reticulum leads to axon degeneration through mitochondrial dysfunction." *J Neurosci* **34**(21): 7179-7189.

Voeltz, G. K., W. A. Prinz, Y. Shibata, J. M. Rist and T. A. Rapoport (2006). "A class of membrane proteins shaping the tubular endoplasmic reticulum." *Cell* **124**(3): 573-586.

Wagner, W., S. D. Brenowitz and J. A. Hammer (2011). "Myosin-Va transports the endoplasmic reticulum into the dendritic spines of Purkinje neurons." *Nature Cell Biology* **13**(1): 40-48.

Wagner, W., S. D. Brenowitz and J. A. Hammer, 3rd (2011). "Myosin-Va transports the endoplasmic reticulum into the dendritic spines of Purkinje neurons." *Nat Cell Biol* **13**(1): 40-48.

Wan, L., D. J. Battle, J. Yong, A. K. Gubit, S. J. Kolb, J. Wang and G. Dreyfuss (2005). "The survival of motor neurons protein determines the capacity for snRNP assembly: biochemical deficiency in spinal muscular atrophy." *Mol Cell Biol* **25**(13): 5543-5551.

Wang, S., F. B. Romano, C. M. Field, T. J. Mitchison and T. A. Rapoport (2013). "Multiple mechanisms determine ER network morphology during the cell cycle in *Xenopus* egg extracts." *J Cell Biol* **203**(5): 801-814.

Waterman-Storer, C. M. and E. D. Salmon (1998). "Endoplasmic reticulum membrane tubules are distributed by microtubules in living cells using three distinct mechanisms." *Curr Biol* **8**(14): 798-806.

West, M., N. Zurek, A. Hoenger and G. K. Voeltz (2011). "A 3D analysis of yeast ER structure reveals how ER domains are organized by membrane curvature." *Journal of Cell Biology* **193**(2): 333-346.

Wieckowski, M. R., C. Giorgi, M. Lebedzinska, J. Duszyński and P. Pinton (2009). "Isolation of mitochondria-associated membranes and mitochondria from animal tissues and cells." *Nature Protocols* **4**(11): 1582-1590.

Wiese, S., T. Herrmann, C. Drepper, S. Jablonka, N. Funk, A. Klausmeyer, M.-L. Rogers, R. Rush and M. Sendtner (2009). "Isolation and enrichment of embryonic mouse motoneurons from the lumbar spinal cord of individual mouse embryos." *Nature Protocols* **5**(1): 31-38.

Willis, D. E., E. A. van Niekerk, Y. Sasaki, M. Mesngon, T. T. Merianda, G. G. Williams, M. Kendall, D. S. Smith, G. J. Bassell and J. L. Twiss (2007). "Extracellular stimuli specifically regulate localized levels of individual neuronal mRNAs." *J Cell Biol* **178**(6): 965-980.

Windpassinger, C., M. Auer-Grumbach, J. Irobi, H. Patel, E. Petek, G. Hörl, R. Malli, J. A. Reed, I. Dierick, N. Verpoorten, T. T. Warner, C. Proukakis, P. Van den Bergh, C. Verellen, L. Van Maldergem, L. Merlini, P. De Jonghe, V. Timmerman, A. H. Crosby and K. Wagner (2004). "Heterozygous missense mutations in *BSCL2* are associated with distal hereditary motor neuropathy and Silver syndrome." *Nat Genet* **36**(3): 271-276.

Wiseman, P. W. (2015). "Image correlation spectroscopy: principles and applications." *Cold Spring Harb Protoc* **2015**(4): 336-348.

Woźniak, M. J., B. Bola, K. Brownhill, Y. C. Yang, V. Levakova and V. J. Allan (2009). "Role of kinesin-1 and cytoplasmic dynein in endoplasmic reticulum movement in VERO cells." *J Cell Sci* **122**(Pt 12): 1979-1989.

Wu, H., P. Carvalho and G. K. Voeltz (2018). "Here, there, and everywhere: The importance of ER membrane contact sites." *Science* **361**(6401).

Wu, K. Y., U. Hengst, L. J. Cox, E. Z. Macosko, A. Jeromin, E. R. Urquhart and S. R. Jaffrey (2005). "Local translation of RhoA regulates growth cone collapse." *Nature* **436**(7053): 1020-1024.

Wu, Y., C. Whiteus, C. S. Xu, K. J. Hayworth, R. J. Weinberg, H. F. Hess and P. De Camilli (2017). "Contacts between the endoplasmic reticulum and other membranes in neurons." *Proc Natl Acad Sci U S A* **114**(24): E4859-E4867.

Wu, Y., C. Whiteus, C. S. Xu, K. J. Hayworth, R. J. Weinberg, H. F. Hess and P. De Camilli (2017). "Contacts between the endoplasmic reticulum and other membranes in neurons." *Proceedings of the National Academy of Sciences* **114**(24): E4859-E4867.

Xu, L., X. Wang and C. Tong (2020). "Endoplasmic Reticulum-Mitochondria Contact Sites and Neurodegeneration." *Front Cell Dev Biol* **8**: 428.

Yalçın, B., L. Zhao, M. Stofanko, N. C. O'Sullivan, Z. H. Kang, A. Roost, M. R. Thomas, S. Zaessinger, O. Blard, A. L. Patto, A. Sohail, V. Baena, M. Terasaki and C. J. O'Kane (2017). "Modeling of axonal endoplasmic reticulum network by spastic paraplegia proteins." *eLife* **6**: e23882.

Yamamoto, Y., A. Yoshida, N. Miyazaki, K. Iwasaki and T. Sakisaka (2014). "Arl6IP1 has the ability to shape the mammalian ER membrane in a reticulon-like fashion." *Biochem J* **458**(1): 69-79.

Yang, F., X.-p. He, L. Feng, K. Mizuno, X.-W. Liu, J. Russell, W.-C. Xiong and B. Lu (2001). "PI-3 kinase and IP3 are both necessary and sufficient to mediate NT3-induced synaptic potentiation." *Nature Neuroscience* **4**(1): 19-28.

Yang, Y. S. and S. M. Strittmatter (2007). "The reticulons: a family of proteins with diverse functions." *Genome Biol* **8**(12): 234.

Yao, J., Y. Sasaki, Z. Wen, G. J. Bassell and J. Q. Zheng (2006). "An essential role for β -actin mRNA localization and translation in Ca²⁺-dependent growth cone guidance." *Nature Neuroscience* **9**(10): 1265-1273.

Yoon, B. C., H. Jung, A. Dwivedy, C. M. O'Hare, K. H. Zivraj and C. E. Holt (2012). "Local translation of extranuclear lamin B promotes axon maintenance." *Cell* **148**(4): 752-764.

Yoon, B. C., K. H. Zivraj and C. E. Holt (2009). "Local translation and mRNA trafficking in axon pathfinding." *Results Probl Cell Differ* **48**: 269-288.

Younts, T. J., H. R. Monday, B. Dudok, M. E. Klein, B. A. Jordan, I. Katona and P. E. Castillo (2016). "Presynaptic Protein Synthesis Is Required for Long-Term Plasticity of GABA Release." *Neuron* **92**(2): 479-492.

Zhao, B., D. P. Meka, R. Scharrenberg, T. Konig, B. Schwanke, O. Kobler, S. Windhorst, M. R. Kreutz, M. Mikhaylova and F. Calderon de Anda (2017). "Microtubules Modulate F-actin Dynamics during Neuronal Polarization." *Sci Rep* **7**(1): 9583.

Zhao, L., A. L. Sheng, S. H. Huang, Y. X. Yin, B. Chen, X. Z. Li, Y. Zhang and Z. Y. Chen (2009). "Mechanism underlying activity-dependent insertion of TrkB into the neuronal surface." *J Cell Sci* **122**(Pt 17): 3123-3136.

Zhu, Y., G. Zhang, S. Lin, J. Shi, H. Zhang and J. Hu (2018). "Sec61 β facilitates the maintenance of endoplasmic reticulum homeostasis by associating microtubules." *Protein Cell* **9**(7): 616-628.

Zivraj, K. H., Y. C. L. Tung, M. Piper, L. Gumy, J. W. Fawcett, G. S. H. Yeo and C. E. Holt (2010). "Subcellular Profiling Reveals Distinct and Developmentally Regulated Repertoire of Growth Cone mRNAs." *The Journal of Neuroscience* **30**(46): 15464-15478.

Zufferey, R., T. Dull, R. J. Mandel, A. Bukovsky, D. Quiroz, L. Naldini and D. Trono (1998). "Self-inactivating lentivirus vector for safe and efficient in vivo gene delivery." *J Virol* **72**(12): 9873-9880.

8. Appendix

8.1 List of figures

Figure 5.1.1	ER distributes in the growth cone core and filopodia of cultured motoneurons	Page 75
Figure 5.1.2	ER moves into growth cone filopodia and these movements are different from membrane filopodia movements	Page 76
Figure 5.1.3	In cultured motoneurons, ER movements in filopodia are coordinated by actin filaments	Page 77
Figure 5.2.1	ER dynamics in growth cone filopodia and core after different treatments.	Page 80
Figure 5.2.2	ER dynamics in growth cone filopodia are higher than those in the growth cone core.	Page 81
Figure 5.2.3	Filopodia ER are correlated especially with actin filaments.	Page 81
Figure 5.2.4	Core ER dynamics are regulated by actin and microtubules.	Page 82
Figure 5.3.1	Survival assay of cultured motoneurons after pharmacological treatment with myosin inhibitors.	Page 84
Figure 5.3.2	Myosin VI mediates filopodia ER movements in growth cones of cultured motoneurons.	Page 85
Figure 5.3.3	Knockdown of drebrin isoforms in cultured motoneurons.	Page 87-88
Figure 5.3.4	Drebrin A facilitates actin and microtubule regulated ER dynamics in axon terminals.	Page 88-89
Figure 5.4.1	Specificity of antibodies against pTrkB and TrkB.	Page 91-92
Figure 5.4.2	Extracellular BDNF stimulates TrkB activation on a time scale of seconds in cultured motoneurons.	Page 92-93
Figure 5.4.3	Redistribution of ribosomes is triggered by BDNF stimulation.	Page 95-96
Figure 5.5.1	A short exposure to BDNF triggers ribosome assembly in growth cones of motoneurons.	Page 98
Figure 5.5.2	BDNF promotes ribosomes in growth cones of motoneurons into the stage of elongation.	Page 99
Figure 5.5.3	Loss of TrkB repeals BDNF-induced increase in Y10B immunoreactivity in growth cones of motoneurons.	Page 100-101
Figure 5.6.1	Puromycin assay reveals increased global protein synthesis in growth cones within 1 min BDNF stimulation.	Page 102
Figure 5.6.2	No obvious increase in immunoreactivity of puromycin in soma of motoneurons is observable in the puromycin assay.	Page 103
Figure 5.6.3	BDNF stimulation triggers translation of the transmembrane protein Cav2.2.	Page 104
Figure 5.6.4	Translation of cytosolic protein β -actin in growth cones is induced by extracellular BDNF.	Page 105

Figure 5.7.1	Increased number of fully assembled ribosomes attach to ER as a result of extracellular BDNF stimulation.	Page 107
Figure 5.7.2	BDNF-induced ribosomes at the elongation stage are associated with ER in axonal growth cones of motoneurons.	Page 108
Figure 5.8.1	In Smn-deficient motoneurons, ER dynamics in growth cone filopodia are reduced.	Page 110
Figure 5.8.2	ER in the growth cone core of Smn-deficient motoneurons shows reduced dynamics compared to that in the control group.	Page 111
Figure 5.8.3	Association between ER and F-actin in growth cone cores of Smn-deficient motoneurons.	Page 112
Figure 5.8.4	Overlap of ER with F-actin in growth cone filopodia is altered when SMN is deficient.	Page 113
Figure 5.9.1	Ribosomal response to BDNF is altered in axonal growth cones of Smn-deficient motoneurons.	Page 115
Figure 5.9.2	Global protein synthesis stimulated by BDNF is not detectable in growth cones of Smn-deficient motoneurons using puromycin incorporation assay.	Page 115
Figure 5.10.1	BDNF-induced assembly of ribosomes and their association with ER in growth cones of Smn-deficient motoneurons.	Page 117
Figure 5.10.2	In Smn-deficient motoneurons, ribosomes and ER tethering is impaired during translation elongation phase.	Page 118
Figure 5.11.1	Total TrkB level of Smn-deficient motoneurons is similar with the control group.	Page 120
Figure 5.11.2	TrkB levels on the surface of growth cones of Smn-deficient motoneurons are comparable to the control.	Page 120
Figure 5.12.1	BDNF can stimulate activation of Trkb in Smn-deficient motoneurons.	Page 122
Figure 5.12.2	BDNF does not trigger phosphorylation of Trkb receptor in growth cones of Smn-deficient motoneurons.	Page 123

8.2 List of tables

Table 4.1.4.1	List of plasmids used for cloning and lentivirus production
Table 4.1.5.1	List of primary antibodies used for immunofluorescence
Table 4.1.5.2	List of secondary antibodies used for immunofluorescence
Table 4.1.5.3	List of primary antibodies used for western blot
Table 4.1.5.4	List of secondary antibodies used for western blot
Table 4.1.6.1	List of used primers for genotyping

Table 4.1.6.2	List of used primers for cloning
Table 4.2.8.1	RCP program for amplification of KDEL fragments
Table 4.2.8.2	RCP program for amplification of mCherry-KDEL fragments
Table 4.2.8.3	RCP program for amplification of GFP-actin fragments
Table 4.2.13.1	Table of RCP program for Smn KO and WT genotyping
Table 4.2.13.2	Table of RCP program for <i>SMN2tgtg</i> genotyping
Table 4.2.13.3	Table of RCP program for TrkB KO and WT genotyping

8.3 List of abbreviations

°C	Celsius grad
4EBPs	Eukaryotic initiation factor 4E-binding proteins
AChE	Acetylcholinesterase E
AD	Alzheimer's disease
ADP	Adenosine diphosphate
ALS	Amyotrophic lateral sclerosis
AMPA	α -amino-3-hydroxy-5-methyl-4-isoxazole propionic acid
AMPArs	AMPA receptors
APH	Amphipathic Helix
APS	Ammonium persulfate
ARL6IP1	ADP-ribosylation factor-like 6 interacting protein 1
ATF-6	Activating transcription factor 6
ATP	Adenosine triphosphate
ATP5G1	ATP synthase lipid-binding protein
BACE1	Beta-secretase 1
BDNF	Brain-derived neurotrophic factor

BiP	Binding immunoglobulin protein
BNIP1	BCL2 Interacting Protein 1
BSA	Bovine serum albumin
C9ORF72	Chromosome 9 open reading frame 72
cAMP	Cyclic adenosine monophosphate
Cav2.2	α -1 β subunits of the N-type Ca ²⁺ channels
CI-MPR	Cation-independent mannose 6-phosphate receptor
CNTF	Ciliary neurotrophic factor
COX4I1	Cytochrome oxidase subunit 4 isoform 1
CRE	cAMP-responsive element
CREB	CRE-binding Protein
CytoD	Cytochalasin D
DCC	Colorectal carcinoma
DiOC6(3)	3,3'-Dihexyloxacarbocyanine iodide
DIV	Days in vitro
DMEM	Dulbecco's modified eagle medium
DMSO	Dimethyl sulfoxide
DNA	Deoxyribonucleic acid
DNs	Dystrophic Neurites
dNTPs	Deoxyribonucleosides
DP1	Deleted in polyposis 1
DRG	Dorsal root ganglion
Drp1	Dynamin related protein 1
<i>E.coli</i>	<i>Escherichia coli</i>
EB1	End-binding protein 1

EB3	End-binding protein 3
ECL	Enhanced chemiluminescence
EDTA	Ethylenediaminetetraacetic acid
eEF2	eukaryotic elongation factor 2
eIFs	Eukaryotic initiation factors
EM	Electron microscopy
ER	Endoplasmic reticulum
ERGIC	ER-Golgi intermediate compartment
ERK	Extracellular signal-regulated protein kinase
ESCRT	Endosomal sorting complexes required for transport
FCS	Fetal calf serum
Fmr1	synaptic functional regulator
FMRP	Fragile X mental retardation protein
FUS	Fused in sarcoma
FXS	Fragile X syndrome
G6P	Glucose-6-phosphate
G6Pase- α	Glucose-6-phosphatase- α
GM130	Golgi matrix protein 130
GRP78	Glucose-regulated protein 78
GTP	Guanosine triphosphate
GTPase	Guanosine triphosphatase
HBSS	Hanks' balanced salt solution
HEK	Human embryonic kidney
HEPES	4-(2-hydroxyethyl)-1-piperazineethanesulfonic acid
HS	Horse serum

HSPs	Hereditary spastic paraplegias
ICS	Image Correlation Spectroscopy
INPP5K	Inositol polyphosphate 5-phosphatase K
IP3Rs	Inositol tris-phosphate receptor
iPSC	Induced pluripotent stem cell
IRE1	Inositol-requiring enzyme 1
IsAHP	Slow afterhyperpolarization current
IST1	IST1 Factor Associated with ESCRT-III
JACoP	Just Another Colocalization Plugin
JIR	Jackson ImmunoResearch
JPH3	Junctophilin 3
JPH4	Junctophilin 4
KD	Kilo base pair
KIF5	Kinesin heavy chain isoform 5A
KO	knockout
L	Liter
LB	Lysogeny broth
LDLR	Low-density-lipoprotein receptor
M6PR	Mannose 6-phosphate
MAMs	Mitochondria-associated membranes
MAPK	Mitogen-activate protein kinase
MCSs	Membrane contact sites
MCTPs	Multiple C2 domain and transmembrane region proteins
MFN2	Mitofusin2
MgCl ₂	Magnesium chloride 2

mGluRs	Metabotropic glutamate receptors
min	Minute
MKP-1	Mitogen-activated protein kinase phosphatase 1
ml	Milliliter
mRNAs	Messenger messenger ribonucleic acids
ms	millisecond
MTB1	microtubule-binding domain
mTOR	Mammalian target of rapamycin
MTs	Microtubules
mV	Millivolt
NB	Neurobasal
NGF	Nerve growth factor
NMJs	Neuromuscular junctions
NP-40	Nonidet P-40
NT3	Neurotrophin-3
Ntrk2	Neurotrophic receptor tyrosine kinase 2
P/S	Penicillin-Streptomycin
PBS	Phosphate buffered saline
PCR	Polymerase chain reaction
PD	Parkinson's disease
PDZD8	PDZ domain containing 8
PFA	Paraformaldehyde
PFS	Perfect focus system
PI3K	Phosphatidylinositol 3-kinase
Pink1	Pten-induced putative kinase 1

PLC γ	Phospholipase C γ
PLS3	Plastin 3
PM	Plasma membrane
polyQ	Polyglutamin
PORN	Poly-DL-Ornithine
PSD-95	Postsynaptic density protein 95
PTPIP51	Protein tyrosine phosphatase-interacting protein 51
RBPs	RNA-binding Proteins
REEP1	Receptor expression-enhancing protein 1
REEPs	Receptor expression-enhancing proteins
RER	Rough endoplasmic reticulum
RHD	Reticulon homology domain
RHOA	Ras homolog family member A
ROCK	Rho-associated protein kinase
RPL24	Ribosome protein L24
RPL5	Ribosome protein L5
RPS6	Ribosome protein S6
rRNA	ribosomal ribonucleic acid
RT	Room temperature
Rtn1p	Reticulon 1p
Rtn4a	Reticulon 4a
RTNs	reticulons
RyRs	Ryanodine receptors
sAHP	Slow afterhyperpolarization
SCRN1	Secernin-1

SDS	Sodium dodecyl sulfate
Sema3A	Semaphorin 3A
SER	Smooth endoplasmic reticulum
SERCA	Sarcoplasmic/endoplasmic reticulum calcium ATPase
shRNA	short hairpin RNA
SIGMAR1	MAM-associated proteins Sigma 1 receptor
SigR1	Sigma-1 receptor
SIM	Structured Illumination Microscopy
SMA	Spinal Muscular Atrophy
SMN	Survival motor neuron
SNCA	Synuclein Alpha
snRNA	small nuclear RNA
snRNPs	small nuclear ribonucleoproteins
SOD1	Superoxide dismutase 1
STIM1	Stromal interacting molecule 1
SV	Synaptic vesicle
TAC	Tip attachment complex
TBS	Tris buffered saline
TDP43	TAR DNA-binding Protein 43
TEMED	Tetramethylethylenediamine
TfnR	Transferrin receptor
Tg	Transgene
TGN38	Trans-Golgi network protein 38
TrkB	Tropomyosin receptor kinase B
tRNA	transfer ribonucleic acid

U snRNAs	Uridine-rich, small nuclear ribonucleic acids
VAPB	Vesicle-associated membrane protein-associated protein B
VAPs	Vesicle-associated membrane protein-associated proteins
VPS13	Vacuolar Protein Sorting-associated Protein 13
WB	Western blot
WT	Wildtype
ZBP1	Zipcode binding protein 1

9. Affidavit

I hereby confirm that my thesis entitled “Dynamic remodeling of endoplasmic reticulum and ribosomes in axon terminals of wildtype and Spinal Muscular Atrophy motoneurons” is the result of my own work. I did not receive any help or support from commercial consultants. All sources and / or materials applied are listed and specified in the thesis.

Furthermore, I confirm that this thesis has not yet been submitted as part of another examination process neither in identical nor in similar form.

Place, Date

Signature

Eidesstattliche Erklärung

Hiermit erkläre ich an Eides statt, die Dissertation „Dynamische Reorganization des endoplasmatischen Retikulums und der Ribosomen in Axonterminalen von Wildtyp- und Spinaler Muskelatrophie Motoneuronen“ eigenständig, d.h. insbesondere selbstständig und ohne Hilfe eines kommerziellen Promotionsberaters, angefertigt und keine anderen als die von mir angegebenen Quellen und Hilfsmittel verwendet zu haben.

Ich erkläre außerdem, dass die Dissertation weder in gleicher noch in ähnlicher Form bereits in einem anderen Prüfungsverfahren vorgelegen hat.

Ort, Datum

Unterschrift

10. Acknowledgments

Dear Prof. Sendtner, I would like to thank you for offering me the opportunity to work on this exciting project. This precious chance took me out of my comfortable zone and allowed me to experience life as a researcher. I have learned a lot of things including technical approaches and methodologies in neuroscience, scientific thinking and experimental design during my PhD period. Without your patience, massive knowledge, great scientific ideas and technical guidance, this work would not be accomplished so successfully within 4 years. In weekly morning meetings, you gave me good advice to my experiments, inspired and encouraged me all the time to overcome obstacles in science. I really appreciate what you have done and are still doing for me to finish my PhD program here. I would like to thank other members of my thesis committee: Prof. Markus Sauer and Prof. Lars Dölken for giving me precious suggestions and helpful feedbacks in my Start-up meeting and annual meetings. Prof. Markus Sauer provided me with the access to super-resolution microscope and had some small meetings with me to discuss my experiments.

I would like to thank Mehri for helpful guidance during my PhD including good ideas, technical teaching and assistance for cloning, image acquisition and analysis. I have learned so much from you in all these years. Sebastian Reinhard and Sören Doose, working at the Biocenter, helped me with all the analysis of ER dynamics using Image Correlation Spectroscopy. Marcus Behringer assisted me with the manipulation of the Structured Illumination Microscope. Patrick, Changhe, Sibylle and Luisa, thank you guys for helping me with some experiments of the project. Robert, thank you for giving me suggestions and helpful discussion. Many thanks also go to Hildegard for her excellent work in virus production, to Christian for his preparation of cells for virus production and to Regine and all the other members at the animal facility for mouse breeding. I also have to say a special word

of thanks to my colleagues: Bitu, Simon, Alex, Urveen and Judita. Thank you all for the comfortable atmosphere and fantastic collaboration in the lab and for your personal support.

I honestly thank the excellent funding from PicoQuant and further funding from DFG that made this interesting and challenging research work possible. I would also like to thank the Graduate School of Life Science Würzburg for the administrative assistance, organization of amazing workshops on transferable skills and providing international conferences to me to communicate with other young scientists. I pretty much enjoyed the events organized by the Graduate School of Life Science.

Last but not the least, I am very thankful to my family and friends. First, I would like to thank my family members for their love and continuous support during this hard time. My friends in Würzburg Meiqi, Mengshi and Kunkun, many thanks for sharing happiness and frustrations, discussing solutions to daily life problems, and encouraging me to stay positive. Without your accompanying, I would not have had this colorful and fantastic life in Germany.

11. Curriculum Vitae

Deng, Chunchu

Birthdate: Jan. 11th 1990

Birthplace: China

Nationality: Chinese

Bahnhofstraße 22

97070 Würzburg, Germany

+49 17636651680

dengchunchu@sina.com

Education

11.2017-present	PhD, Neuroscience, Julius-Maximilians-University of Wuerzburg, Germany
09.2014-06.2017	MSc in Neurology, Huazhong University of Science and Technology, China
09.2008-06.2014	BSc in Clinical Medicine, Huazhong University of Science and Technology, China

Research experience

11.2017-present	<ul style="list-style-type: none"> • University of Wuerzburg, Germany • Institute of Clinical Neurobiology • Doctoral researcher • Doctoral thesis: Dynamic remodeling of endoplasmic reticulum and ribosomes in axon terminals of wildtype and Spinal Muscular Atrophy motoneurons. • Supervision: <ol style="list-style-type: none"> 1. Prof. Michael Sendtner 2. Prof. Markus Sauer 3. Prof. Lars Dölken
09.2014-06.2017	<ul style="list-style-type: none"> • Huazhong University of Science and Technology, China • Department of Neurology • Master thesis: Clinical features and severe type associated factors of Guillain-Barré Syndrome • Supervision: Zhang Sumin
09.2011-12.2012	<ul style="list-style-type: none"> • Huazhong University of Science and Technology, China • Institute of Biochemistry • Research Project for Students: Effect of PTD4-Apoptin on VEGF expression in cancer cells and on M1-type macrophages • Supervision: Sun Jun

Clinical experience

09.2014-05.2017	<ul style="list-style-type: none"> • Huazhong University of Science and Technology, China • Department of Neurology, Tongji Hospital • Clinical standardized training in Neurology
08.2013-09.2013	<ul style="list-style-type: none"> • Heidelberg University, Germany • Stroke Unit and Dermatology Department, Heidelberg Hospital • Exchange Program student for Practice

Awards and honors

11.2017-10.2020	Fellowship from the Institute of Clinical Neurobiology, University Hospital Wuerzburg, Germany
2014-2016	Academic Scholarship, China
2013	Self-improvement Student Scholarship, China
2009	<ul style="list-style-type: none"> • Outstanding Student Award, China • National Scholarship for Encouragement, China

Conferences

<ul style="list-style-type: none"> • 10.2021 • 10.2019 • 10.2018 	<ul style="list-style-type: none"> • International Symposium “EUREKA” organized by the PhD students at the Graduate School of Life Sciences, Würzburg, Germany. • Contribution: Poster
<ul style="list-style-type: none"> • 09.2019 • 09.2018 	<ul style="list-style-type: none"> • International Workshop on “Single Molecule Spectroscopy and Super-resolution Microscopy in the Life Sciences” organized by PicoQuant, Berlin, Germany. • Contribution: Poster
<ul style="list-style-type: none"> • 09.2017 	<ul style="list-style-type: none"> • The 20th National Conference of Neurology. • Contribution: Thesis talk

Publication list

<ul style="list-style-type: none"> • Dynamic remodeling of ribosomes and endoplasmic reticulum in axon terminals of motoneurons. Deng, C., M. Moradi, S. Reinhard, C. Ji, S. Jablonka, L. Hennlein, P. Lüningschrör, S. Doose, M. Sauer and M. Sendtner (2021). <i>J Cell Sci</i> 134(22).doi: 10.1242/jcs.258785 • Impaired dynamic interaction of axonal endoplasmic reticulum and ribosomes contributes to defective stimulus-response in Spinal Muscular Atrophy. Deng, C., S. Reinhard, L. Hennlein, S. Doose, S. Jablonka, M. Sauer, M. Moradi and M. Sendtner. Manuscript submitted to <i>Translational Neurodegeneration</i>. Status: in Revision. 2021 Nov 13. • Loss of Tdp-43 disrupts the axonal transcriptome of motoneurons accompanied by impaired axonal translation and mitochondria function. Briesse, M., L. Saal-Bauernschubert, P. Lüningschrör, M. Moradi, B. Dombert, V. Surrey, S. Appenzeller, C. Deng, S. Jablonka and M. Sendtner. <i>Acta Neuropathol Commun</i>. 2020 Jul 24;8(1):116. doi: 10.1186/s40478-020-00987-6 • A case of neuromyelitis optica combined with anti-NMDA receptor encephalitis. Huang Liangjiang, Deng Chunchu, Li Dayong, Xiong Yongjie, Zhang Sumin and Huang Xiaojiang. <i>Stroke and Nervous Diseases (in Chinese)</i>. 2017,24(1):18-20. doi: 10.3969/j.issn.1007-0478.2017.01.004 • Clinical characteristics and etiology analysis of acute intracerebral hemorrhage in 694 young adults. Huang Liangjiang, Li Dayong, He Yongpei, Deng Chunchu, Xiong Yongjie and Zhang Sumin. <i>Acta Medicinae Universitatis Scientiae et Technologiae Huazhong (in Chinese)</i>. 2017,46(3), 5. doi: 10.3870/j.issn.1672-0741.2017.03.017
